NASA Contractor Report 178019

NASA-CR-178019
19860006217

EFFECTS OF LOAD PROPORTIONING ON THE CAPACITY OF MULTIPLE-HOLE COMPOSITE JOINTS

M. W. Hyer and P. A. Chastain

VIRGINIA POLYTECHNIC INSTITUTE
AND STATE UNIVERSITY
Blacksburg, Virginia

Grant NAG1-343
November 1985

National Aeronautics and
Space Administration

Langley Research Center
Hampton, Virginia 23665

ENTER:

9 1 1 RN/NASA-CR-178019

DISPLAY 09/6/1

86N15687*# ISSUE 6 PAGE 960 CATEGORY 39 RPT#: NASA-CR-178019 NAS 1.26:178019 CNT#: NAG1-343 85/11/00 176 PAGES UNCLASSIFIED DOCUMENT

UTTL: Effects of load proportioning on the capacity of multiple-hole composite joints TLSP: Final Report, Mar. 1984 - Mar. 1985

AUTH: A/HYER, M. W.; B/CHASTAIN, P. A. PAA: A/(Maryland Univ., College Park); B/(Aerojet Strategic Propulsion Co., Sacramento, Calif.)

CORP: Virginia Polytechnic Inst. and State Univ., Blacksburg. CSS: (Dept. of Engineering Science and Mechanics.) AVAIL.NTIS

SAP: HC A09/MF A01

CIO: UNITED STATES Sponsored in part by Army Aviation Systems Command

MAJS: /*ALGORITHMS/*BOREHOLES/*COMPOSITE MATERIALS/*FAILURE ANALYSIS/*JOINTS (JUNCTIONS)/*LOADS (FORCES)

MINS: / FINITE ELEMENT METHOD/ LAMINATES/ STRESS ANALYSIS/ THICKNESS

ABA: Author

EFFECTS OF LOAD PROPORTIONING

ON THE

CAPACITY OF MULTIPLE-HOLE COMPOSITE JOINTS

M.W. Hyer*

Department of Mechanical Engineering
University of Maryland
College Park, MD 20742

P.A. Chastain*

Advanced Engineering
Aerojet Strategic Propulsion Co.
Sacremento, CA 95813

*both authors were formerly associated with the Department of Engineering Science and Mechanics, Virginia Polytechnic Institute and State University.

ABSTRACT

This study addresses the issue of adjusting the proportion of load transmitted by each hole in a multiple-hole composite joint so that the joint capacity is a maximum. Specifically two-hole-in-series joints are examined. The results indicate that when each hole reacts 50% of the total load, the joint capacity is not a maximum. One hole generally is understressed at joint failure. The algorithm developed to determine the load proportion at each hole which results in maximum capacity is discussed. The algorithm includes two-dimensional finite-element stress analysis and a failure criteria. The algorithm is used to study the effects of joint width, hole spacing, and hole to joint-end distance on load proportioning and capacity. To study hole size effects, two-hole diameters are considered. Three laminates are considered: a quasi-isotropic laminate; a cross-ply laminate; and a 45 degree angle-ply laminate. By proportioning the load, capacity can be increased generally from 5 to 10%. In some cases a greater increase is possible.

ACKNOWLEDGEMENT

The research which led to the results presented was supported by a grant from the Structures Laboratory of the United States Army Research and Technology Laboratory (AVCSOM). The grant was monitored by Donald J. Baker of the NASA Langley Research Center. The authors wish to thank the Structures Laboratory for the support and thank Donald J. Baker for helpful comments and suggestions on the research.

TABLE OF CONTENTS

LIST OF TABLES

LIST OF FIGURES

CHAPTER 1

INTRODUCTION

Composite materials are widely used in many structural applications such as aircraft, automobiles and spacecraft. Currently the widespread use of composites is dependent upon many factors. Among these are material performance, cost, and compatibility of the composite material with the existing structure. In the future, when entire structures are manufactured with composite materials, the compatibility of the composite material with other materials within a structure may no longer be an issue. However, current applications require an interface between the composite component and other materials. This interface, which is in many cases a mechanical joint, has been the focus of much research.

In most applications of composite materials, the joint becomes the critical factor in the determination of failure loads. Therefore, joints often utilize many bolts or fasteners to distribute the loads throughout the joint to reduce the risk of failure and to increase load capacity. These types of joints, called multiple-hole joints, generally have two main configurations. One configuration is a series arrangement. In this arrangement the bolts are in a line and parallel to the line of load application. The second configuration is called a parallel arrangement. In a

parallel arrangement the bolts are aligned perpendicular to the line of load application. In some cases a joint uses a combination of these two configurations to distribute the load over a larger area. These multifastener joints are in contrast to the much simpler single-hole configuration. Though not often used, the single hole configurations are frequently studied, serving as a starting point for the analysis of composite bolted joints.

In addition to the number and configuration of fasteners used in a joint, the overall geometry of the joint varies with different designs. Some joints are in a single-lap configuration with two plates overlapping each other. The fastener holes are drilled through the two plates. This type of joint is rather simple. However, due to the separation distance between the geometric midplanes of the two plates, the plates experience bending stresses, in addition to the applied tensile or compressive stresses. Scarf joints are used to minimize this bending effect by tapering the thicknesses of the two plates in the joint area. With tapering, the total joint thickness is the same as the thickness of a single plate and the midplanes of the two plates coincide. This joint can be useful in some applications but there are some disadvantages to it. Compared to a single lap joint, the capacity of a scarf joint is usually lower. Also, the thicknesses of the plates

to be joined need to be nearly the same. Quite often this is not the case in actual structural applications. Also, the taper in the plate has to be created by machining or some other additional step in the manufacturing process. This adds to the cost of the joint.

Another popular joint used is the double-lap joint. The plate thicknesses need not be uniform. This configuration also eliminates the bending stresses caused by eccentricities. This can be explained by examining the symmetry of the joint. Fig. 1.1 depicts the joints discussed and the symmetric nature of the double lap joint is evident in the figure. In the figure it is assumed the joints must transmit, or react, a load of P. The primary mode of deformation of a double-lap joint is extensional. Though having more components, this joint is in some respects simpler to analyze than a single-lap joint.

This study will focus on a specific joint configuration, namely a two-hole-in-series double-lap joint. The configuration is shown at the bottom of Fig. 1.1. The study will be aimed at determining what proportion of the total load, P, should be reacted at each hole so that the load capacity of the joint is a maximum. The load capacity will be assumed to be limited by the failure of the material around the holes. Specifically, the Yamada-Sun failure criteria is used in conjunction with the idea of a

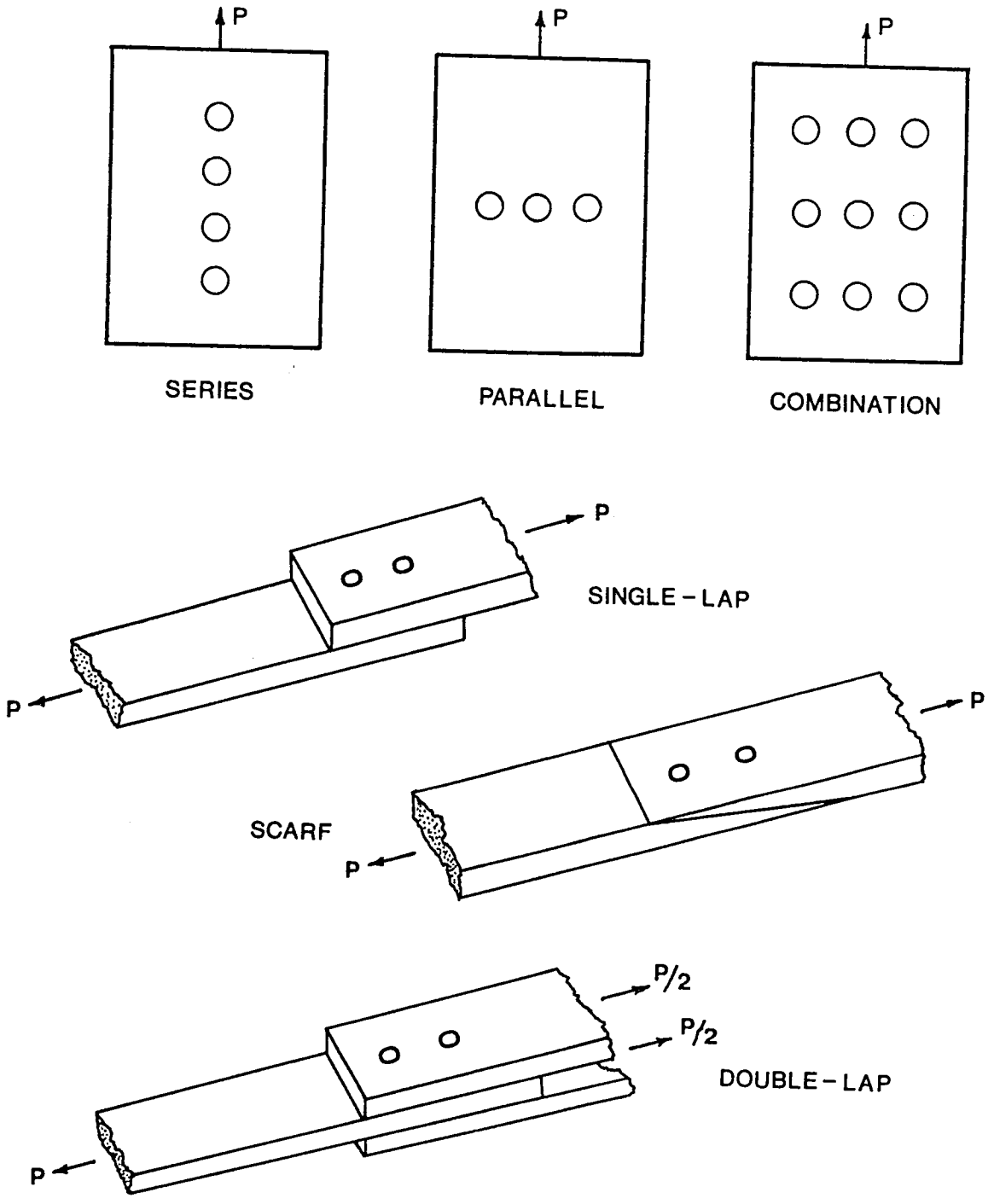

Fig. 1.1 Joint Configurations.

characteristic distance to determine what proportion of the total load should be reacted by each hole so that the failure load of the joint is a maximum. Oftentimes in actual applications the total load is divided equally among each hole. It does not seem obvious a priori that having one-half the load being reacted by each hole (in the two-hole series joint) results in the maximum load capacity. If the material around one hole is understressed while the material around the other hole is failing, the joint is not operating efficiently. Material, and thus weight-savings, are compromised.

This study centers on looking at the inner lap of a double-lap joint. The lap is considered as a finite-width plate with two holes. The holes are loaded at their edge, in the plane of the plate. The load on the holes is reacted on one end of the plate. Considering only the inner lap is not restrictive. The single plate with two holes could as easily be thought of as one of the two outer laps of a double-lap joint. Here, however, the discussion will proceed as if it is an analysis of the inner lap. For purposes of the analysis, the plate is assumed to be in a state of plane stress.

The study begins by reviewing the relevant past work in the area of bolted joints. The review is not meant to be a critical or comprehensive review of the past work, rather it

is meant to illustrate the context of the present work. Attention is then turned to the method of analysis used in the study, namely the displacement-based finite-element method. Since the method is so well known, this discussion is short and related only to the specific element used. Results obtained from the analysis of a single-hole joint using the particular element are compared with past work of other investigators. This step essentially confirms the validity of the present analysis and provides a means of determining proper mesh density and mesh size.

The study then turns to the analysis of the two-hole joint. Results of the present analysis, assuming each bolt reacts 50% of the total load, are compared with past work which have assumed the 50-50 load proportion. This step is also viewed as a validation step.

The remainder of the study deals with the determination of the load proportion which results in the maximum joint capacity. The failure theory used will be presented and discussed. An appendix will be used to compare the failure theory used with other failure theories. Then the discussion turns to the computational procedure used to find what proportion of load should be reacted by each hole if load capacity is to be maximized. The determination of the maximum load capacity is discussed in the context of a fixed joint geometry and a given material.

However, the effects on joint capacity, and on the load proportion that gives the maximum capacity, of varying joint geometry and material properties is then explored. The study ends by summarizing the findings

CHAPTER 2

LITERATURE REVIEW

Of all the work done which relates to the joining of composite materials, the vast majority of work has focused on determining the stress distribution around a single hole in an orthotropic plate. The plate has represented a portion of the joint, the orthotropy has represented the effect of the fiber-reinforcing, and the single hole has represented a 'typical' hole in the joint. The hole is loaded in some fashion to represent the effects of the bolt bearing on the hole. Recognizing that single hole connections are rarely used, some work has been conducted with more than one loaded hole in an orthotropic plate. This single-hole and double-hole work will be reviewed in order to establish the findings of research and to motivate the need for the work presented here.

In studying the stress state in a bolted joint, various assumptions have been used by the many researchers. The most common of these is that a state of plane stress exists in the plate and any through-the-thickness effects can be ignored. This approach was used by Bickley [1], in his study of a pin-loaded hole in an isotropic plate. The terminology 'pin' is used to denote the fact that a bolt, when tightened, would induce a through-the-thickness stress state. This is contrary to the plane-stress assumption. A

pin, on the other hand, would simply slip into the hole and bear on the edge of the hole in the plane of the plate. Bickley assumed the contact stresses imposed on the plate by the pin could be represented by means of a cosinusoidal distribution of the radial stress acting on the hole edge in the plane of the plate. Any frictionally-induced stresses were ignored. This stress distribution has been used widely by many investigators for both isotropic and orthotropic problems.

Oplinger [2] used another popular approach in modelling the pin-plate interface stresses. Oplinger assumed a rigid pin. For purposes of analysis, this translates into displacement boundary conditions on the edge of the hole. Oplinger used this assumption in conjunction with an elasticity solution. Such an assumption results in a stress distribution at the pin-plate contact region that is different than a cosinusoidal distribution. The study shows that plate material properties have a substantial effect on the shape of the stress distribution. Oplinger summarized the radial stress issue by saying that in some cases the cosinusoidal stress distribution can be used to represent pin-plate interaction. In other cases it could not be used with any degree of accuracy. The study concluded that displacement boundary conditions (rigid-pin assumptions) produced a more accurate analysis.

Waszcak and Cruse [3] compared the cosinusoidal distribution assumption with the rigid pin assumption in their studies. They employed finite-element methods. The primary conclusion of their work was that ultimate prediction of failure was not highly dependent on the pin-plate interface assumption. However, their correlation with laboratory data was, in some cases, quite poor.

Crews, Hong, and Raju [4] have studied the case of an orthotropic plate loaded with an elastic frictionless pin. This analysis utilized springs between the pin and hole boundary, resulting in a separation between the pin and hole edge on the unloaded portion of the hole. This meant that a contact angle of less than 180° was possible, and indeed occurred, for most cases. This analysis was also based on finite-elements, using extremely refined meshes. Radial, circumferential, shear stresses, and stress concentration factors were found for many different laminate configurations and different plate geometries. The results emphasized the influence of orthotropy and geometry upon these stress distributions and the magnitudes of the stresses.

Collings [5] has performed experimental work with both one-hole and two-hole composite joints. He determined the type of laminates which most effectively react the stresses induced by the bolt. In addition to investigating the

effect of various laminates, he also examined the effect of bolt clamping pressure. Subsequent work by Collings and Beauchamp [6] examined the deflection behavior of various laminates. The purpose of their study was to evaluate the joint stiffnesses by understanding the load-deflection characteristics.

Pyner and Matthews [7] have also experimentally examined single and multiple-bolted joints in composites. Various parallel and series configurations were studied. The main aim of this study was to determine the best bolt-hole configuration in terms of joint capacity. The conclusion of the study was that simpler bolt hole configurations yield higher capacities than more complex configurations. It was recommended that testing be employed when strengths of multiple hole joints are needed. In other related work Godwin, Matthews, and Kilty [8] experimentally investigated multiple-bolt joints. It was found that bolts in series yielded lower joint capacity than bolts in a parallel configuration. The existence of a bolt hole within the stress field generated by another bolt hole was found to be important. It was this superposition of stress fields which the authors recognized as the reason why joint capacities were lower for the series configurations. Godwin and Matthews [9] also presented a fine review of composite joint strengths. Various parameters such as material

properties, fastener types, joint type, fastener tolerance, and geometry were discussed.

Eisenmann and Leonhardt [10] presented experimental findings concerning laminate in-plane elastic property tailoring to improve composite joint efficiency. They examined the effect of replacing some of the laminate within the bearing region with compliant (+45/-45) plies. This uncoupled the global laminate strain level from local hole-region strains. Such uncoupling allowed the composite joint to achieve higher strain-to-failure values, extending the range of applications.

Soni [11] studied the failure of a variety of composite plates with a single fastener hole. He used finite-element analysis with displacement boundary conditions in conjunction with the Tsai-Wu tensor polynomial criterion [12]. The ultimate failure strength of the strongest ply at the weakest point in the laminate was used as a definition of failure. Soni's predictions, compared with available data, were conservative.

Hart-Smith [13] presented a study containing a massive amount of data collected during a test program of bolted graphite/epoxy and graphite-glass/epoxy joints conducted at McDonnell Douglas Corporation. The main object of the study was to determine the nature of the stress interactions in a multiple-bolt joint. Major findings include: 1) multiple-

bolt joints increase strength over single-bolt joints only when bearing failure governs; 2) a linear stress interaction exists, i.e., a direct superposition of stress fields caused by the individual holes, can be assumed in tensile loading cases. In compressive loading cases, however, non-linear stress interaction occurs; 3) The ultimate joint strength is, at best, about one-half of the basic laminate plate strength; 4) Capacities of joints with bolts were about twice that of joints with simple pins; 5) The use of glass fiber is almost always beneficial in terms of strength when compared to all graphite fiber cases. Subsequent work by Hart-Smith [14] summarized this data and presented a methodology to compute failure loads in orthotropic plates by using the analysis from isotropic plates and an empirically determined correlation factor.

Garbo and Ogonowski [15] developed a two-dimensional finite-element model to study the multiple-bolt problem. In addition, an excellent overview of design problems from an industry point of view is presented. Such parameters as fastener depth-to-plate thickness, hole tolerance, plate geometry, and laminate elastic properties were addressed. In addition the distribution of load among the bolts was addressed for the first time in any detail in this study. The model which was developed used cosinusoidal radial stress distributions for boundary conditions on the holes.

Although good information is presented, reported results are limited to specific laminates.

In other work by Garbo and Buchanan [16], the model previously developed by Garbo and Ogonowski was used in conjunction with an experimental program to design high-load transfer joints. They incorporated the 'softening' technique proposed by Eisenmann to increase the capacity. A seven-bolt joint in the series configuration was designed. The percentage of total load reacted by each bolt increased linearly along the length of the joint with the first bolt reacting the highest portion of the joint load. Additional work by Garbo and Becker [17] focused on a single-hole joint with the addition of a bypass load. This situation is in essence a section of a multiple-bolt joint in the series configuration. Again predictions were made with the finite-element model and tests were conducted for correlation. Bypass-stress vs. bearing-stress relations were developed for three different laminates.

Work by Hyer, Perry, and Lightfoot [18] reported experimental results obtained in investigating the superposition of the stress fields in a two hole joint. An averaging hypothesis was defined. This was defined as a technique of superimposing the stress fields due to an open hole in a tensile stress field and the stress field generated by a loaded hole. This hypothesis was was used to

predict the strength of joints with various width-to-diameter ratios. Good experimental verification was shown. The study was confined to quasi-isotropic laminates. Later work by Hyer and Klang [19-22] showed the effect of bolt friction, bolt elasticity, and bolt clearance on the stress distribution around the hole in a pin loaded orthotropic plate. A complex variable form of elasticity solution was used. This work indicated, like Oplinger's, that the rigid pin assumption is a better representation of the effects of the interaction of the pin with the hole than is the cosinusoidal representation. Clearance was shown to have a dramatic effect on the value and the location of the peak stresses, and on the overall stress distribution. Friction was also shown to influence the value and location of the peak stresses.

Rowlands, Rahman, Wilkinson, and Chiang [23] have also studied single-hole and double-hole joints in orthotropic materials. Both finite-element and experimental analyses were conducted. Moire interferometry and strain gage measurements were made and the investigation was extended to wood as well as boron-epoxy and glass-epoxy composites. Primarily, the contact stress distribution was reported for a variety of bolt load ratios, tolerances of bolt vs. hole diameters, and materials. In other work, Rahman [24] conducted a strength and stress analysis of two-hole

composite joints. Finite-element modelling with displacement boundary conditions was used to describe the bolt contact with the plate. Numerous failure criteria were used for failure analysis. Various load ratios were examined, in addition to different material types. An incremental loading technique was used to determine the contact region between the bolt and hole. Moire interferometry was used again to determine the accuracy of finite-element results.

Chang, Scott, and Springer [25] have extended the characteristic distance concept of Whitney-Nuismer [26] to study failure of bolted joints. Their work will be elaborated on later because it forms the basis for the failure criteria used in the present study. Briefly, Chang, Scott, and Springer postulated that a locus of characteristic distances exists around the hole. At the net section the distance coincides with the original distance proposed by Whitney and Nuismer to study tension and compression failures at the net section. However, at other circumferential positions around the hole, the characteristic distance varies. This variation reflects other possible failure modes, namely bearing and shearout. The locus is called by Chang, et al a 'characteristic curve' and it is a function of material properties and angular location. This characteristic curve was used by them in

conjunction with the Yamada-Sun [27] polynomial failure criteria for evaluation of joint failure loads. The mode of failure was indicated by the location on the characteristic curve where the Yamada-Sun criteria predicted failure. The method of analysis accounts for the well-observed hole size effect. Various laminates and joint geometries were investigated and experimentally tested for verification. Moderate correlation was achieved. The most accurate prediction occurred for quasi-isotropic laminates.

Of all the literature reviewed, Garbo has been the only author to pursue non-uniform bolt load distribution and its possible benefit in increasing load capacity. He achieved a nonuniform distribution by varying the compliance of the material in the vicinity of each bolt. The present study will assume this technique or others can be used to to allow nonuniform bolt loads to occur within a joint.

CHAPTER 3

METHOD OF ANALYSIS

The geometry and nomenclature associated with the analysis of the two-hole-in-series joint are illustrated in Fig. 3.1. As mentioned previously, only the inner lap will be analyzed in this study of bolt load distribution. Fig. 3.1, then, is a plate which represents the inner lap with its two holes in series. The width of the plate is W, the hole diameter is D (only equal hole diameters are considered), the centers of the holes are a distance G apart, and the center of second (bottom) hole is a distance E from the free end. The overall joint length is L. The plate is of thickness H. Here the geometric parameters W/D, E/D, and G/D will be used to represent variations in joint geometry.

Locations on the plate are defined in terms of an X-Y coordinate system, the Y-axis being the loading direction. **Laminae orientations will be with respect to the X-axis.** Locations at the hole edges will be referred to using polar coordinate systems centered at each hole. Each hole is loaded with known compressive radial stresses of the form

$$\sigma_r = \sigma_{r_o} \cos\theta \qquad -\pi/2 < \theta < \pi/2,$$
$$\sigma_r = 0 \qquad \text{otherwise,} \tag{3.1}$$

σ_{r_o} being a constant. Such a distribution produces a total

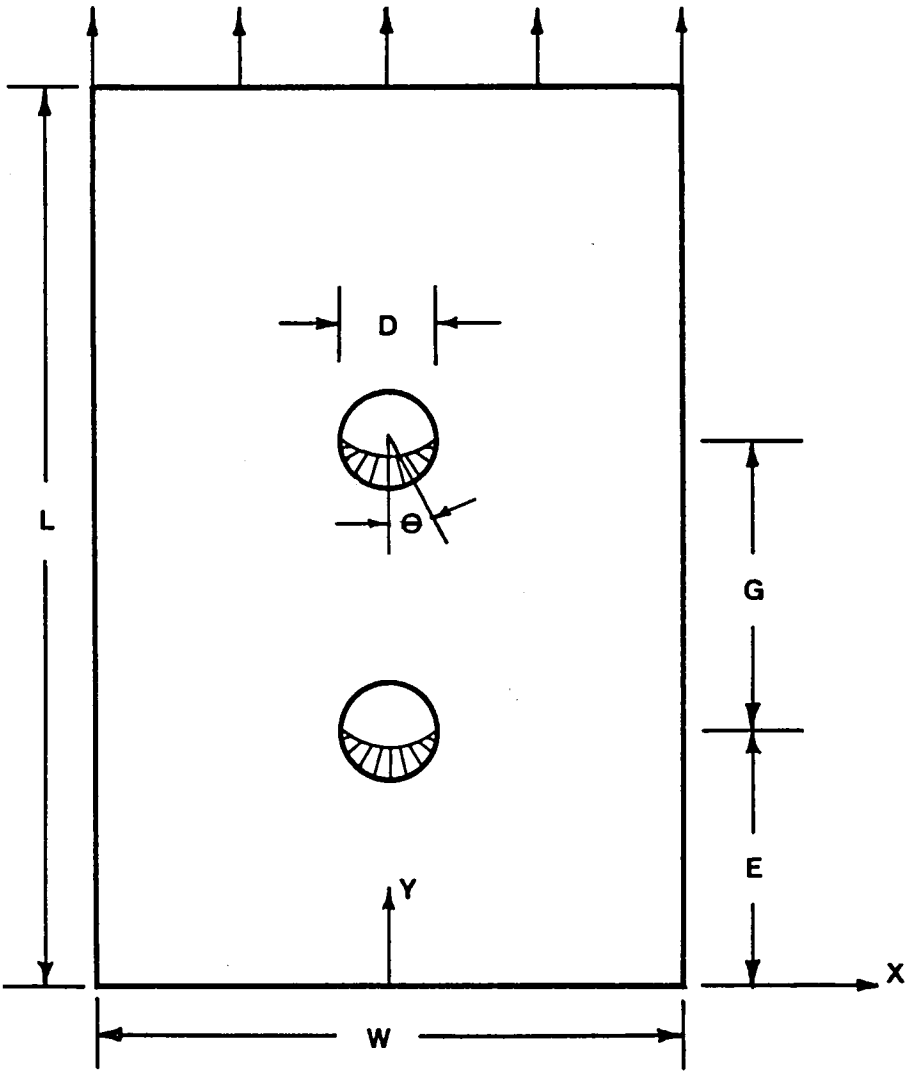

Fig. 3.1 Plate Nomenclature.

load on the hole of

$$P_{total} = \sigma_{r_o} DH\pi/4 \qquad (3.2)$$

For the first (top) hole, the subscript 1 will be used while for the second hole the subscript 2 will be used. Using this nomenclature

$$\sigma_{r_1} = (4/\pi)(P_1/DH)\cos\theta \qquad (3.3)$$

$$\sigma_{r_2} = (4/\pi)(P_2/DH)\cos\theta \qquad (3.4)$$

where P_1 is the load reacted by the top hole and P_2 is the load reacted by the bottom hole. The total load, $P_1 + P_2$, is reacted by a load at the end of the plate.

The finite-element method was used to determine the stresses in the plate. This method allowed for the solution of this complex problem which otherwise could not be solved. The nodal forces acting on the hole edges were used to represent the cosinusoidal distributions of Eqns. 3.3 and 3.4. A version of the well-known program STAP [28] was used to model this problem. Modifications to the original version were made previously for analysis of laminated plates with the program. The analysis was limited to a plane-stress condition in the laminate. In addition, bending effects were not permitted. Therefore, the stiffness matrices were composed only of elements from the A_{ij}, or extensional stiffness, matrix [29].

An 8-node isoparametric element was chosen for the analysis. This higher-order element allowed for a slightly less dense mesh to be used when compared to the mesh using a 4-node element. In addition, the 8-node element also allowed for curved element boundaries. Such boundaries were needed on the hole edge. The general element with its local coordinate system is shown in Fig. 3.2. The displacements for this element are given as

$$u(\xi,\eta) = \sum_{i=1}^{8} U_i \Psi_i(\xi,\eta) \qquad (3.5a)$$

$$v(\xi,\eta) = \sum_{i=1}^{8} V_i \Psi_i(\xi,\eta) \qquad (3.5b)$$

where the constants $U_1,\ldots,U_8$, and $V_1,\ldots,V_8$ are the unknown nodal coordinates. The interpolation functions are defined as

$$\psi_1 = (1/4)(1 + \xi)(1 + \eta)(-1 + \xi + \eta) \qquad (3.6a)$$

$$\psi_2 = (1/2)(1 + \xi)(1 + \eta^2) \qquad (3.6b)$$

$$\psi_3 = (1/4)(1 + \xi)(1 - \eta)(-1 + \xi - \eta) \qquad (3.6c)$$

$$\psi_4 = (1/2)(1 - \xi^2)(1 - \eta) \qquad (3.6d)$$

$$\psi_5 = (1/4)(1 - \xi)(1 - \eta)(-1 - \xi - \eta) \qquad (3.6e)$$

$$\psi_6 = (1/2)(1 - \xi)(1 - \eta^2) \qquad (3.6f)$$

$$\psi_7 = (1/4)(1 - \xi)(1 - \eta)(-1 - \xi + \eta) \qquad (3.6g)$$

$$\psi_8 = (1/2)(1 - \xi^2)(1 + \eta) \qquad (3.6i)$$

The finite-element grid used to represent the plate

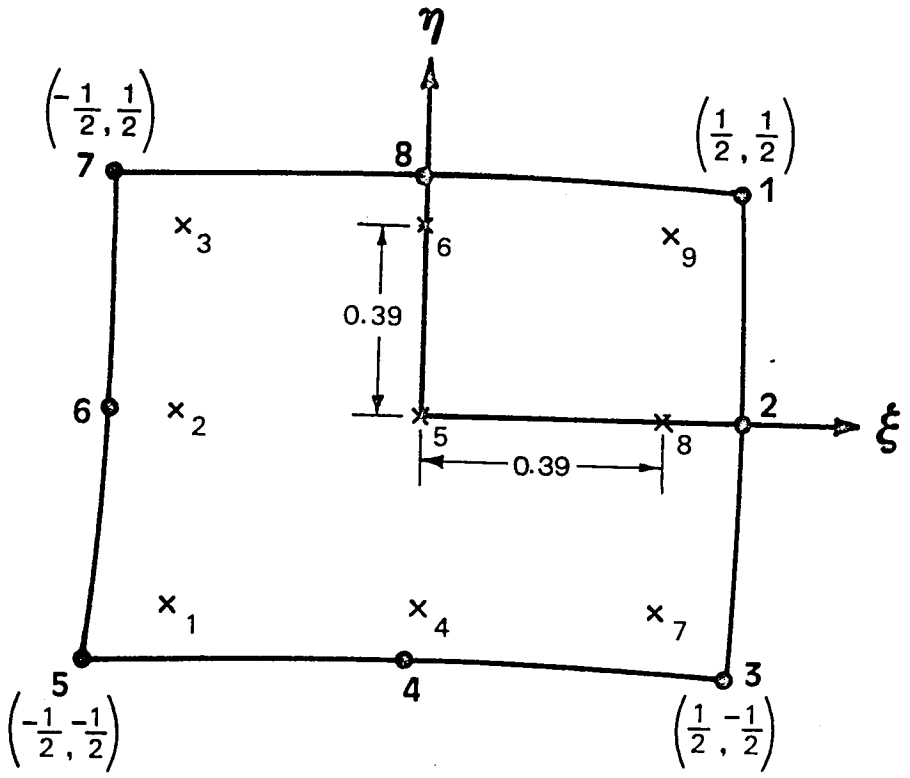

Fig. 3.2 8-Node Isoparametric Element.

with two holes is shown in Fig. 3.3. A total of about 350 elements with 1200 nodes were used to model one-half the plate. Centerline symmetry of both the applied loading and material properties permitted the analysis to be confined to one-half the plate. This figure also shows the boundary conditions used in the analysis. The top edge of the plate is fixed against movement in the Y direction. The centerline of the plate is fixed against movement in the X direction. The bottom and right sides are free of tractions and have unrestricted motion. Except for the fixed top edge, these boundary conditions are consistent with the conditions experienced by an inner lap of a double-lapped joint. In reality, the top edge would have an applied stress instead of being fixed. However, the finite-element analysis with a traction boundary condition on the holes works more conveniently with the top boundary subjected to a displacement boundary condition.

The cosinusoidal stress distribution on the hole edge is represented using nodal forces. The distribution of nodal forces is shown in Table 3.1. The distribution is given for a unit load, i.e., P_1 or P_2 of Eqns. 3.3 or 3.4 equals one. A close-up section of the hole area is shown in Fig. 3.4. The figure illustrates that there are element nodes every 4.5° around the hole.

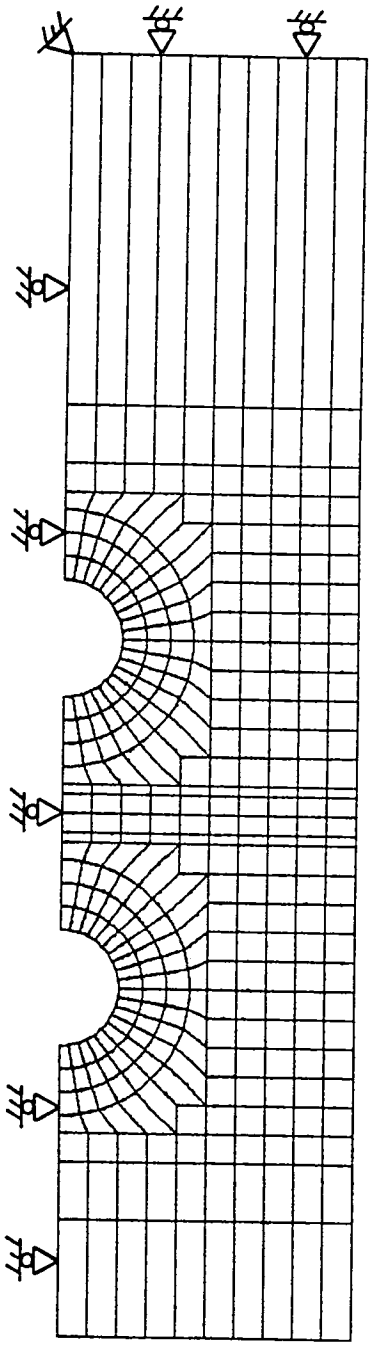

Fig. 3.3 Finite-Element Mesh.

Table 3.1 Hole Boundary Nodal Loadings

ANGLE degrees	Y-DIRECTION nodal loading	X-DIRECTION nodal loading	Node letter
0.0	-0.01668	0.00000	a
4.5	-0.06622	0.00522	b
9.0	-0.03254	0.00516	c
13.5	-0.06302	0.01512	d
18.0	-0.03018	0.00980	e
22.5	-0.05688	0.02356	f
27.0	-0.02648	0.01348	g
31.5	-0.04846	0.02968	h
36.0	-0.02182	0.01586	i
40.5	-0.03852	0.03290	j
45.0	-0.01668	0.01668	k
49.5	-0.02810	0.03290	l
54.0	-0.01152	0.01586	m
58.5	-0.01818	0.02968	n
63.0	-0.00688	0.01350	o
67.5	-0.00976	0.02356	p
72.0	-0.00320	0.00982	q
76.5	-0.00362	0.01512	r
81.0	-0.00082	0.00512	s
85.5	-0.00042	0.00528	t
90.0	0.00000	0.00000	u

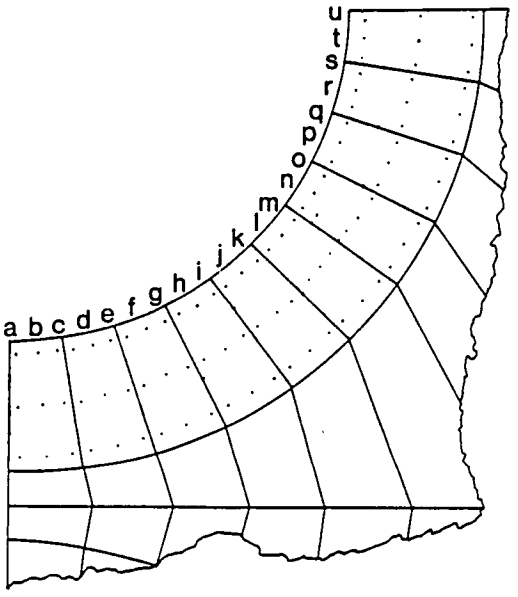

Fig. 3.4 Hole Boundary Nodal Locations.

As mentioned earlier, in order to develop the stiffness matrices for the elements, the finite-element program required the components of the extensional stiffness array, A_{ij}. In classical lamination theory the extensional stiffness array is a part of a larger array which relates the laminate midplane strains and curvatures to the applied inplane and bending loads. In the case where a symmetric laminate is used, and no bending loads exist, the extensional stiffness matrix is the only important component in the entire stiffness matrix. This reduces the relationship between strain and applied load. The relationship is of the form

$$\begin{Bmatrix} N_x \\ N_y \\ N_{xy} \end{Bmatrix} = \begin{bmatrix} A_{11} & A_{12} & A_{16} \\ A_{12} & A_{22} & A_{26} \\ A_{16} & A_{16} & A_{66} \end{bmatrix} \begin{Bmatrix} \varepsilon_x^{\,o} \\ \varepsilon_y^{\,o} \\ \gamma_{xy}^{\,o} \end{Bmatrix} \qquad (3.7)$$

The quantities N_x, N_y, and N_{xy} are the loads per unit width. N_x and N_y are extensional loads and N_{xy} is the shear load. By dividing the N's by the plate thickness, H, the average inplane laminate stresses are obtained. The strain vector consists of the inplane strains $\varepsilon_x^{\,o}$, $\varepsilon_y^{\,o}$, and $\gamma_{xy}^{\,o}$. These strains are referred to the global laminate coordinate system. The finite-element analysis uses the nodal forces at the hole elements, written in terms of N_x, N_y, and N_{xy},

and the boundary conditions to compute the displacement of each point in the plate. Using the strain-displacement relations, the strains at each point in the plate are computed. A post-processor for the finite-element program was written to linearly interpolate the strains from the Gauss points to the points of interest within the plate. Once the laminate strains at the desired locations were determined, the post-processor then transformed these global laminate strains into lamina strains in the lamina coordinate system. This transformation is given by Jones [29]

$$\begin{Bmatrix} \varepsilon_1 \\ \varepsilon_2 \\ \gamma_{12} \end{Bmatrix} = \begin{bmatrix} \cos^2\theta & \sin^2\theta & \sin\theta\cos\theta \\ \sin^2\theta & \cos^2\theta & -\sin\theta\cos\theta \\ -2\sin\theta\cos\theta & 2\sin\theta\cos\theta & \cos^2\theta-\sin^2\theta \end{bmatrix} \begin{Bmatrix} \varepsilon_x^{\,o} \\ \varepsilon_y^{\,o} \\ \gamma_{xy}^{\,o} \end{Bmatrix} \quad (3.8)$$

The strains ε_1 and ε_2 are the elongation strains parallel to the fibers and perpendicular to the fibers, respectively, and γ_{12} is the engineering shear strain in the plane of the lamina. The angle θ is measured positive from the global x-axis counterclockwise to the 1-axis of the lamina.

Once the strains are determined for each lamina, the reduced stiffness matrix, Q_{ij}, for the lamina is used to compute lamina stresses in the lamina coordinate system.

The reduced stiffness matrix is a function of material constants E_1, E_2, G_{12}, and ν_{12}. The relation between lamina stresses and strains in the principal material coordinate system is

$$\begin{Bmatrix} \sigma_1 \\ \sigma_2 \\ \tau_{12} \end{Bmatrix} = \begin{bmatrix} Q_{11} & Q_{12} & 0 \\ Q_{12} & Q_{22} & 0 \\ 0 & 0 & Q_{66} \end{bmatrix} \begin{Bmatrix} \varepsilon_1^{\,o} \\ \varepsilon_2^{\,o} \\ \gamma_{12}^{\,o} \end{Bmatrix} \tag{3.9}$$

The stress σ_1 is the normal stress in the lamina in the fiber direction, σ_2 is the normal stress perpendicular to the fibers, and τ_{12} is the shear stress in the plane of the lamina. The Q_{ij} are defined by,

$$\begin{aligned} Q_{11} &= E_1/(1-\nu_{12}\nu_{21}) & Q_{12} &= \nu_{21}Q_{11} \\ Q_{22} &= E_2/(1-\nu_{12}\nu_{21}) & Q_{66} &= G_{12} \end{aligned} \tag{3.10}$$

In order to determine the failure load of a joint, failure of the laminate must be defined. The application of a material failure criterion is often used for this purpose. This study will utilize the Yamada-Sun failure criterion [27].

The Yamada-Sun criterion takes the form

$$\left(\frac{\sigma_1}{X}\right)^2 + \left(\frac{\tau_{12}}{S_{0/90}}\right)^2 = F^2 \qquad (3.11)$$

Failure is predicted to occur when F=1. The quantity X is the ultimate strength of a unidirectional laminate loaded in the fiber direction. The quantity X can have two values, depending on the sign of σ_1. The quantity $S_{0/90}$ is the shear strength of a cross-ply laminate. This value is usually two to three times larger than the shear strength of an individual lamina. This laminate strength value is thought to more closely represent the shear strength of a lamina when it is a part of a laminate. The strength of a lamina within a laminate is referred to as in-situ strength. Generally in-situ strength is higher than the strength of a single lamina. The Yamada-Sun criteria is applied on a lamina level. Since the stresses are not uniform through the thickness in a laminate, each lamina has to be evaluated for failure.

The criterion given in Eqn. 3.11 uses the values of σ_1 and τ_{12} but assumes the value of σ_2 is not important. This assumption is based on the observation that prior to laminate failure, each lamina contains many matrix cracks. With the existence of these cracks, the lateral stiffness, E_2, drops dramatically. This in turn reduces the capacity

to transmit load in this direction. The shear stress, however, and its relation to the failure stress is still considered important. Appendix A discusses this issue. However, it is premature to turn to that appendix at this point. The reader will be referred to that appendix at the appropriate time.

Chang [30] utilized this criterion in his study of single and double-hole bolted joints. In addition, he extended Whitney-Nuismer's characteristic distance concept to a continuous locus around a hole. The equation for this locus was given by Chang, et al to be

$$r(\theta) = D/2 + R_t + (R_c - R_t)\cos(\theta) \qquad (3.12)$$

This function, which varies cosinusoidally, defines a locus of points where the failure criteria is applied. The locus is the same for each lamina. Here D is the diameter of the hole around which the failure criteria is applied. R_t and R_c are experimentally derived constants which are a function of the material properties. A physical interpretation of R_t and R_c are shown on Fig. 3.5. Table 3.2 presents numerical values of R_t and R_c used here. Other material properties used in the present study are also presented in this table. The function $r(\theta)$ then is a cosinusoidal fit between these two constants, spanning the region from the bearing area to the net-tension area. One

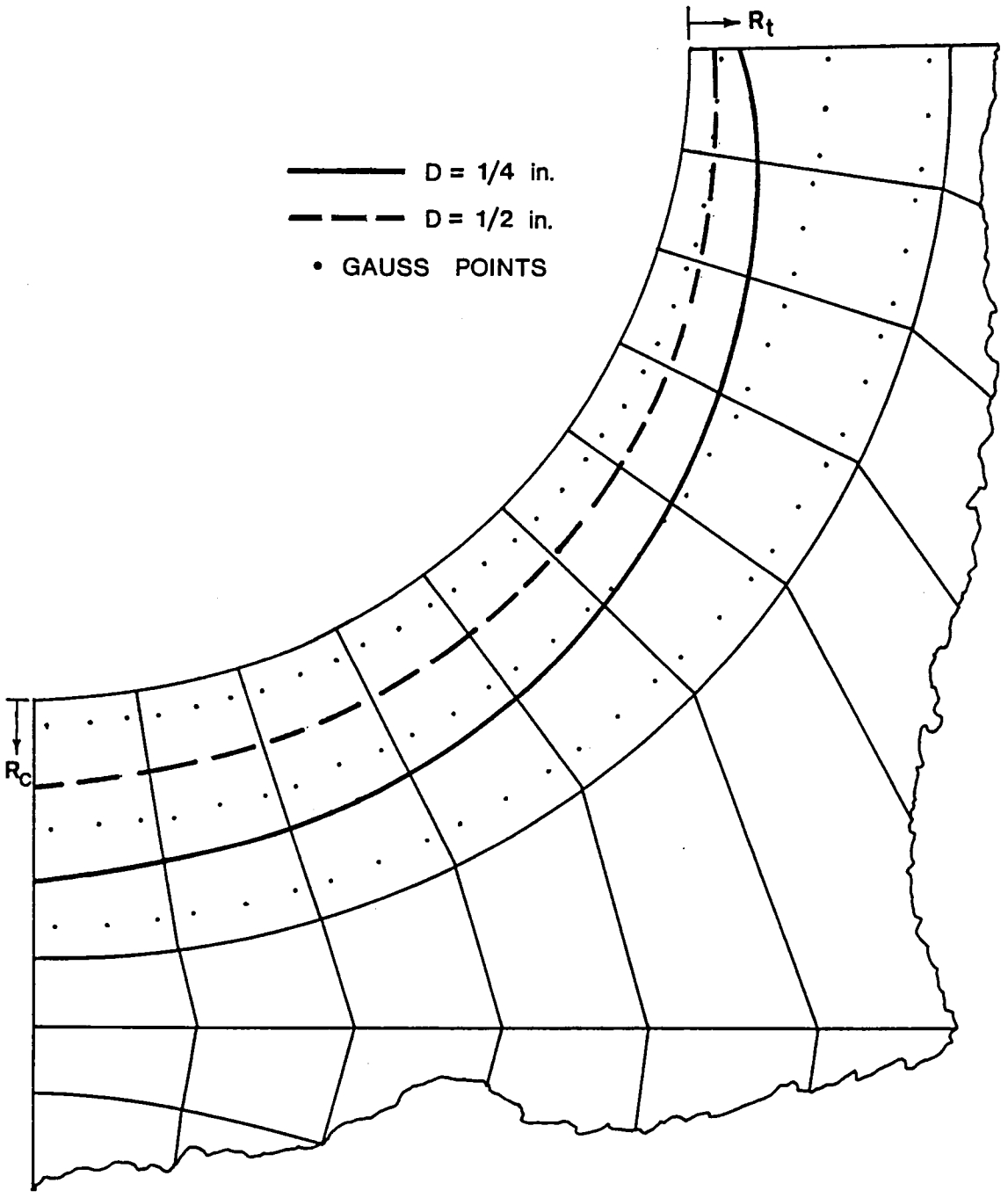

Fig. 3.5 Characteristic Curve Locations.

Table 3.2 Material Properties

R_t	= 0.018 in.
R_c	= 0.070 in.
E_1	= 21300000 psi
E_2	= 1700000 psi
G_{12}	= 897000 psi
ν_{12}	= 0.30
X_t	= 251000 psi
X_c	= 200000 psi
$S_{0/90}$	= 19400 psi

benefit in this procedure is that the stresses which are substituted into the Yamada-Sun criterion are stresses which are in the interior of the plate. Stress values on the hole edge are not required. This eliminates many problems. First, the extrapolation of stress values from a Gauss point to the hole edge is not required. Second, at the hole edge region there is a three-dimensional state of stress involving interlaminar normal and shear stresses, in addition to the inplane stresses. These additional stresses can have a large influence on the localized failure of the plate at the hole edge. With the criterion being applied away from the hole edge, not modelling those interlaminar stresses in the plane stress analysis was not a problem.

Another advantage to the characteristic curve approach is that the hole size effect is accounted for. This well observed phenomena indicates that for two identical single-hole plates with the same value of W/D, the plate with the smaller diameter hole will have a higher ultimate strength. This hole size effect is accounted for by including the diameter in the expression for the characteristic curve equation. For large holes, the diameter term dominates the equation and the locus is closer to the hole edge. With the characteristic curve close to the hole edge, the stresses on the locus are higher, so the failure criteria is met at a lower overall load level than when small diameter holes are

considered. Also with the diameter term dominating the expression, the dependence of the characteristic curve on angular location is minimal. Fig. 3.5 shows the location of the characteristic curve for the two hole sizes considered in this study, namely 1/4 in. diameter holes and 1/2 in. diameter holes.

When the Yamada-Sun criterion is evaluated along the characteristic curve, there is a load level, a point, and a lamina where F = 1. According to Chang et al, the angular location of F = 1 defines the mode of failure. Normally there are three different failure modes which occur in a pin-loaded plate. These modes are called net-tension failure, bearing failure, and shear-out failure. A net-tension failure causes separation of the plate near the net-section. A bearing type failure mode is defined to occur when material crushing occurs beneath the bolt. Shear-out failure occurs when separation or tearing occurs near the line which extends from the hole edge at the net-section area toward the free edge of the plate. This line is commonly called the shear-out plane and is depicted in Fig. 3.6. The bounds on angular location associated with the three failure modes are shown in Table 3.3.

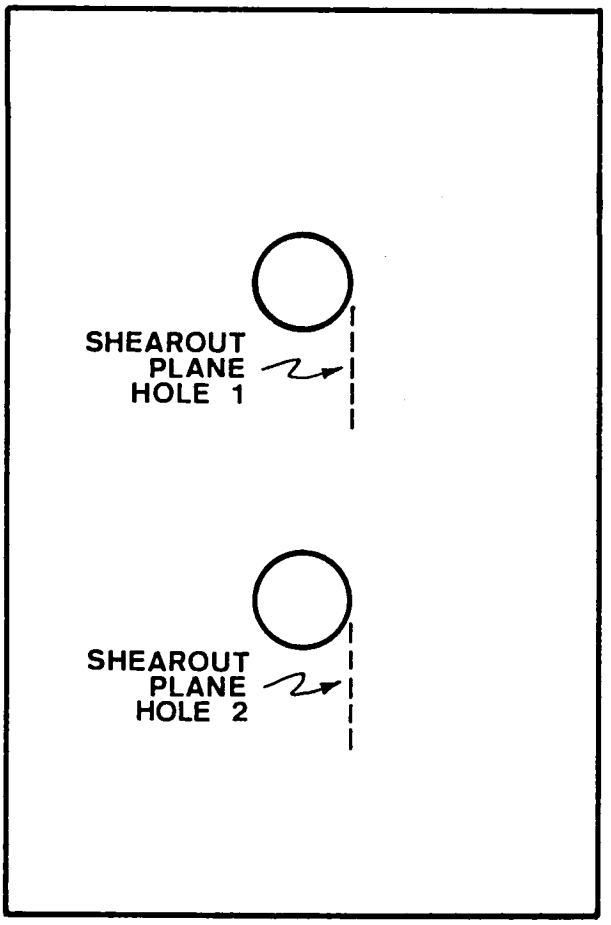

Fig. 3.6 Location of Shearout Planes.

Table 3.3 Definition of a Failure Mode

Mode of Failure	Angular Position, θ^* (degrees)
Net-Tension	75 - 90
Shearout	30 - 60
Bearing	0 - 15

* see Fig. 3.1 for definition of θ.

CHAPTER 4

COMPARISON WITH PAST WORK

In order to judge the ability of the finite-element analysis to predict the stresses for this problem, and to gain insight in the character of the stress state for various laminates, the stresses predicted by the present analysis were compared to the stress predictions in work by other researchers.

Figs. 4.1-4.3 shows Crews' calculations and the calculations of the present study for the radial and circumferential stresses around the hole, and the shear-out stresses in three pin-loaded laminates. The stresses have been normalized by the average bearing stress, S_b. The average bearing stress, which is often used as a normalization factor, is defined as

$$S_b = P / D*H \qquad (4.1)$$

where as described previously, P is the total load acting on the hole, D is the hole diameter, and H is the laminate thickness. Results from Crews are shown in Fig. 4.1 for a quasi-isotropic laminate with width-to-diameter ratios, W/D, of 3 and infinity. The distance from the center of the hole to the end of the joint, E/D, was 10. Here a value of 3 was used. The results are shown by dashed and solid lines, respectively, in the figure. The stresses computed in the

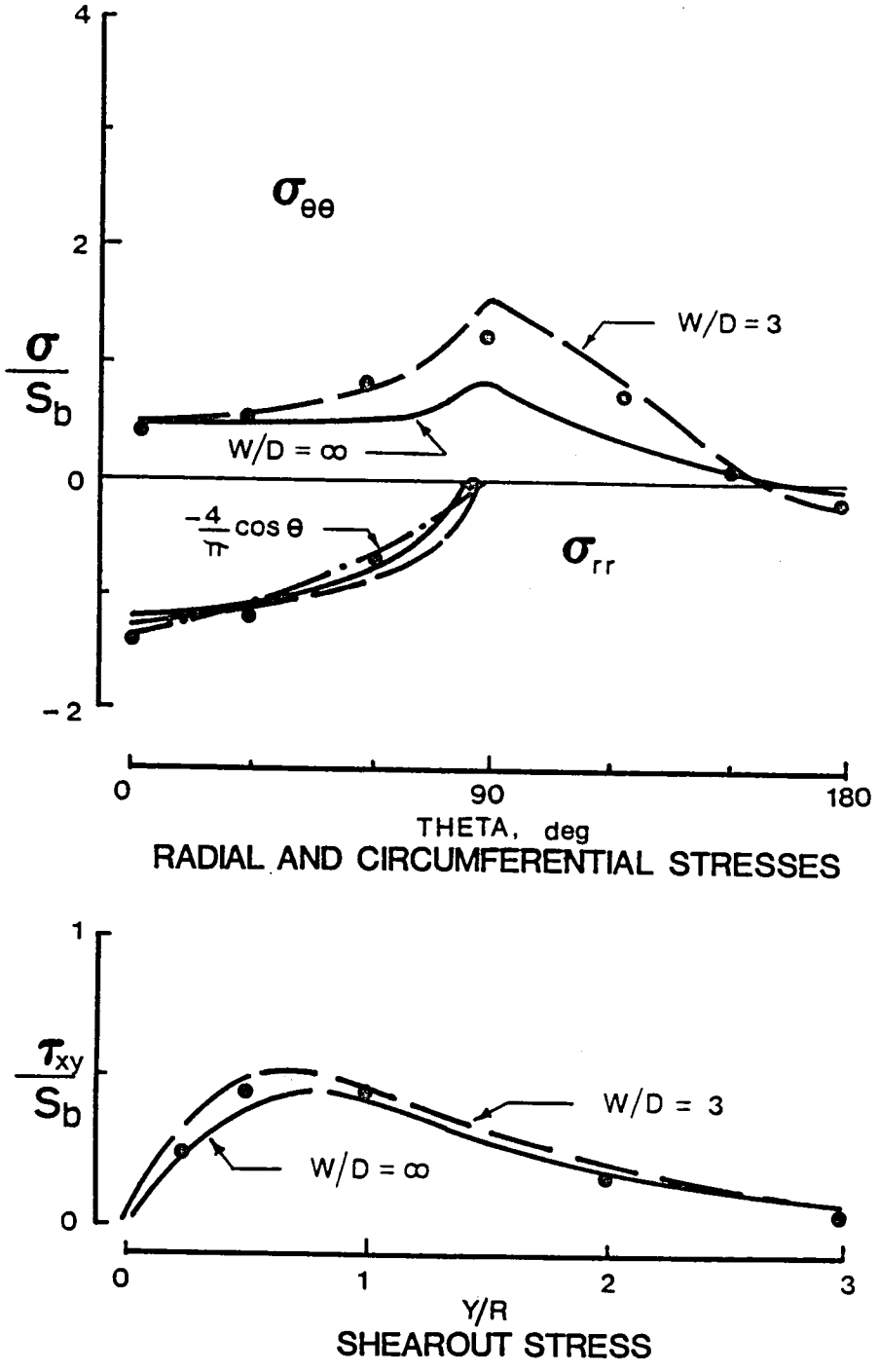

Fig. 4.1 Stresses in a Single-Hole Quasi-Isotropic Laminate.

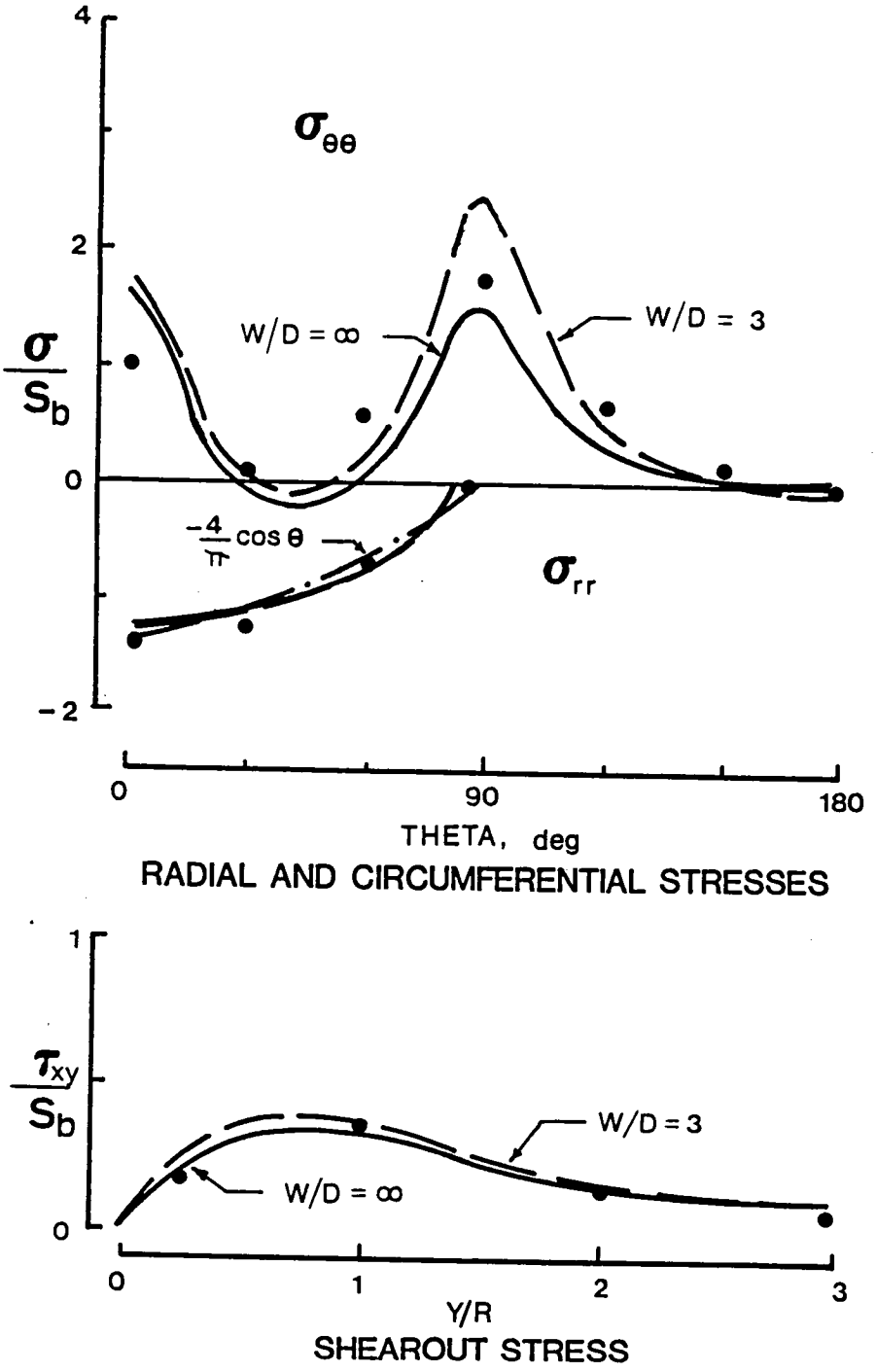

Fig. 4.2 Stresses in a Single-Hole Cross-Ply Laminate.

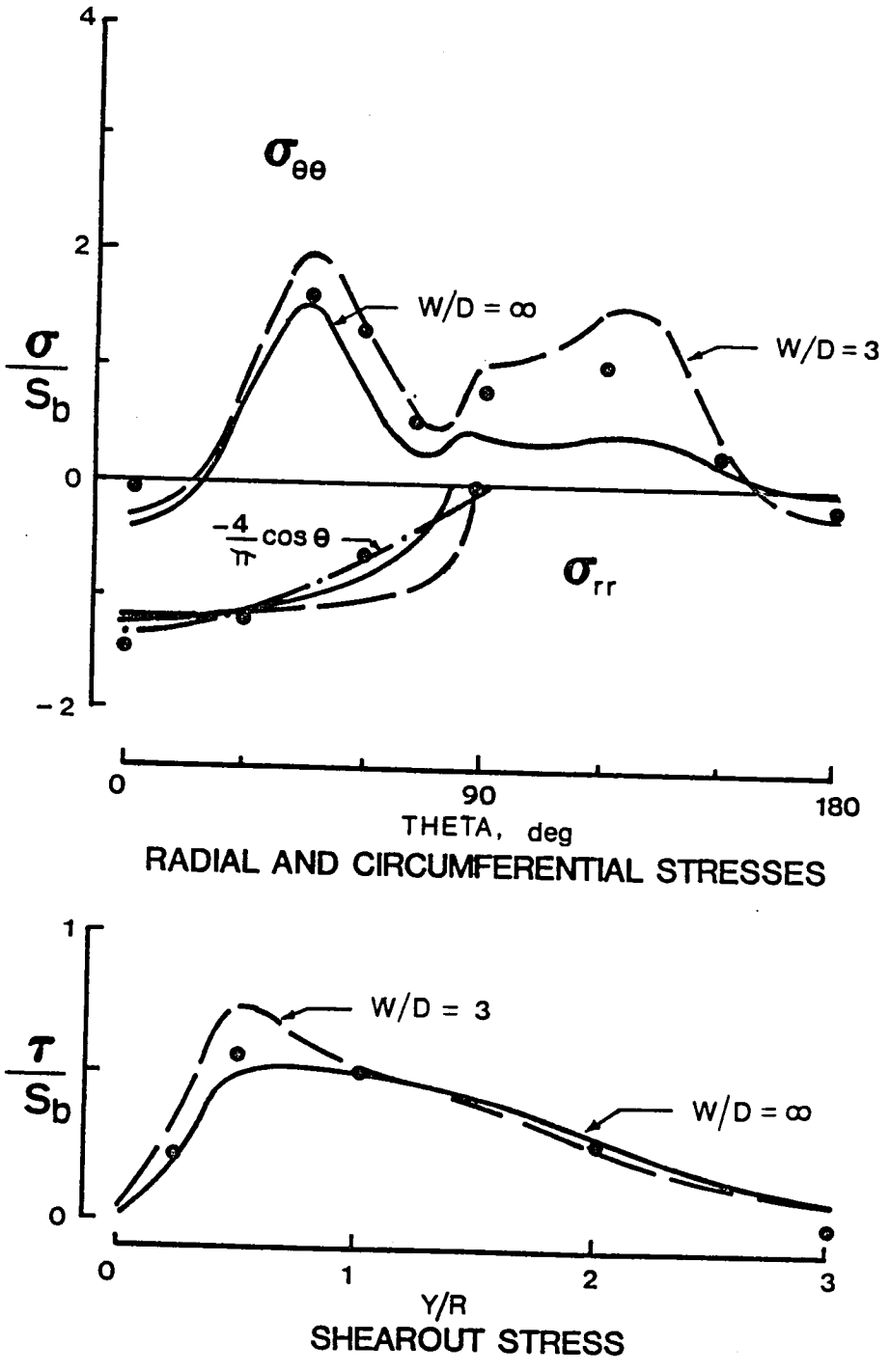

Fig. 4.3 Stresses in a Single-Hole Angle-Ply Laminate.

present study are shown by solid dots. For the present study, W/D was 5. As can be seen, the comparison between the present study and Crews' results is quite good. The equation for cosinusoidal radial stress distribution is shown on the figure. The comparison for the radial stresses should be very good since these values are essentially used for input to the analysis. Differences that do arise are due to the fact that in the finite-element analysis the stresses are computed at the Gauss points while the input stresses are applied at the nodes. Spatially, these are different points.

There is similar good agreement for the shear-out stress calculations. Again, Crews' results are given for W/D of 3 and infinity. The solid dots are from the present study for W/D of 5. At a value of Y/R equal to three, which is a distance of three radii from the hole centerline towards the bottom edge of the plate, the current finite-element results predict a somewhat lower shearout stress. This is due to the fact that the element mesh for the plate was generated for a smaller edge distance, E/D, than Crews used in his investigations. This causes the shearout stresses to diminish quicker than Crews' predicted values.

Fig. 4.2 shows these same results for a cross-ply laminate. There is a slightly higher variance between the current predictions and those of Crews. This is primarily

caused by the higher stress gradients that are typical in this type of laminate. This in turn means a greater difference in the values of stress at Gauss points and at the hole edge. However, there is a fair agreement between both the circumferential and radial stresses. The shearout stresses, which should be in better agreement, are quite close. Again, as the bottom edge of the plate is approached, the current prediction of shearout stress drops off a bit faster due to a shorter edge distance.

The results for a 45 degree angle-ply laminate are illustrated in Fig. 4.3. Again, there are some discrepancies between current and past predicted circumferential stresses. The radial stress distribution is slightly different. This is expected, since the current model uses a cosinusoidal distribution to model the the contact stresses between the bolt and the hole edge. Crews used displacement boundary conditions. This results in a slightly different distribution for some laminates. The shearout stresses compare quite well. The only major deviation occurs towards the plate bottom.

These results confirmed the validity of the current finite-element model and the degree of refinement of the mesh. Two different mesh densities were used in this study to model the single-hole problem. It was found that the lower density mesh gave answers which agreed quite well with

the higher density mesh. The less dense mesh was subsequently used in modelling.

Further comparisons were made for a single-hole joint by using the work of Chang [30]. The comparisons were made for three laminates used in that work: a quasi-isotropic $[(0/+45/-45/90)_3]s$; a cross-ply $[(0/90)_6]_s$; and an angle-ply $[(+45/-45)_6]_s$. However, Chang did not report stress distributions. Chang reported on failure loads using the Yamada-Sun - characteristic curve criterion. Hence comparison with Chang's work afforded a change to check the implementation of the failure criteria. Chang reported joint strengths normalized with respect to bearing stress.

Fig. 4.4 shows the comparison between Chang's work and the present study. The solid curves in Fig. 4.4 represent the finite-element failure predictions of Chang. The solid dots indicate the present study's prediction for selected situations. The letters accompanying the dots refer to the present study's predicted mode of failure. In some cases this can be a combined mode. The symbols are experimental data that Chang measured as a part of that study. The variation of normalized joint strength vs. hole diameter is shown. The increase of strength with decreasing hole diameter is well represented in Chang's calculations and in the calculations of the present study. The upper curve in

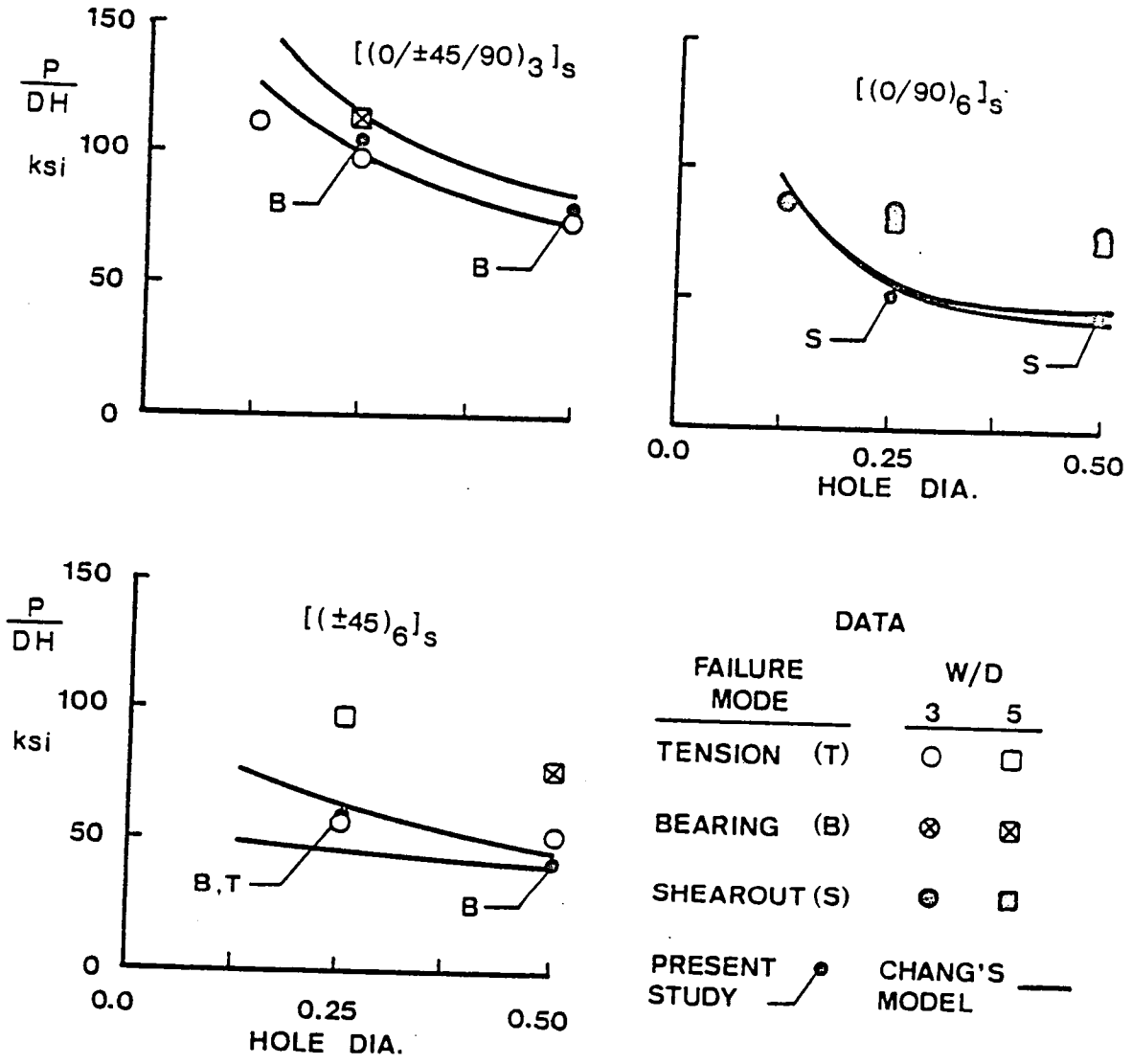

Fig. 4.4 Comparison with Chang's Single-Hole Results.

each figure corresponds to a W/D of 5 while the lower curve represents a W/D of 3. The solid dots from the present study were determined for a W/D of 5.

Considering the quasi-isotropic case, the agreement between Chang's model and the present model is quite good. Agreement of the present model with the strengths determined experimentally by Chang is also quite good. The failure mode prediction by both Chang's and the present study's results are the same and concur with the experimental data. Experimentally, for the W/D ratio of 5, this mode is bearing. For the narrower plate, W/D of 3, the mode switches to net-tension mode.

Good agreement is also found between the two models for the angle-ply case. However, the experimental work shows a higher joint strength than predicted. The mode of failure is predicted quite well however, and in some cases, the present study is more accurate in this mode prediction than is Chang's. For W/D = 5, the mode of failure for the 1/2 in. diameter hole is predicted by the present study to be bearing. The data also indicates this type of failure mode, i.e. a square with a cross in it. Chang's analysis predicted a tensile failure for this case. When the hole diameter is reduced to 1/4 in., the experimentally determined mode changes to net-tension (open square). The present study predicts a mixture of bearing failure and

tension failure while Chang's analysis predicts tension.

For the cross-ply laminate, predictions by Chang and the predictions of the present study are quite close. Chang shows there is not much sensitivity to W/D. The data shows a higher joint strength when compared to both finite-element predictions. The mode of failure is predicted to be shearout by both the present study and Chang's model, and his experiments show this to be true.

Similar to the single-hole figure, the solid lines in Fig. 4.5 represent finite-element results obtained by Chang for a two-hole joint. The solid dots and their accompanying letters indicate the numerical results of the present study. The other symbols are experimental data gathered by Chang.

Considering the quasi-isotropic case, the predictions by Chang and the present study agree quite well. The correlation of the predicted joint strength with the data by the present study is slightly better when compared to Chang's finite-element predictions. The failure mode is accurately predicted by both models to be tension.

The angle-ply case shows a moderate discrepancy between Chang's finite-element predictions and the present study's predictions of ultimate joint capacity. The present study's strength predictions are closer to the experimental data than Chang's predictions. Again, the mode of failure is accurately predicted by both finite-element models to be

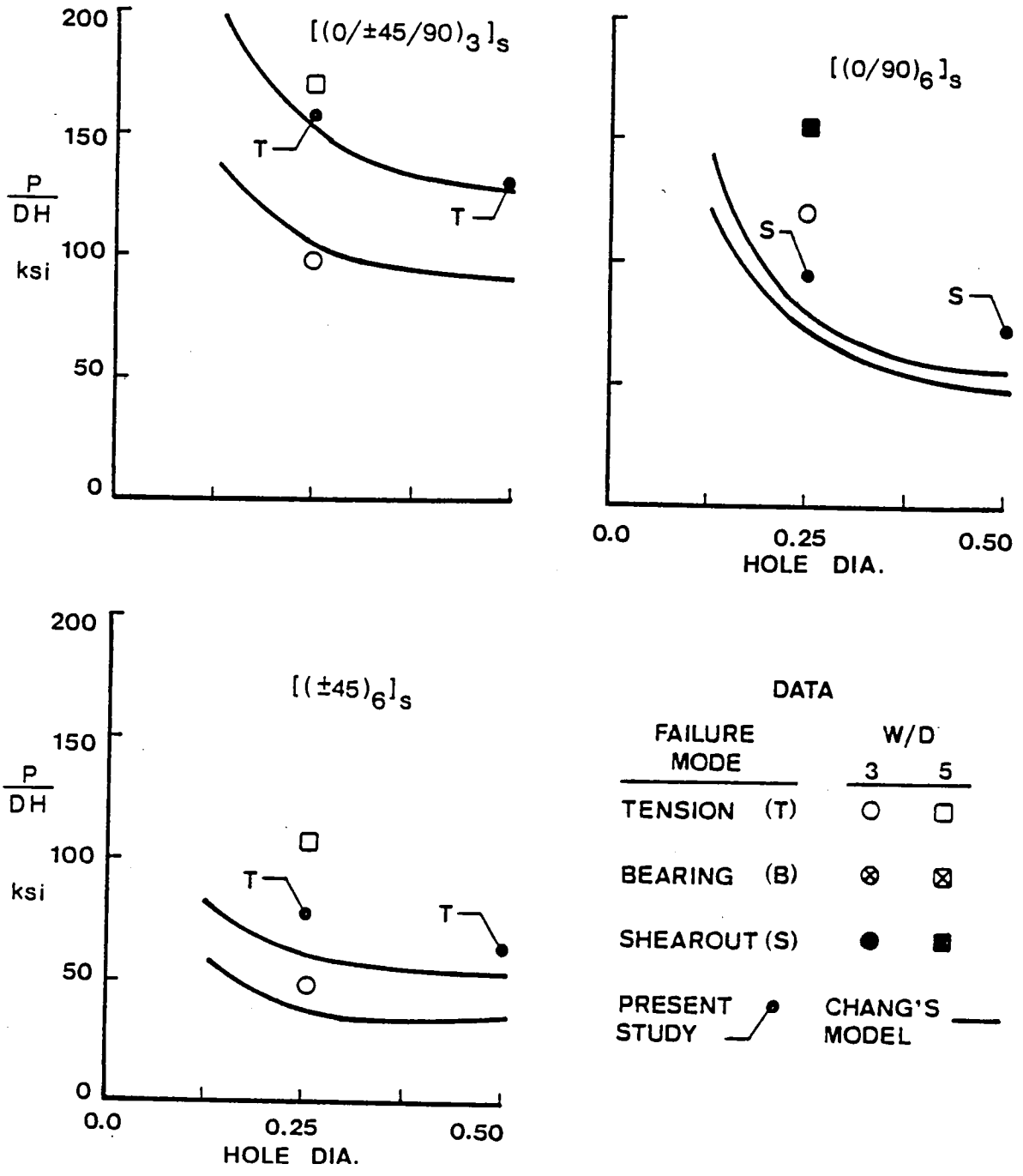

Fig. 4.5 Comparison with Chang's Double-Hole Results.

net-section tension.

The cross-ply case shows trends similar to the angle-ply case. The present study's strength predictions are closer to the experimental data than Chang's predictions. For the W/D = 5 curve, both models predict a shearout failure mode and this correlates with the data. For the W/D = 3 curve, the present study predicts a tension and this also matches the experimental results. Chang's analysis predicts a shearout mode for this case also.

The comparison with Chang's two-hole studies indicate that the present study's predictions are close to the experimental values and the modes of failure are accurately predicted for all cases. This correlation enabled the current study to be expanded to variations in geometry and load ratios with confidence in the ability to predict results.

CHAPTER 5

STRESS CALCULATIONS FOR TWO-HOLE JOINTS

Many of previous reports concerning single hole plates have presented details of the predicted stress distribution at the hole edge, at the net-section, along the shear-out line, and at other locations. No such information has been presented for plates with two loaded holes. This chapter will present the results of stress analysis of a plate with two holes. This information fills a gap in the present literatures where no comprehensive results for the two-hole case exists.

A typical two hole joint geometry was chosen for this task. A width-to-diameter ratio of 5, an edge-distance to bolt-diameter ratio, E/D, of 3, and a bolt-pitch to bolt-diameter ratio , G/D, of 3 were chosen to represent a standard joint. The bolt pitch refers to the spacing between subsequent bolt holes in a joint (refer to fig 3.1). In addition, a hole diameter of 1/2 in. was also chosen. Results for the quasi-isotropic, angle-ply, and cross-ply laminates are presented. It is assumed that each hole reacts 50% of the total applied load.

CROSS-SECTION STRESSES

The stress distribution along four specific loci on the plate are presented. These loci include: the net-section at

both hole locations; both hole edges; the vertical centerline of the plate; and the horizontal mid-section of the plate. The mid-section is the line which is equidistant between both holes. These sections are highlighted in Fig. 5.1. In addition, stress contours are presented for all three inplane components of stress.

Figs. 5.2-5.4 show the net-section stresses at both holes for the three laminates. These stresses are normalized with respect to the gross, or far-field, stress. The gross stress is defined as

$$\sigma_{y_{gross}} = P/W*H \qquad (5.1)$$

The quasi-isotropic case in Fig. 5.2 shows the top hole σ_y stress increasing from a value less than 1.0 at the edge of the plate to about 4.0 at the innermost Gauss point. The bottom hole stress is somewhat lower, reaching a value of 2.25. The difference in net-section stress magnitudes between the upper and lower holes is a graphic illustration of stress field superposition. The upper hole has stresses due to the pin reaction, and stresses occurring due to the load being passed to the lower hole. This phenomena causes the longitudinal tensile stresses at the top hole to be higher than the corresponding stress at the top hole for all laminate cases, and for all geometries. Only when the 50-50 load ratio is changed does this difference disappear.

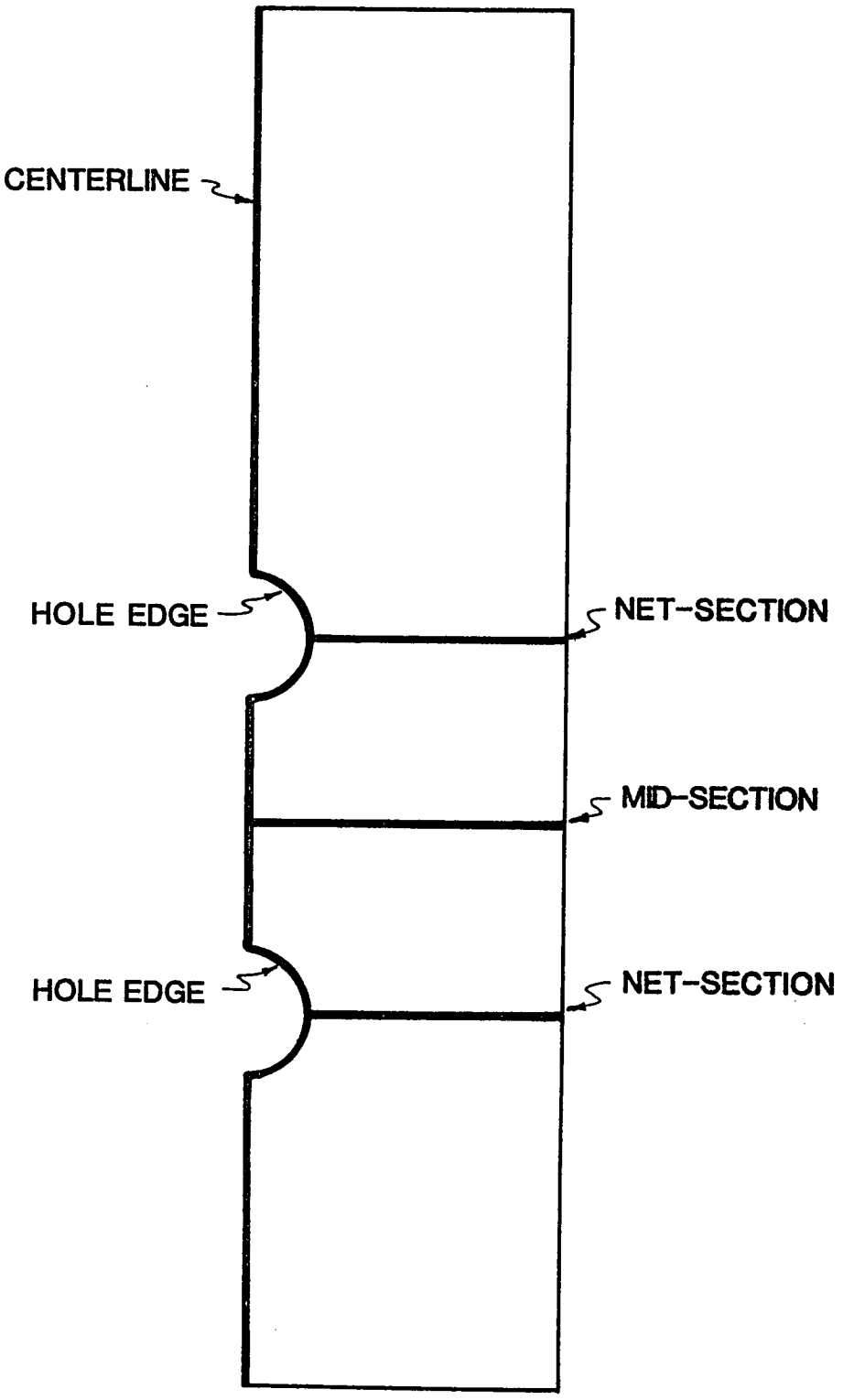

Fig. 5.1 Stress Presentation Sections.

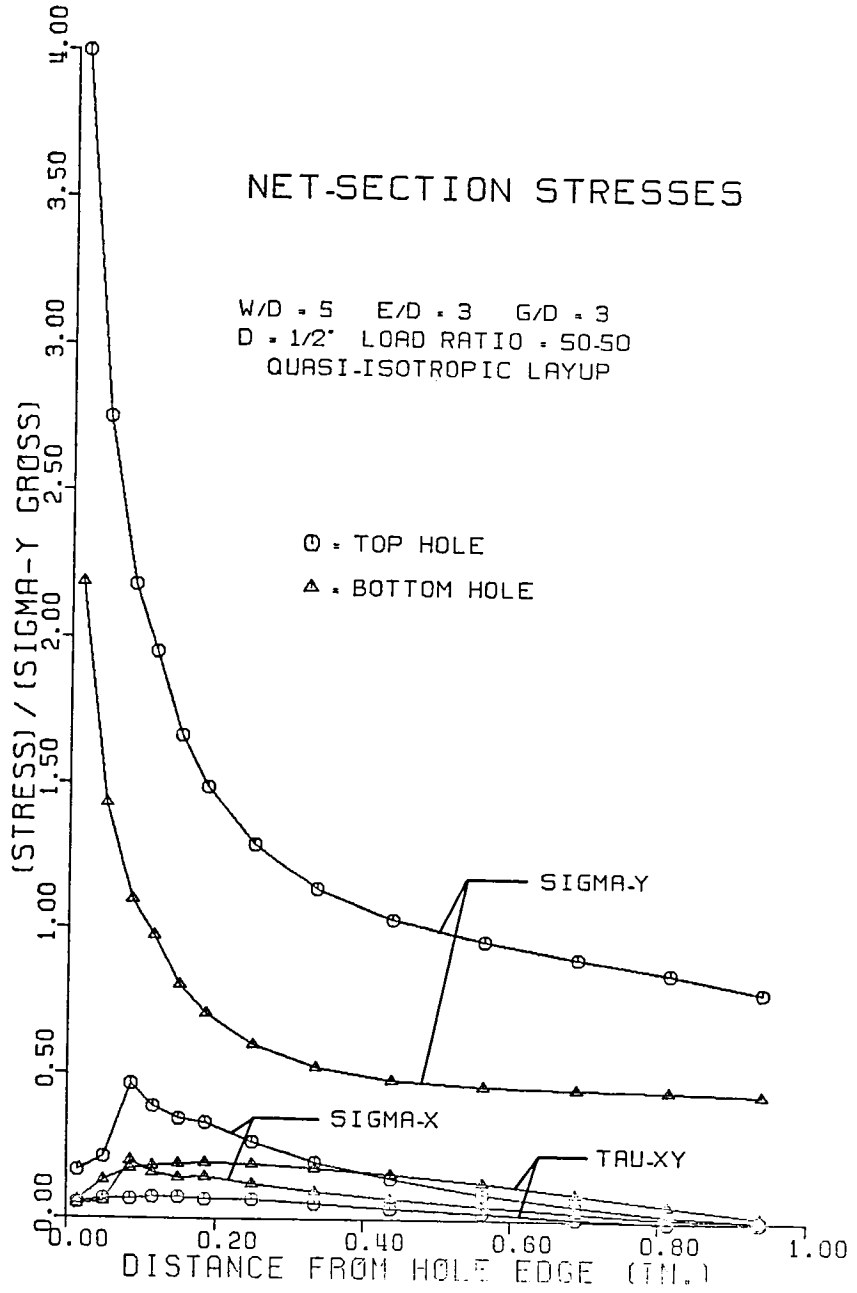

Fig. 5.2 Net-Section Stresses for a Quasi-Isotropic Laminate.

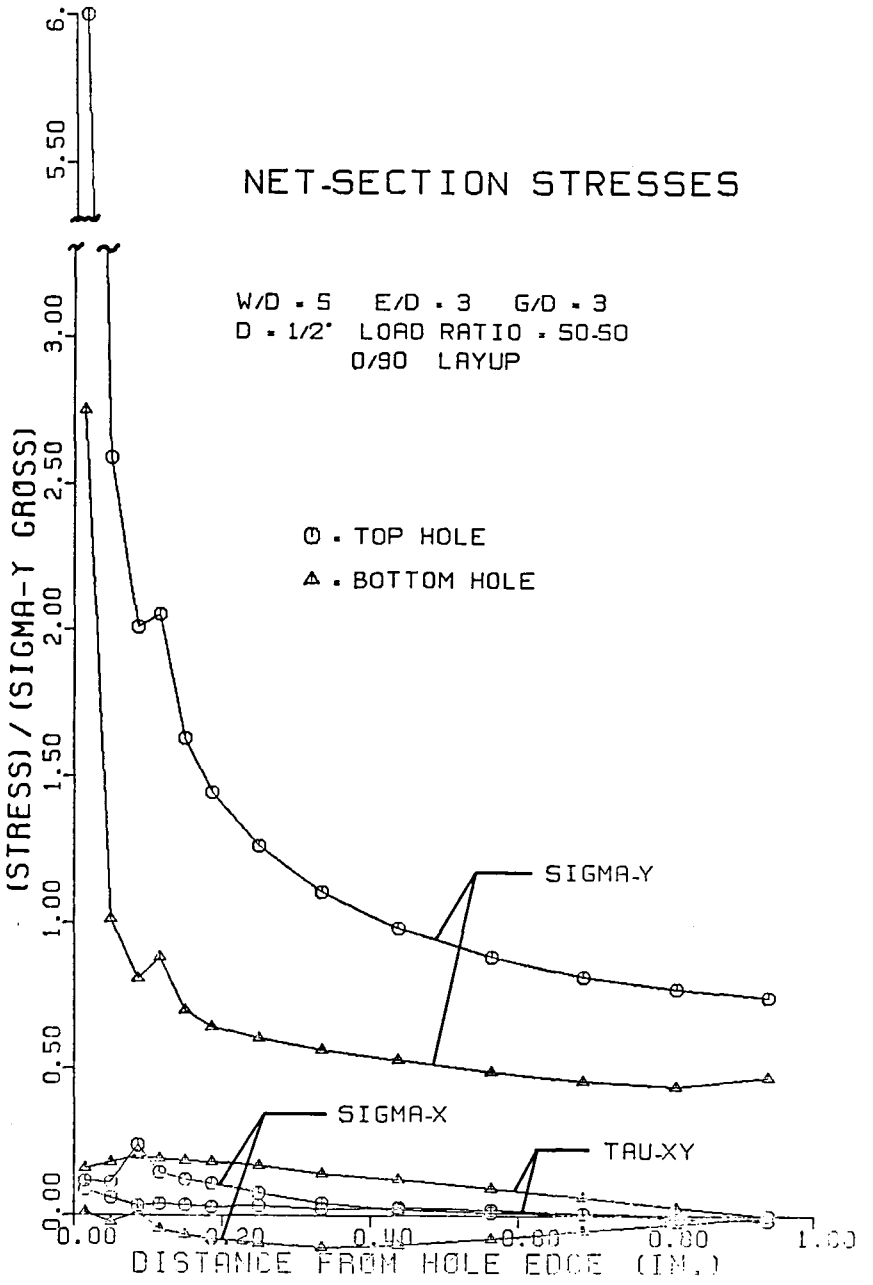

Fig. 5.3 Net-Section Stresses for a Cross-Ply Laminate.

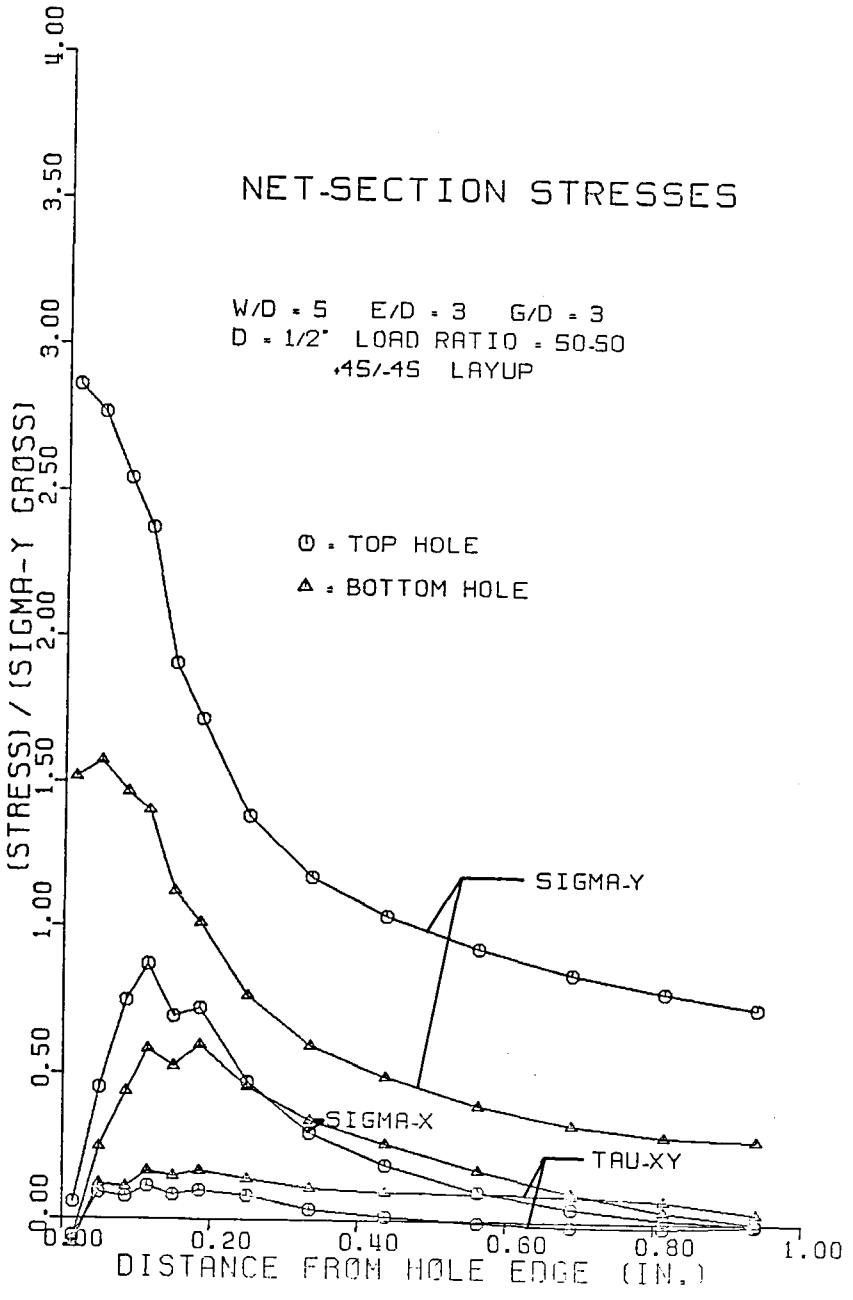

Fig. 5.4 Net-Section Stresses for an Angle-Ply Laminate.

The σ_x and τ_{xy} stresses at these sections are quite small when compared to the σ_y stresses. Again, at the top hole σ_x stress is higher than at the bottom hole. At both holes the σ_x stress has a small peak prior to decreasing as the hole edge is approached. This peak is due to a Poisson contraction effect. The shear stress is higher at the bottom hole than at the top hole. The higher shear stress at the lower hole is caused by the proximity of the bottom hole net-section to the free edge of the plate. The magnitudes of the shear and transverse tensile stresses are of no consequence at the net-section locations.

Fig. 5.3 shows these same stresses for the cross-ply laminate. Due to the higher percentage 0° plys, as compared with the quasi-isotropic case, the σ_y stresses are much higher at the hole edge. At the top hole the tensile stress has a maximum value of about 6.0 while the peak tensile stress at the bottom hole is about 2.75. The other inplane stresses are much smaller, and are for the most part insignificant in causing failure.

Fig. 5.4 shows the stresses for an angle-ply laminate. One interesting point illustrated here is the absence of any steep asymptotic behavior of the σ_y stresses near the hole edges. Of the three laminates considered, the tensile stresses for this laminate are the lowest. On the other hand, the σ_x stresses are much higher than in the other two

laminates. The peak σ_x stress occurs a small distance from the hole edge. Note here that once again the top hole stresses are, for the most part, greater in magnitude than those at the lower hole. The shear stresses are relatively small compared to the other in-plane stresses.

Stresses at the midsection of the plate are shown in Figs. 5.5-5.7. Fig. 5.5 illustrates the results for the quasi-isotropic case. All three components of inplane stresses are shown. Near the centerline of the plate the σ_y stress is negative. This is interesting in light of the fact that, overall, the plate must transmit tension at the midsection. This effect is due to the compressive stresses caused by the pin-plate interaction at the bottom of the top hole, just above the midsection. As the spatial coordinate approaches the free edge of the plate, the σ_y stress approaches the gross stress value. The σ_x stress shows opposite behavior. This is due to Poisson contraction effects. Near the plate centerline, the σ_x stress is positive, goes negative, and then drops to zero at the free edge of the plate. The shear stress starts at zero at the centerline becomes positive, and then quickly approaches zero as the outer edge of the plate is approached.

Fig. 5.6 shows the mid-section stresses for a cross-ply laminate. Due to the nature of this laminate, the gradients of the σ_y stress near the centerline are much higher than

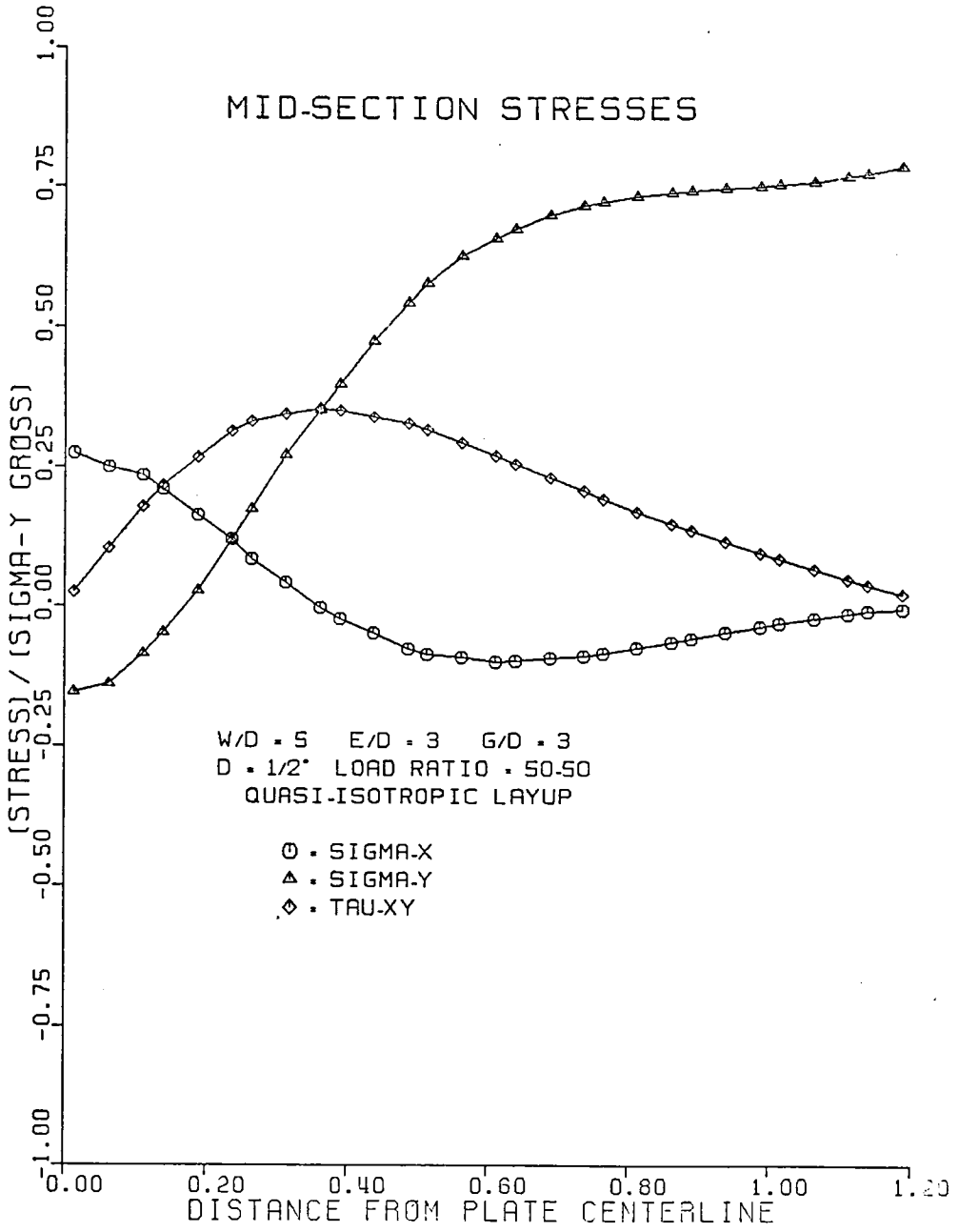

Fig. 5.5 Mid-Section Stresses in a Quasi-Isotropic Laminate.

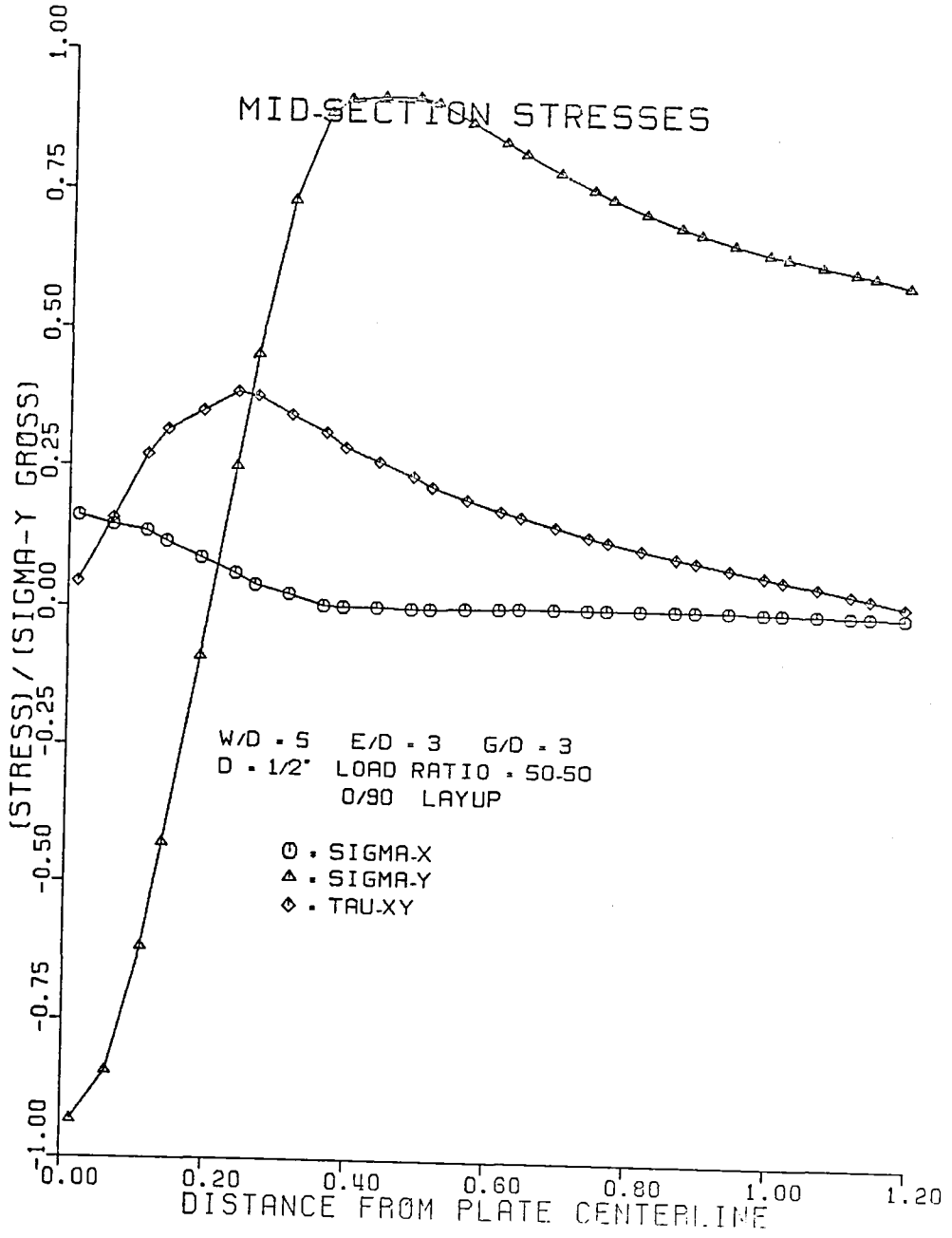

Fig. 5.6 Mid-Section Stresses in a Cross-Ply Laminate.

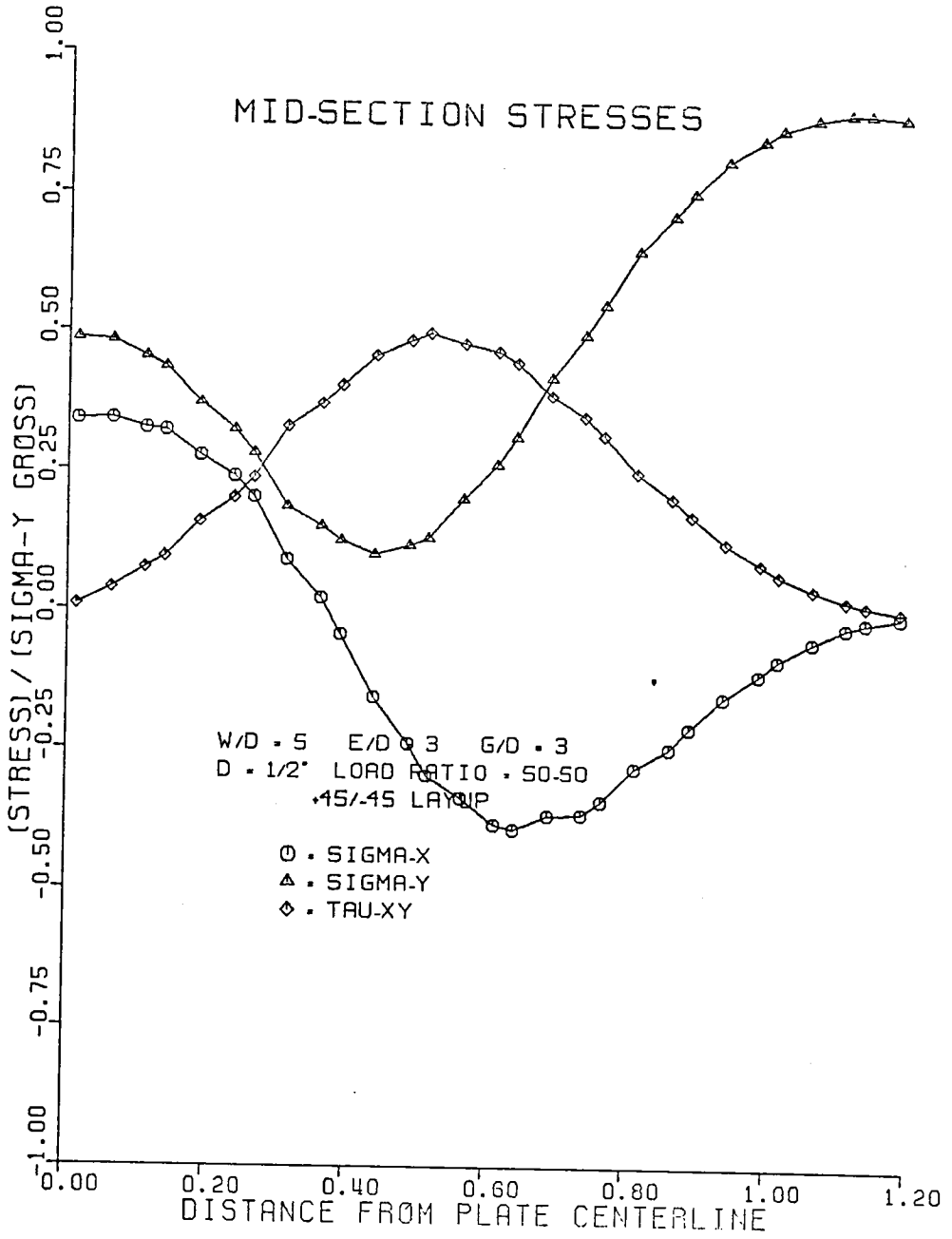

Fig. 5.7 Mid-Section Stresses in an Angle-Ply Laminate.

for the other two laminates. Near the plate centerline the σ_y stress is compressive, much more so than for the quasi-isotropic case. This is caused by the higher percentage of fibers in the direction of load application. For the cross-ply case, as one moves away from the centerline, the σ_y stress changes drastically to a positive value of 1.0. The value then decreases as the free edge of the plate is approached. The σ_x stress starts postive, starting smaller at the centerline than in the quasi-isotropic laminate, and dropping to zero rather quickly. The shear stress reaches a maximum about 20% of the half plate width from the centerline, then gradually decreases to zero at the free edge of the plate.

Fig. 5.7 shows the three mid-section stresses for the angle-ply case. Here the σ_y stress is always positive and shows a minimum at a point about 40% of the way towards the free edge. Further from the centerline the stress increases to a value approximately equal to the gross field stress value. The σ_x stress also varies considerably. It reaches maximum compressive value about 60% of the way towards the free edge of the plate. After the maximum compression is reached, the σ_x stress approaches zero toward the free edge. The shear stress shows a maximum value at about halfway between the centerline and the free edge. This maximum value of stress decreases to zero as the free edge and the

centerline are approached.

Figs. 5.8-5.10 show the variation of σ_y and σ_x stresses, normalized with respect to the gross σ_y stress, as a function of distance along the plate's vertical centerline. Along the centerline the shear stress is, by symmetry, zero. In the figures, the bottom of the graph represents the bottom free edge of the plate while the top of the graph represents the fixed end of the plate. There are two discontinuities shown in each of the figures. These correspond to the hole locations in the plate.

Fig. 5.8 shows the centerline stress distribution for a quasi-isotropic laminate. Near the top of the plate the σ_y stress is unity, basically, by definition. There is a spatially uniform state of stress until the top of the hole is reached. As the top of the upper hole is approached from above, the σ_y stress decreases to zero. This is expected since the unloaded upper half of each hole is traction free. Directly beneath the top hole the σ_y stress has a high negative value. This is the bearing stress. For this laminate the bearing stress has a value of about -3.0. At a point between the two holes the σ_y stress becomes slightly positive. This change from a compressive value to a tensile value is due to the unloading caused by the bypass stress. For the quasi-isotropic laminate, this unloading effect is quite small. Again, at the top of the bottom hole the σ_y

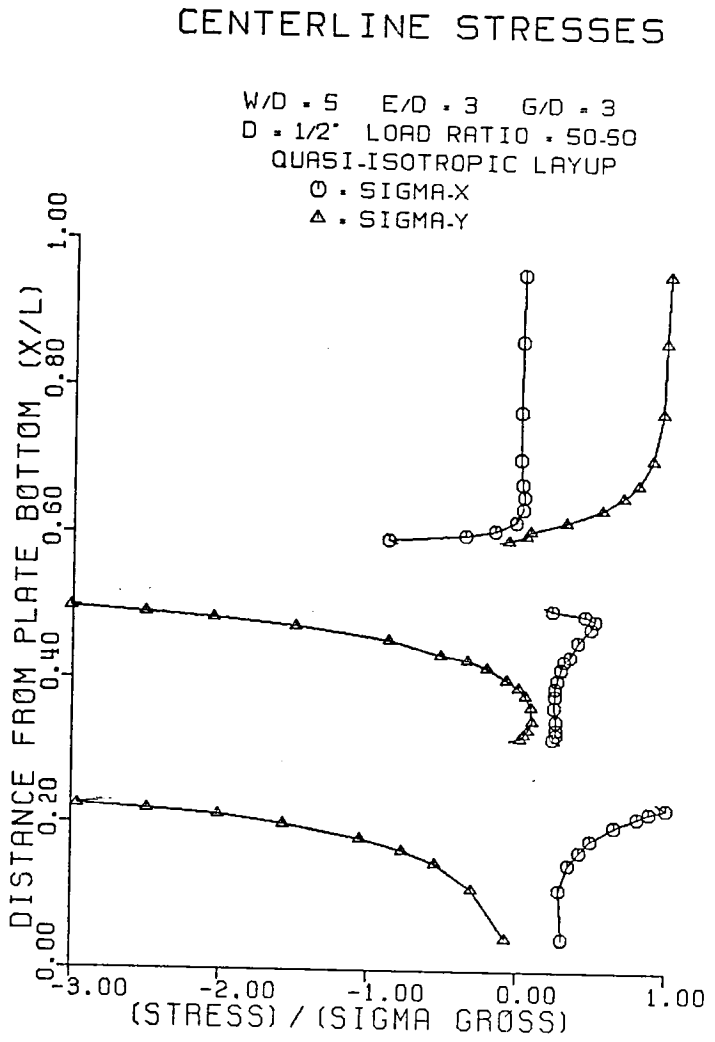

Fig. 5.8 Centerline Stresses in a Quasi-Isotropic Laminate.

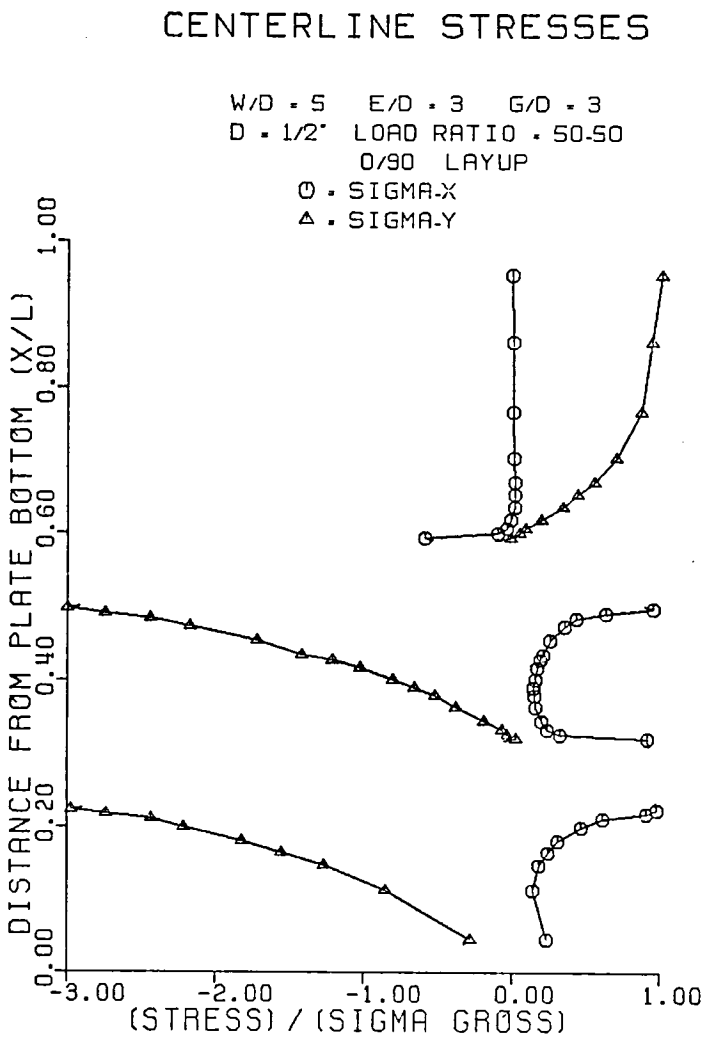

Fig. 5.9 Centerline Stresses in a Cross-Ply Laminate.

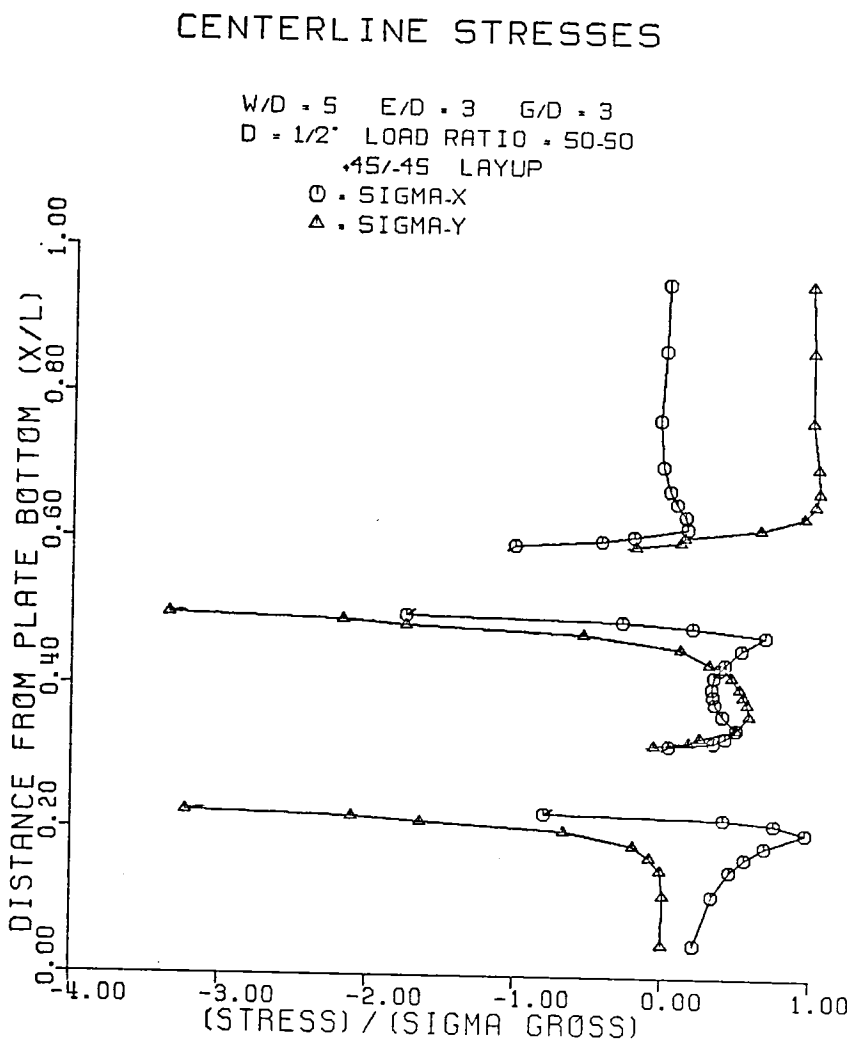

Fig. 5.10 Centerline Stresses in an Angle-Ply Laminate.

stress is zero because this location is traction free. Similar compressive behavior is shown below the bottom hole. Below the bottom hole there is no tensile phenomena as there was below the top hole. The tension has disappeared due to the fact that no bypass load exists at this point in the plate. The σ_y stress approaches zero at the bottom free edge of the laminate.

Starting from the top end of the plate, the σ_x stress is essentially zero until the top edge of the upper hole is reached. At this point a compressive value is shown. This is a familiar effect, at least in isotropic plates and this plate is a close approximation to that case. Below the top hole the σ_x value is quite small, starting positive at the bottom edge of the hole and rising to a slight peak. After the peak is reached the stress remains small to the top edge of the bottom hole. Directly beneath the bottom hole, the value of the σ_x stress is about 1.0. The σ_x stress below the bottom hole is different than the σ_x below the top hole because of a lack of bypass load. As the plate bottom is approached the magnitude of the σ_x stress decreases to a small value.

The centerline stresses in a cross-ply laminate are shown in Fig. 5.9. The stresses for this laminate exhibited characteristics similar to the stresses for the quasi-isotropic case except for the variation of σ_x between the

holes. Unlike the quasi-isotropic case, the magnitude of this stress is about the same directly below each hole. This implies that the unloading effect of the bypass load for the top hole is smaller for this laminate than for the quasi-isotropic laminate. Also it is interesting to note that the σ_x stress is tensile at the top of the bottom hole.

Fig. 5.10 shows the centerline stresses for the angle-ply laminate. Above the top hole, the stress distributions are similar to the other two cases. However, in this case the σ_y stress becomes slightly negative at a point directly above the top hole. Recall that the finite-element method requires output of stresses at Gauss points which are at interior points in the plate and not on the hole edge. The top of the top hole should have a zero σ_y stress value. Since the stress gradient is higher than in the other two cases, the mesh density used may not have had the required refinement to get a zero σ_y stress value at this point. Between the two holes, the σ_y stress starts with a large negative bearing value, -3.4, and then rapidly becomes positive. The positive value of the σ_y stress between the two holes is the largest of the three laminates. At the top of the second hole, the σ_y stress drops to zero. Between the two holes, the σ_x stress also varies rapidly, going from compression directly below the hole, to tension between the holes, to zero at the top of the second hole. Below the

second hole, the σ_y stress changes quite rapidly from a high negative value to approximately zero. The σ_x stress changes rapidly from compression, to tension, and then levels off as the free end of the laminate is approached.

Figs. 5.11-5.13 show the circumferential stresses around the two holes in the three laminates. Since this region is polar in nature the stresses are transformed to the r-θ coordinate system. In addition, since the radial stresses are input to the program to be cosinusoidal, they will not be shown on the graphs. The circumferential stress values are reported for a region starting at the bottom of each hole and varying through 180° to the top of each hole. Fig. 5.11 shows this stress for both top and bottom holes for the quasi-isotropic laminate. It is obvious that bypass effects cause the stress magnitudes around the upper hole to be greater than the magnitudes around the bottom hole. A maximum stress is attained at slightly less than 90° for both holes. The maximum for the top hole is about twice the maximum for the lower hole.

Fig. 5.12 illustrates the circumferential stress for a cross-ply laminate. The maximum values still occur near 90°, the location corresponding to a net-section area. However, overall shape and magnitudes are quite different when compared to the previous quasi-isotropic case. There are secondary maximums of circumferential stress at the

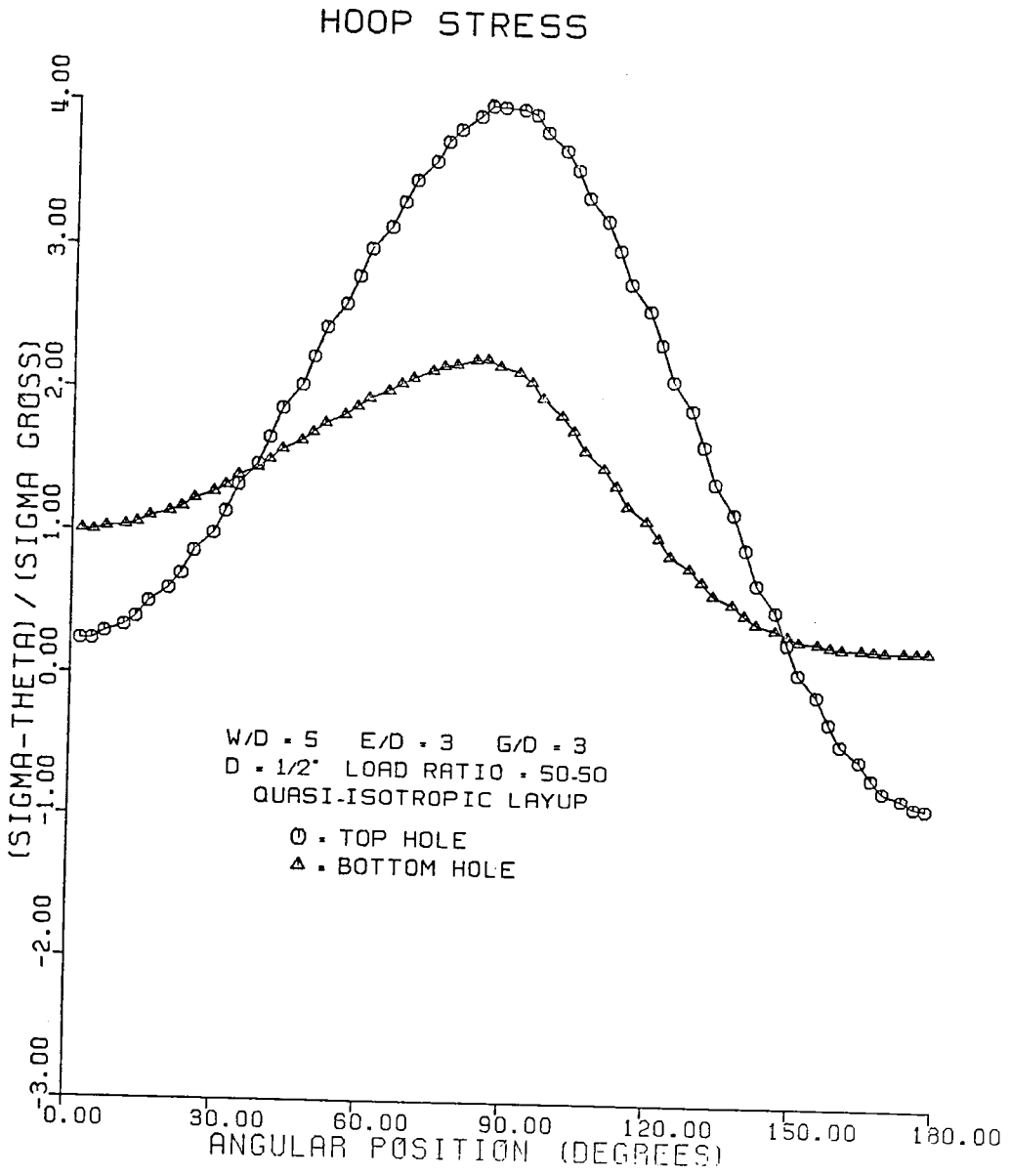

Fig. 5.11 Circumferential Stresses in a Quasi-Isotropic Laminate.

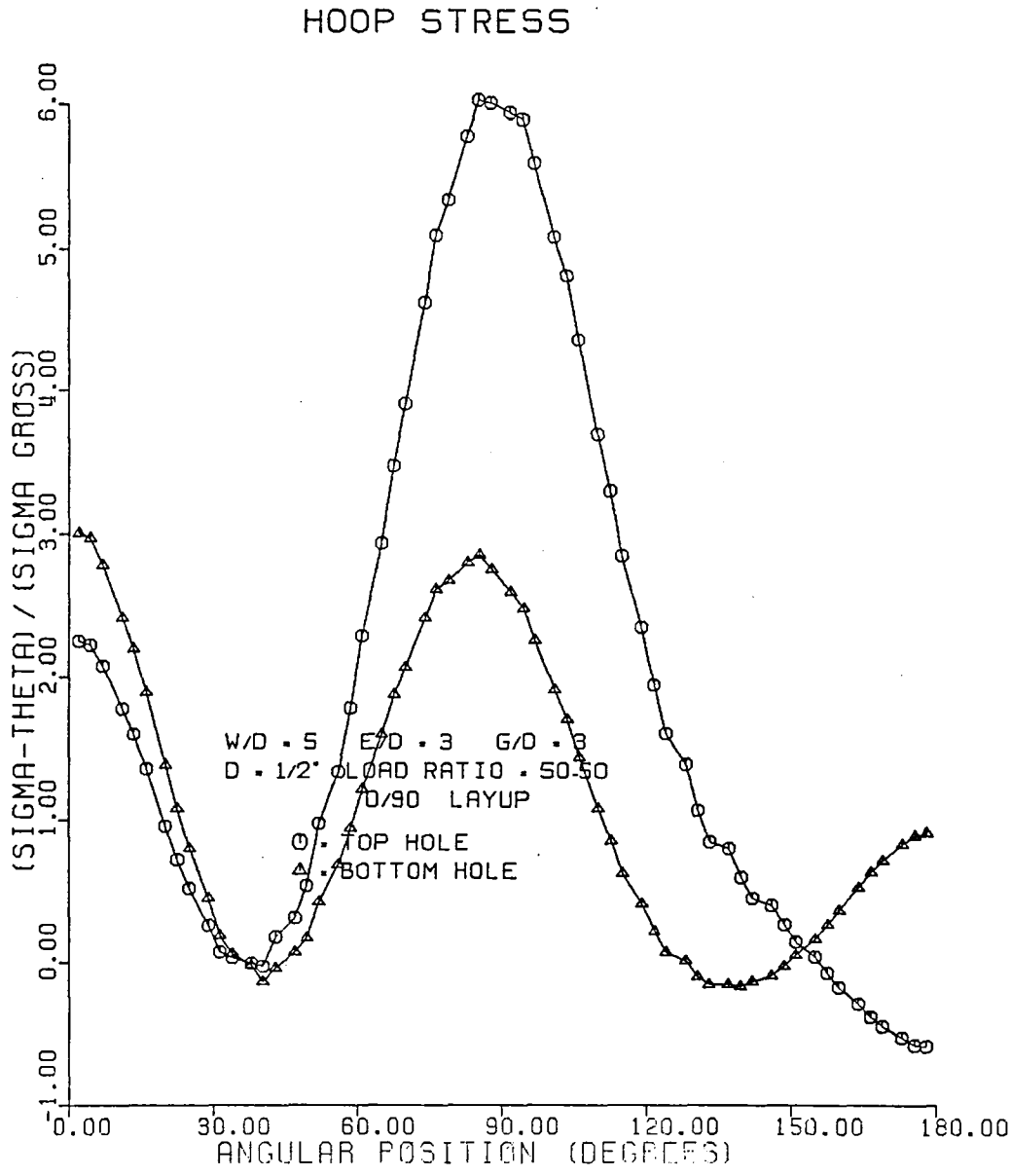

Fig. 5.12 Circumferential Stresses in a Cross-Ply Laminate.

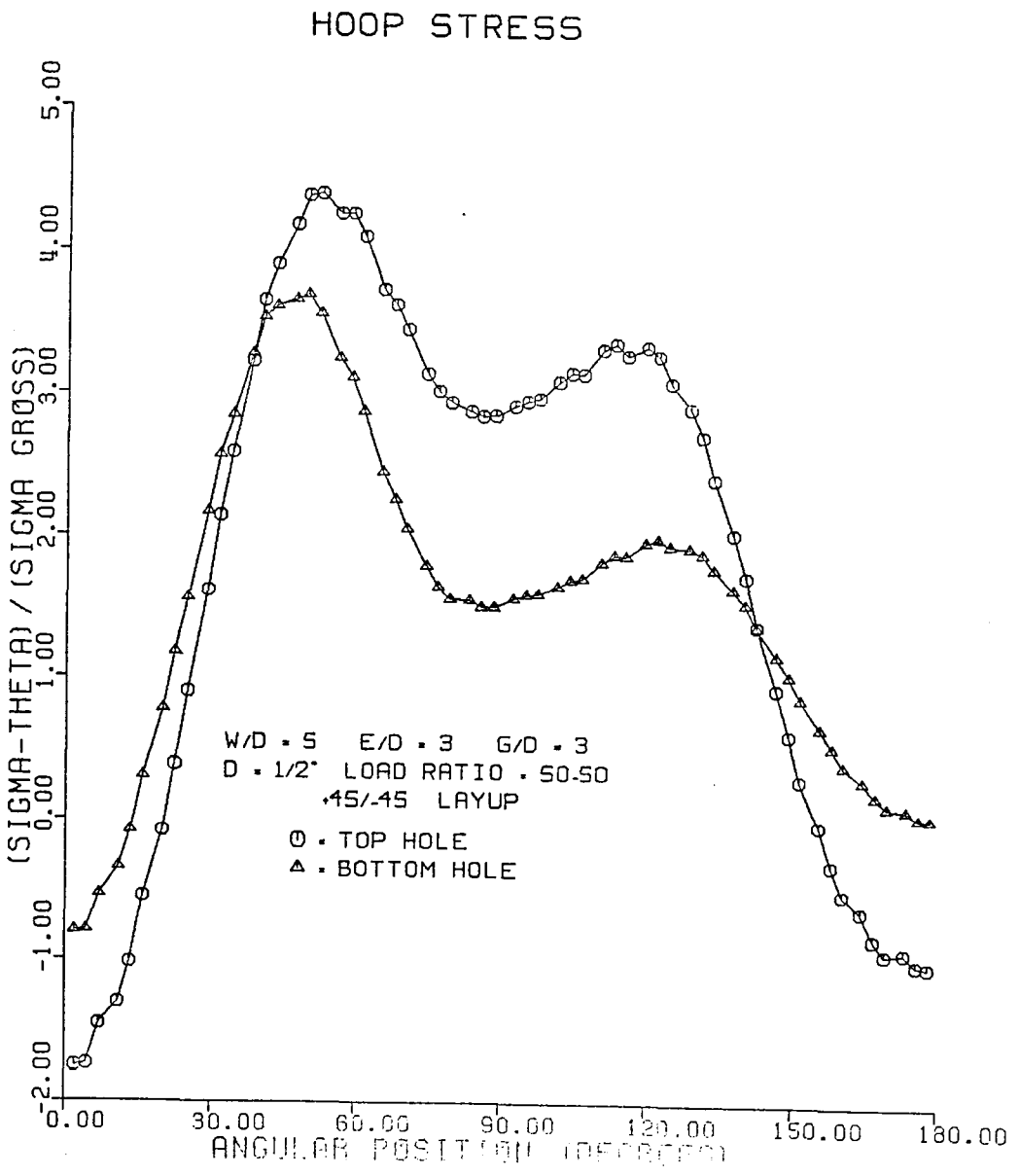

Fig. 5.13 Circumferential Stresses in an Angle-Ply Laminate.

bottoms and tops of each hole on the vertical centerline of the plate. The bottom of each hole is in tension but the top of the upper hole edge is in compression while the top of the bottom hole is in tension. At the net-section, for the top hole, the maximum value is about 6.0 compared to 4.0 for the quasi-isotropic case. The difference between the top hole maximum at the net-section and the bottom hole maximum at the net-section is about a factor of two, as in the quasi-isotropic case. For this cross-ply case, at $\theta = 40^{\circ}$ the circumferential stress is very close to zero for both holes. This is quite unusual. The difference between the cross-ply and the quasi-isotropic case shows the influence of laminate elastic properties on the stress distribution.

Fig. 5.13 shows the circumferential stress distribution for the angle-ply laminate. Obvious are the negative values below both holes. This was shown in the centerline plots. Also the relative maximums occur at about 50° and 120°. This effect is due to half the fibers being tangent to the hole at $\theta = 45^{\circ}$ and $\theta = 135^{\circ}$. The maximum values of the circumferential stress is about 4.5 at 50° for the top hole and 3.5 at 50° for the bottom hole. There is not the factor of two difference in the peaks between the top and bottom holes as there is for the quasi-isotropic and cross-ply cases. At the $\theta = 135^{\circ}$ location, there is about a factor of

two difference between the secondary peak at the top hole and the secondary peak at the bottom hole. In addition, the top of the top hole is in greater circumferential compression than the top of the bottom hole. This difference in stresses at the top and bottom holes also demonstrates the effects caused by the bypass loads.

STRESS CONTOURS

In addition to presenting the stresses in a two-hole joint at particular locations in the plate, stress contours are also plotted to show the whole-field stress state in each laminate, for the baseline case. These stress contours σ_y, σ_x, and τ_{xy} are all normalized to the far-field σ_y stress. Figs. 5.14-5.16 show these contours for the quasi-isotropic laminate. In Fig. 5.14 the contour intervals are equal to 1.0. In some cases, a contour value of 0.50 is shown to clarify the distribution of the stresses. As can be seen, there is the expected stress concentration near the net-section region at both the top and bottom holes. At the top hole this value reaches a magnitude of 3.0 while at the bottom hole the maximum contour shown is 2.0. This is a good illustration of the fact that the bottom hole is understressed in relation to the top hole for a load ratio of 50-50. A negative stress value can also be seen below each hole in the bearing region. For this laminate, the contours reach -3.0 at both holes. This shows that the

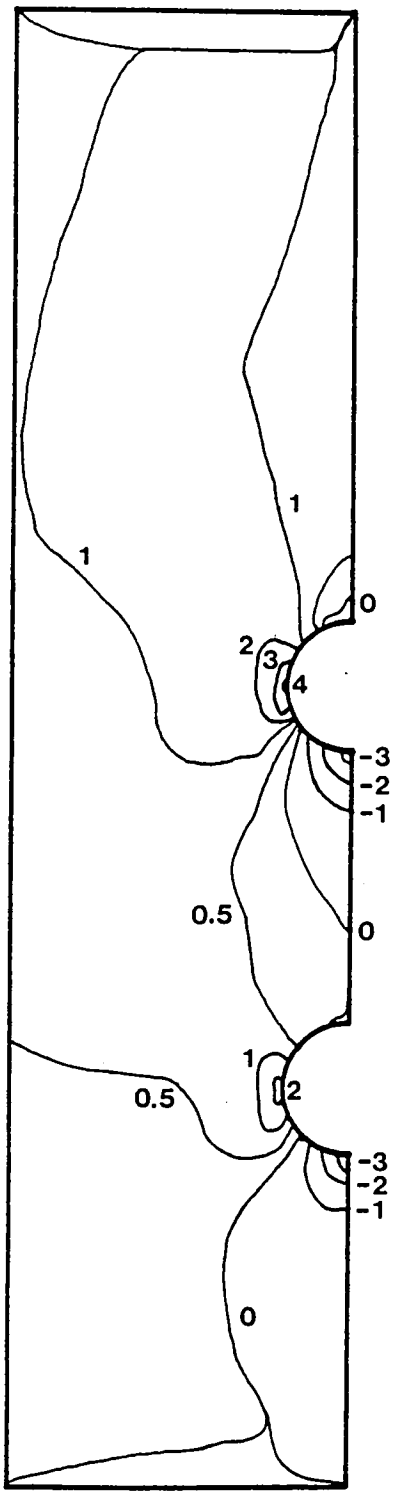

Fig. 5.14 σ_y Stress Contours for a Quasi-Isotropic Laminate.

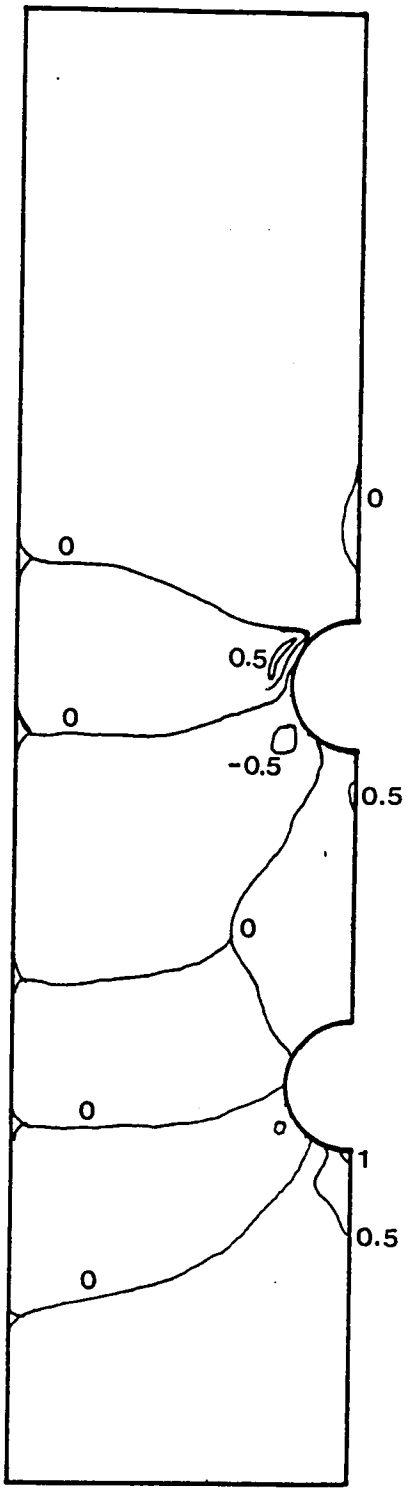

Fig. 5.15 σ_x Stress Contours for a Quasi-Isotropic Laminate.

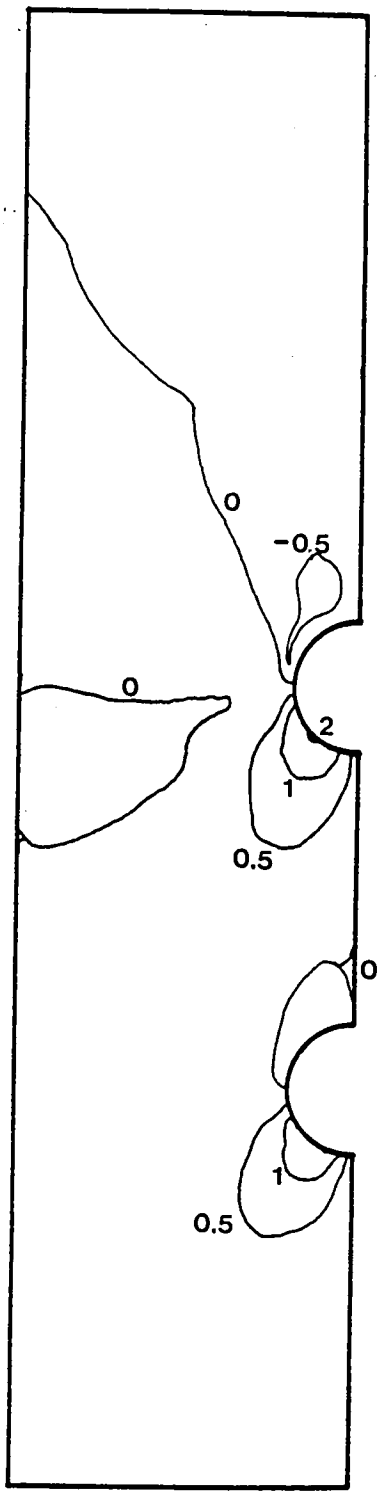

Fig. 5.16 τ_{xy} Stress Contours for a Quasi-Isotropic Laminate.

superposition of stresses does not influence the magnitude of the stresses in the bearing region of the hole since the values are about the same at both the top and bottom holes.

Fig. 5.15 shows the σ_x stress contours for a quasi-isotropic laminate. As expected the values are much less than the σ_y contour magnitudes. Below the holes, the contours are positive, showing the Poisson effects. The intervals for this figure are 0.50 At the net-section region of each hole, a 0 contour interval begins. This is a necessary condition at the hole edge. The free edges of the plate, the left and bottom edges in the figure, also have a value of 0. This matches the boundary conditions.

Fig. 5.16 illustrates the τ_{xy} stress contours for a quasi-isotropic laminate. Again, since the magnitudes are smaller when compared to the σ_y contour plot, the contour interval is 0.50. The most important feature shown in this figure is the fact that the highest values of the shear stress occur near the $\theta = 45^{o}$ position at each hole. In addition, the top hole shows a slightly higher value of shear stress than does the bottom hole. The free edges have a value of 0 as does the net-section point on the edge of each hole. These values must have a zero magnitude to match the boundary conditions.

The σ_y stress contours for a cross-ply laminate are shown in Fig. 5.17. With this laminate type the stress

concentrations at the hole edge as well as the stress gradients are much higher when compared to the quasi-isotropic case. This figure also shows that the far-field contour value of 1.0 is much narrower. This illustrates the high influence of the holes in this laminate type.

Fig. 5.18 shows the σ_x contours for the cross-ply laminate. The main features in this figure are the values of the stress contours directly below each hole. The magnitudes approach 2.0 at the top hole and 3.0 at the bottom hole. The higher value at the lower hole can be linked to an unloading phenomena at the top hole caused by the bypass load which will be reacted at the lower hole.

The shear stress contours for a cross-ply laminate are given in Fig. 5.19. Again, the most prominent feature is the location the maximum values which occur at the $\theta = 45^{o}$ location at each hole. The top hole has a slightly higher value of shear stress. This was also seen in the quasi-isotropic laminate. The centerline and free edges are stress free and show a contour value of 0 to reflect this.

Fig. 5.20 shows the σ_y contours for an angle-ply laminate. The magnitudes of the stress concentrations at the net-section region at each hole are lower than both the cross-ply and the quasi-isotropic laminates. The bearing stress contours are about same as was shown for the quasi-isotropic case, as was the wide dispersion of the far-field

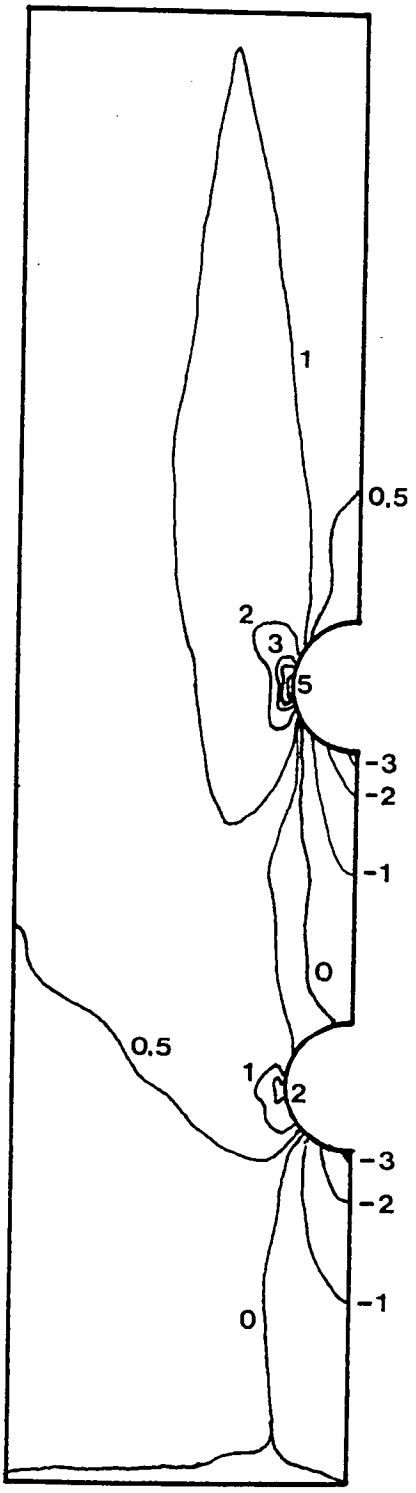

Fig. 5.17 σ_y Stress Contours for a Cross-Ply Laminate.

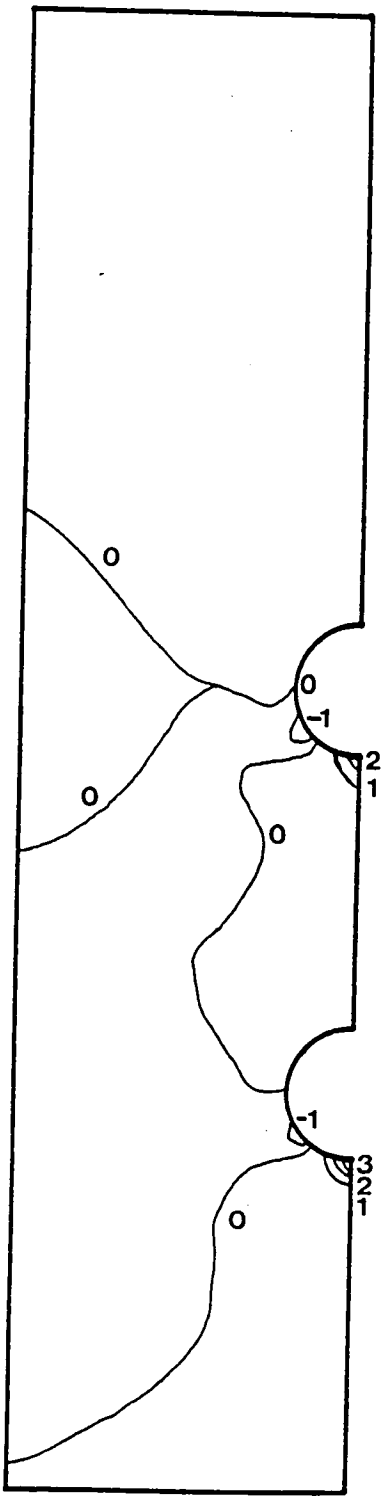

Fig. 5.18 σ_x Stress Contours for a Cross-Ply Laminate.

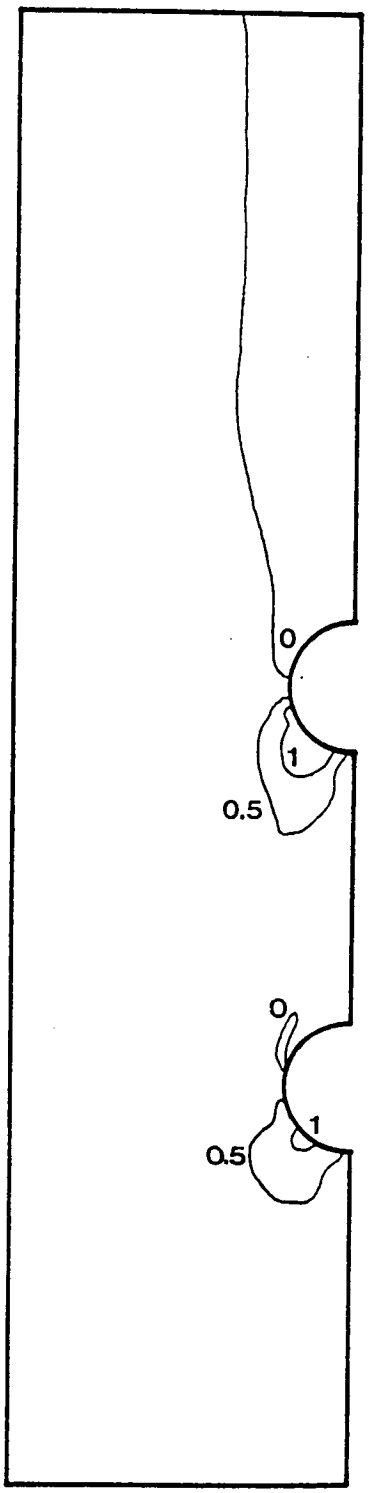

Fig. 5.19 τ_{xy} Stress Contours for a Cross-Ply Laminate.

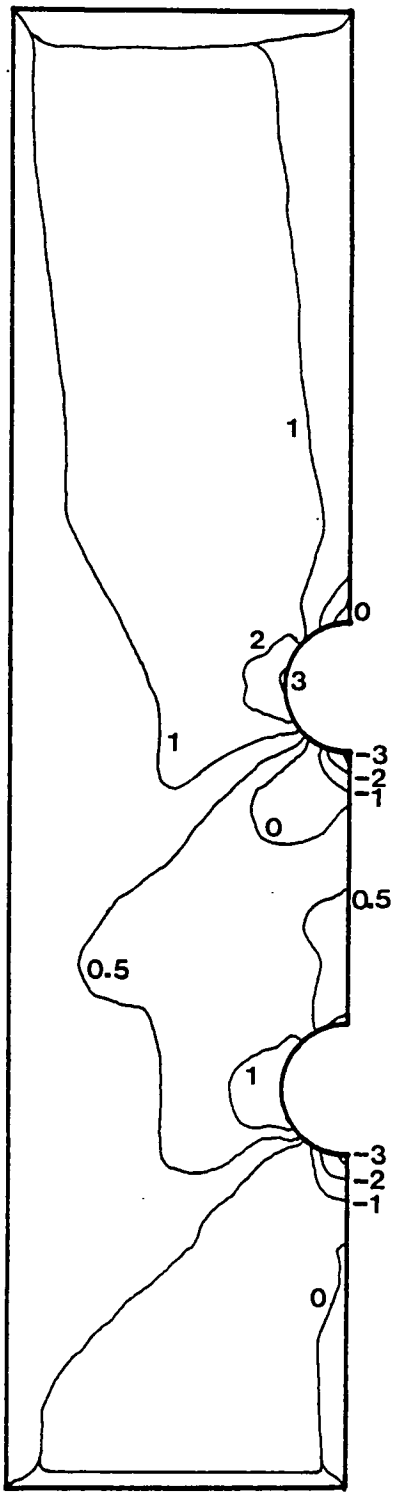

Fig. 5.20 σ_y Stress Contours for an Angle-Ply Laminate.

1.0 contour.

The σ_x stress contours for the angle-ply laminate are given in Fig. 5.21. Again, the magnitudes are much lower when compared to the σ_y contours. The net-section region at both holes and the free edges show a value of 0. Also, the far-field region shows the 0 contour. This illustrates the uniaxial stress state in this region.

Fig. 5.22 shows the shear stress contours for an angle-ply laminate. As was shown earlier in the other two laminates, the highest contour magnitudes occur near the $\theta = 45^{o}$ region at both holes. Also, the top hole shows a higher value of the shear stress than the bottom hole. This again shows the superposition effect on the stresses at the top hole.

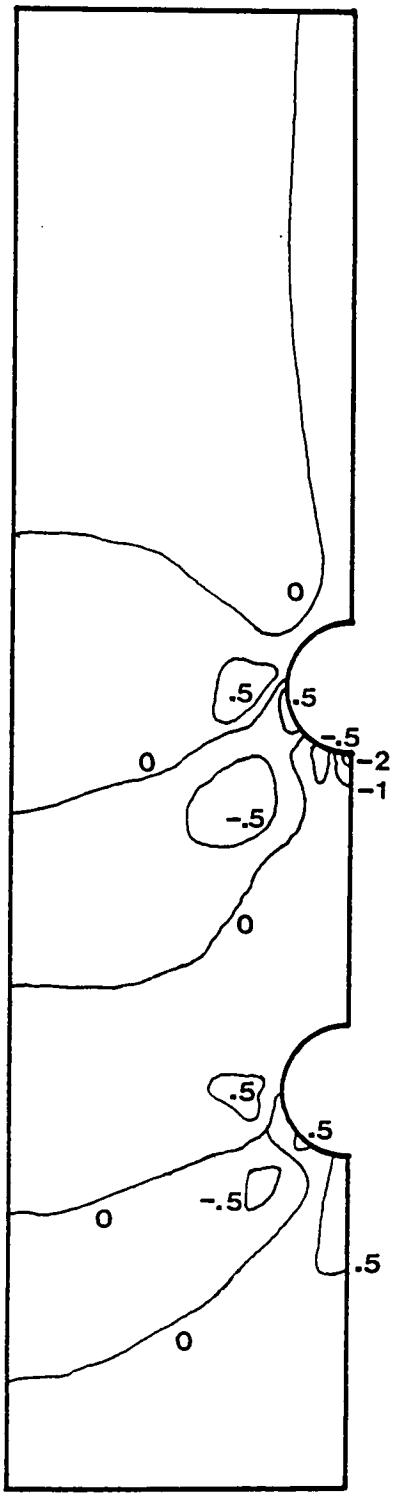

Fig. 5.21 σ_x Stress Contours for an Angle-Ply Laminate.

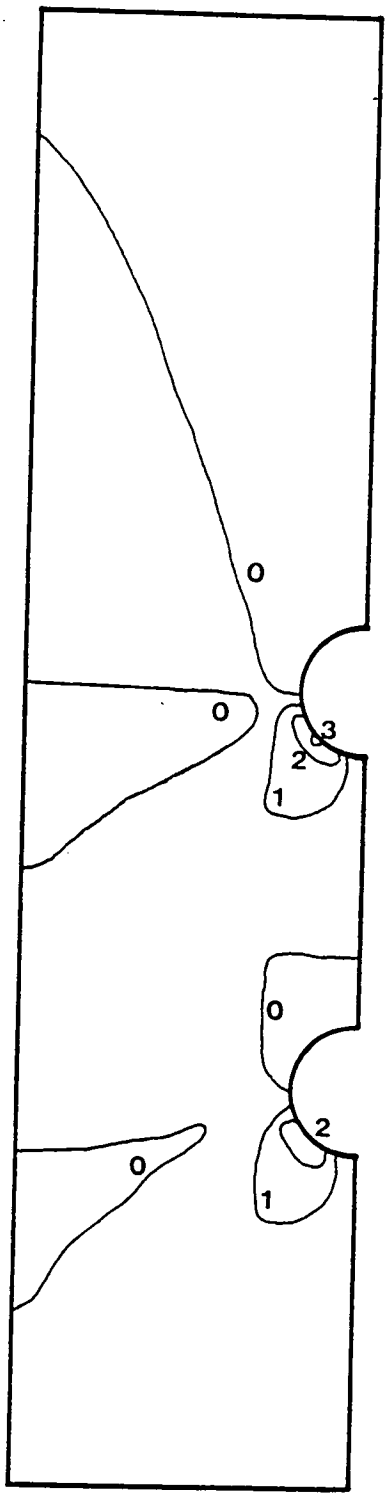

Fig. 5.22 τ_{xy} Stress Contours for an Angle-Ply Laminate.

CHAPTER 6

TUTORIAL ON LOAD PROPORTIONING ALGORITHM AND BASELINE CASE DISCUSSION

Tutorial

Prior to the discussion of any results, a short tutorial will be presented to acquaint the reader with the algorithm used to determine the best load ratio for a particular case. The tutorial will also acquaint the reader with the format of the figures used. The figures which follow in this discussion are not necessarily associated with any particular geometry. The figures are for a quasi-isotropic laminate, however. The figures are only used as being typical of figures to be encountered later.

Fig. 6.1 represents the variation of the quantity F, defined in the Yamada-Sun failure criteria of Eqn. 3.11, as a function of position around the holes. These values of F have been normalized with respect to the maximum value of F at either of the two holes. This joint is loaded so that equal load is reacted by both the top and bottom holes. This is the 50-50 case as referred to earlier. The upper portion of Fig. 6.1 shows the values of F for the top hole of the joint while the lower portion of the figure shows F values around the lower hole. Recall that the Yamada-Sun failure criteria is applied on a lamina-by-lamina basis. Since by classical lamination theory all lamina at a

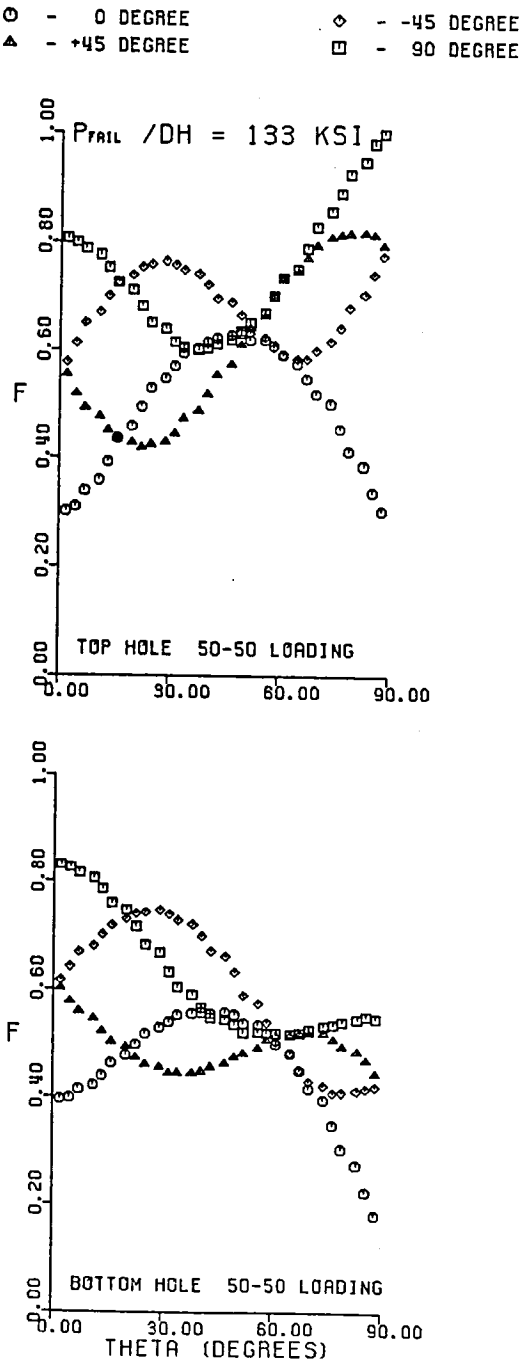

Fig. 6.1 F vs. θ for a Quasi-Isotropic Laminate With a Load Ratio of 50-50.

particular fiber orientation experience the same stress, independent of location through the thickness of the laminate, there are four F vs. θ relations, or curves, on each portion of the figure. Each curve corresponds to the criterion applied to a lamina with a particular fiber orientation. The total load applied in Fig. 6.1 is such that in some lamina at some location around either of the top or bottom holes, F = 1. According to the failure criterion, failure has occurred at this load level, at this particular circumferential location, in this particular lamina. Failure near $\theta = 0^{\circ}$ corresponds to failure beneath the hole in a bearing failure mode. Failure near $\theta = 90^{\circ}$ indicates net-section tensile failure mode. At other locations the failure is considered a shearout failure mode. Using this criteria, the joint of Fig. 6.1 fails in net-section tension at the top hole. Failure is in the 90° lamina, the lamina with the fibers aligned with the load. The actual load to cause F to be 1 at the net-section of the top hole is indicated on the top figure. In this case it is 133 ksi, i.e. P/DH = 133 ksi.

The next highest value of F is 0.83 and it occurs at the bottom hole at $\theta = 0^{\circ}$. If failure at the top hole could be prevented and the load increased, failure would occur at the bottom hole in bearing at a load of P/DH = (1/0.83)(133)=160 ksi. These values of P/DH associated with

top hole and bottom hole failure are important. They will be used shortly.

If the percent of total joint load reacted by the top hole is varied to, say, 40% and then to 30% (the bottom hole reacting 60% and 70% respectively) and the failure criteria is applied to these two load cases, two additional sets of plots similar to Fig. 6.1 are generated. These are shown in Figs. 6.2 and 6.3. In each case there is a load to cause failure at the top hole and a load to cause failure at the bottom hole. If the top hole and bottom hole failure loads for these three cases are plotted as a function of the load ratio, Fig. 6.4 is generated. In this figure the loads associated with top hole failure are connected with a line and the loads associated with bottom hole failure are connected with another line. The open symbols are the failure loads generated for the three cases, circles for the top hole, triangles for the bottom hole. Note that there is a letter is adjacent to each symbol. This letter indicates the mode of failure predicted. It is important to note here that the failure loads shown in some portions of the figure are physically unattainable. This is demonstrated by realizing that once failure has occurred at a particular hole, the joint cannot sustain any additional load. Fig. 6.5 shows physical bounds of the joint load. The locus representing the maximum value of attainable load at any

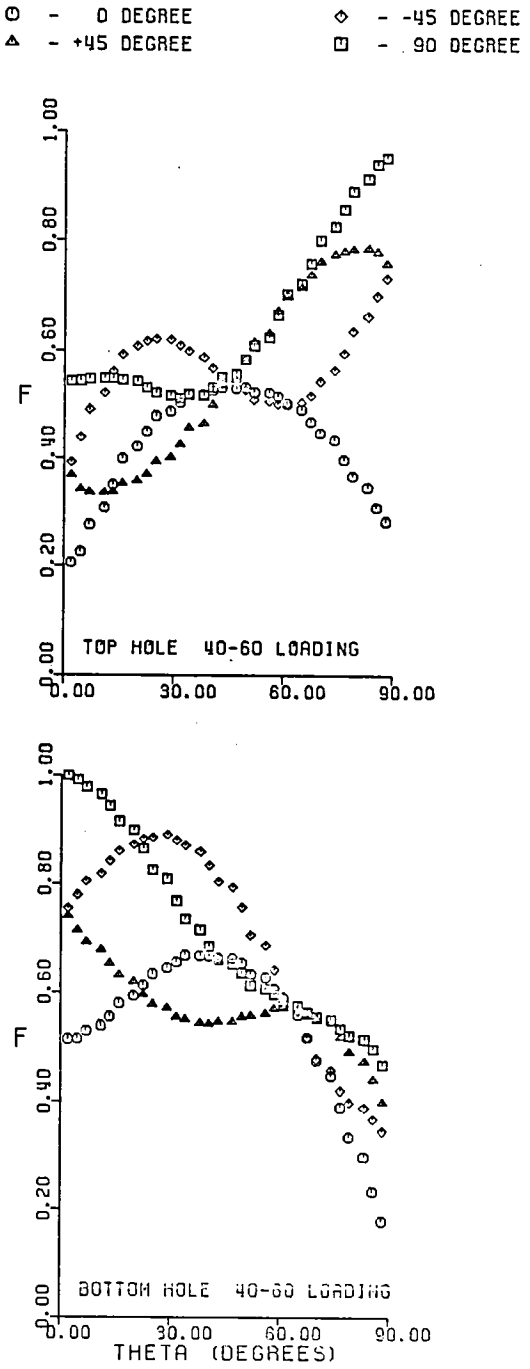

Fig. 6.2 F vs. θ for a Quasi-Isotropic Laminate With a Load Ratio of 40-60.

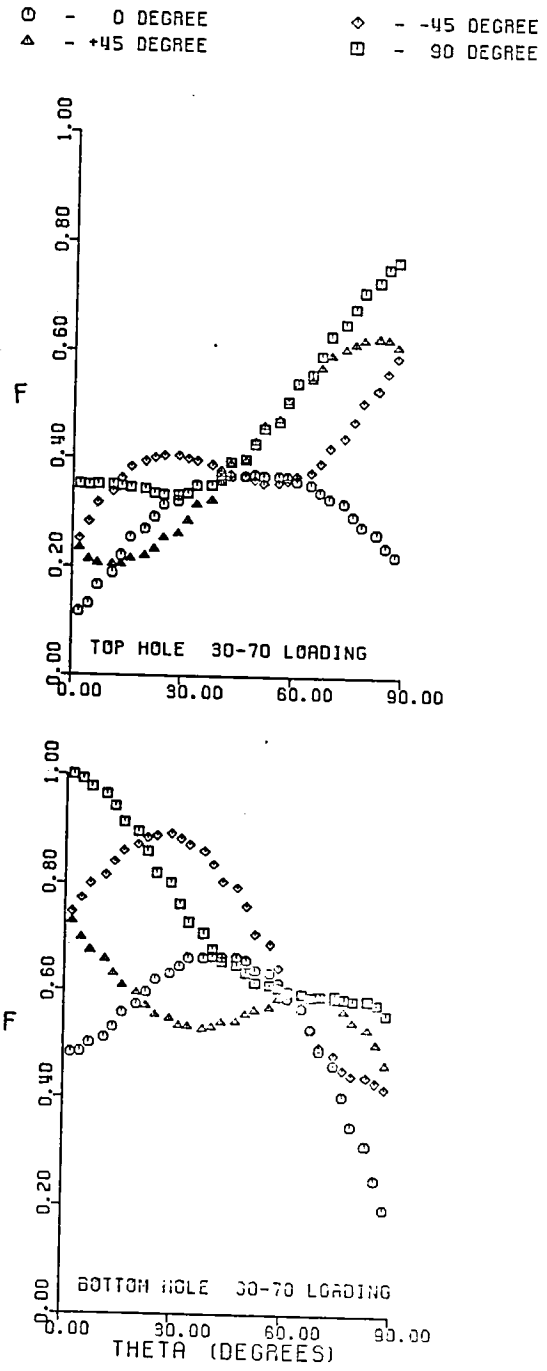

Fig. 6.3 F vs. θ for a Quasi-Isotropic Laminate With a Load Ratio of 30-70.

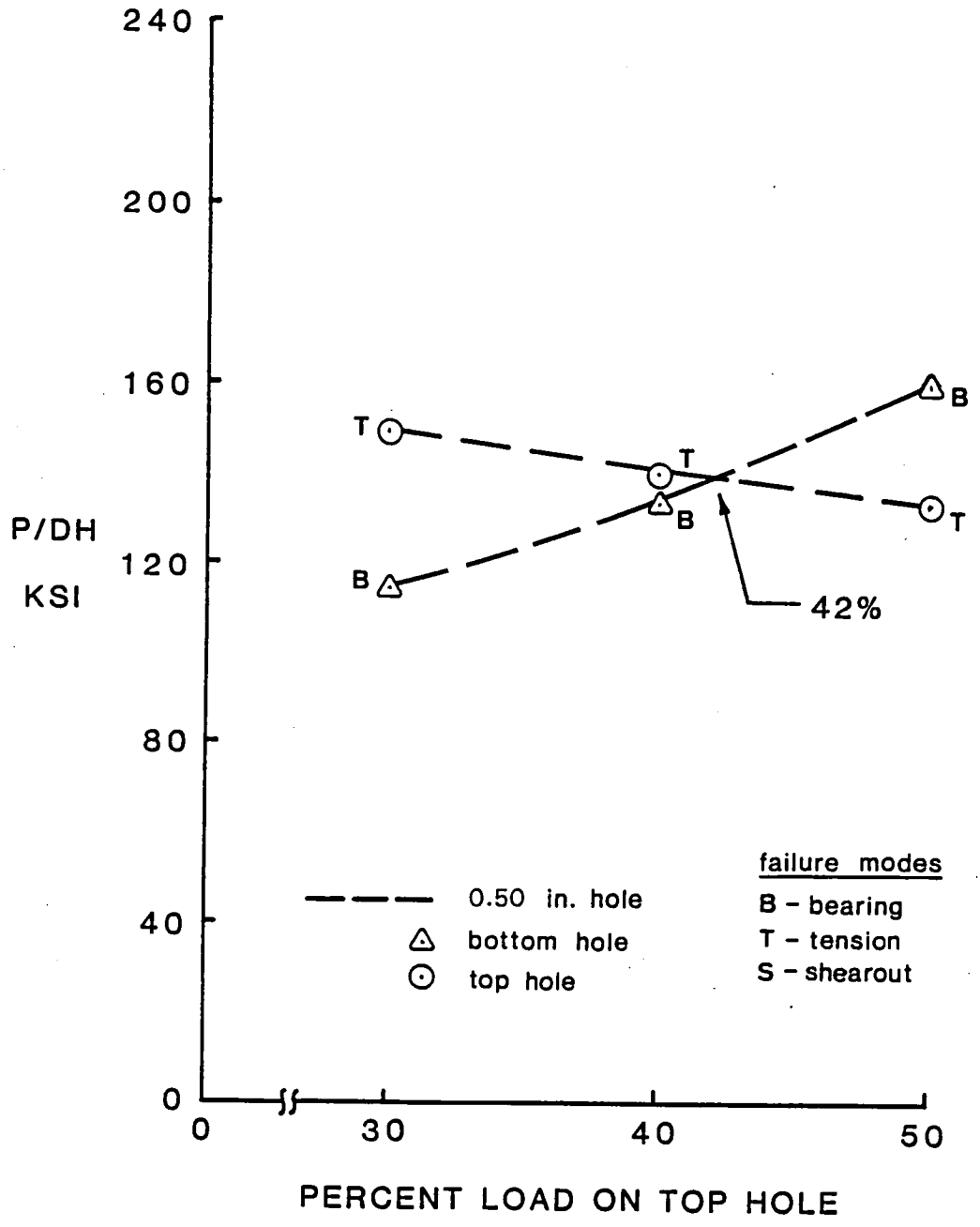

Fig. 6.4 Failure Characteristics for a Quasi-Isotropic Laminate.

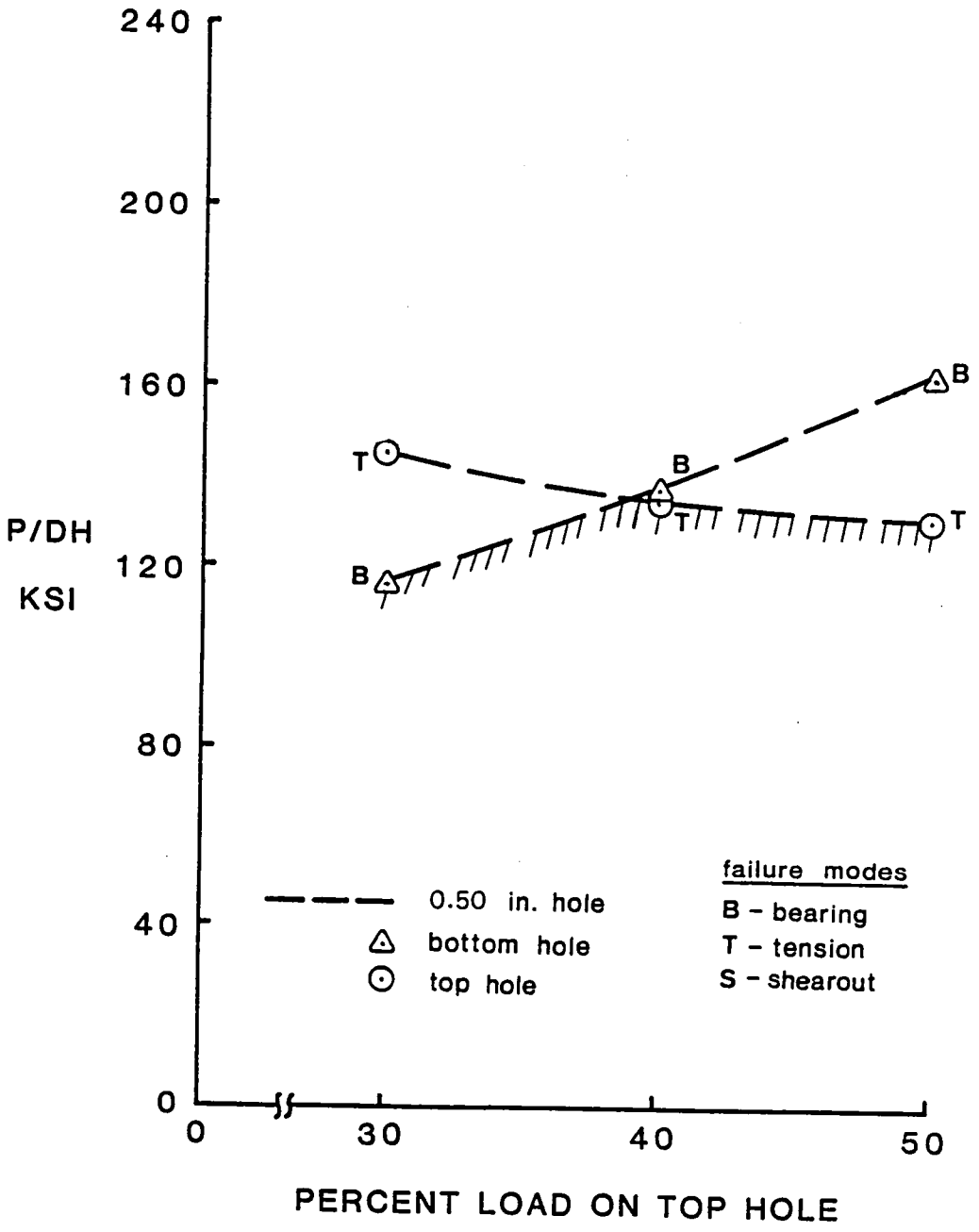

Fig. 6.5 Physical Bounds of Joint Capacity.

particular percent of load on the top hole is indicated by tic marks.

From Fig. 6.4 it is obvious how the load proportion to cause failure at the top hole and bottom hole at the same value of P/DH is determined. At the location where the locus of the bottom hole failures crosses the locus of the top hole failures, simultaneous failure occurs. This is at the apex of the maximum load locus and thus the failure load associated with this load proportion is higher than the failure load associated with any other load proportion. For the joint being discussed, having 42% of the total load on the top hole and 58% on the bottom hole results in the highest failure load for that joint. As a check, the stress analysis and application of the failure criteria is applied to the 42-58 load case. Fig. 6.6 shows the variation of the values of F around the holes. It is clear F is now equal to unity at two locations. The failure value of P/DH associated with this load proportion, 140 KSI, is indicated on the figure. For this hypothetical case, it is seen there is a 5.3% increase in load capacity.

Baseline Case Description

Prior to a general discussion of the effects of load proportioning, joint geometry, and laminate elastic properties on the joint capacity, an in-depth discussion of a baseline geometry for each specific laminate will be

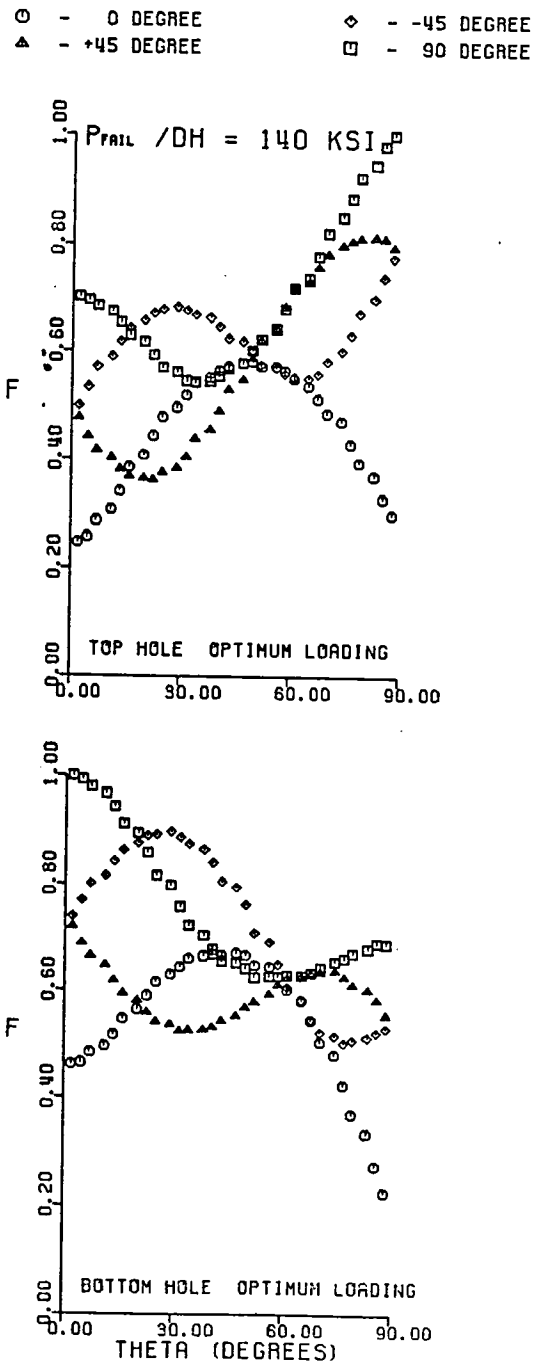

Fig. 6.6 F vs. θ for a Quasi-Isotropic Laminate With an Optimum Load Ratio.

presented. The baseline case will be a plate with a width to hole diameter ratio, W/D, of 5, an edge distance to hole diameter ratio, E/D, of 3, and a hole spacing to hole diameter ratio, G/D, of 3. Two different hole diameters will be discussed with each baseline case. This will permit a close examination of the hole size influence on joint capacity, and also its effect on the optimum load ratio.

The first stacking sequence addressed is a quasi-isotropic layup. This geometry and stacking sequence are typical of current designs in many structural applications. Figs. 6.7a and 6.7b show the value of F around the hole for the baseline quasi-isotropic case when a 1/2 in. diameter hole is used. The maximum load of this joint with the 50-50 load ratio is about 133 ksi. This load produces failure in the 90 degree ply (fiber tension failure) at the net-section portion of the top hole. The other plies at the top hole are at about 80 percent of their capacity, each at a different location around the hole. Fig. 6.7b shows that at the bottom hole the 90 degree ply is the closest to failure, in bearing (fiber compression). None of the plies at the bottom hole are at their maximum capacity. Conducting a stress and failure analysis for the 40-60 and 30-70 load ratios, the dashed loci on Fig. 6.8 are generated, one representing failure at the top hole, the other representing failure at the bottom hole. The open circles are associated

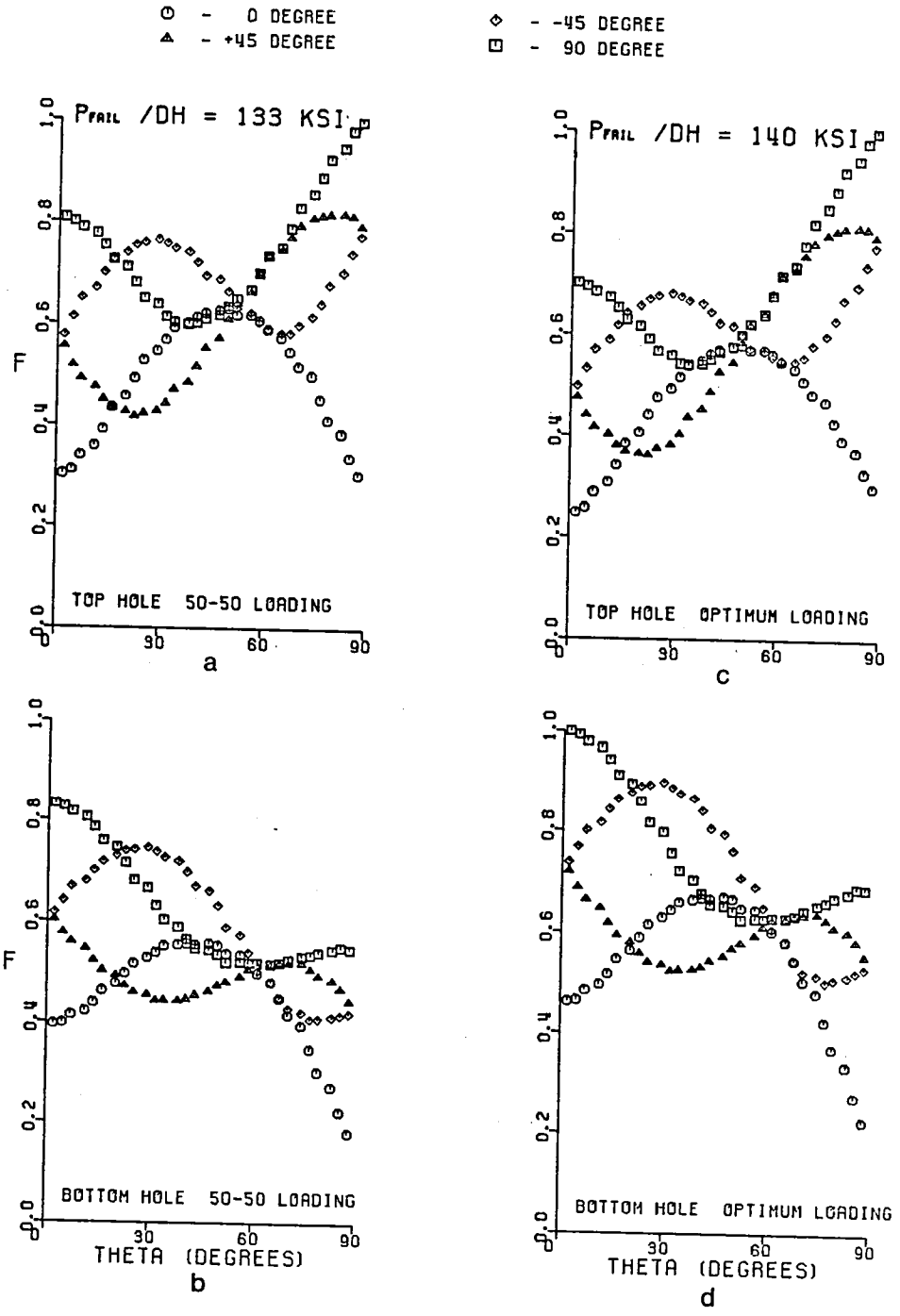

Fig. 6.7 F vs. θ for a Quasi-Isotropic Laminate, W/D=5, E/D=3, G/D=3, D=1/2.

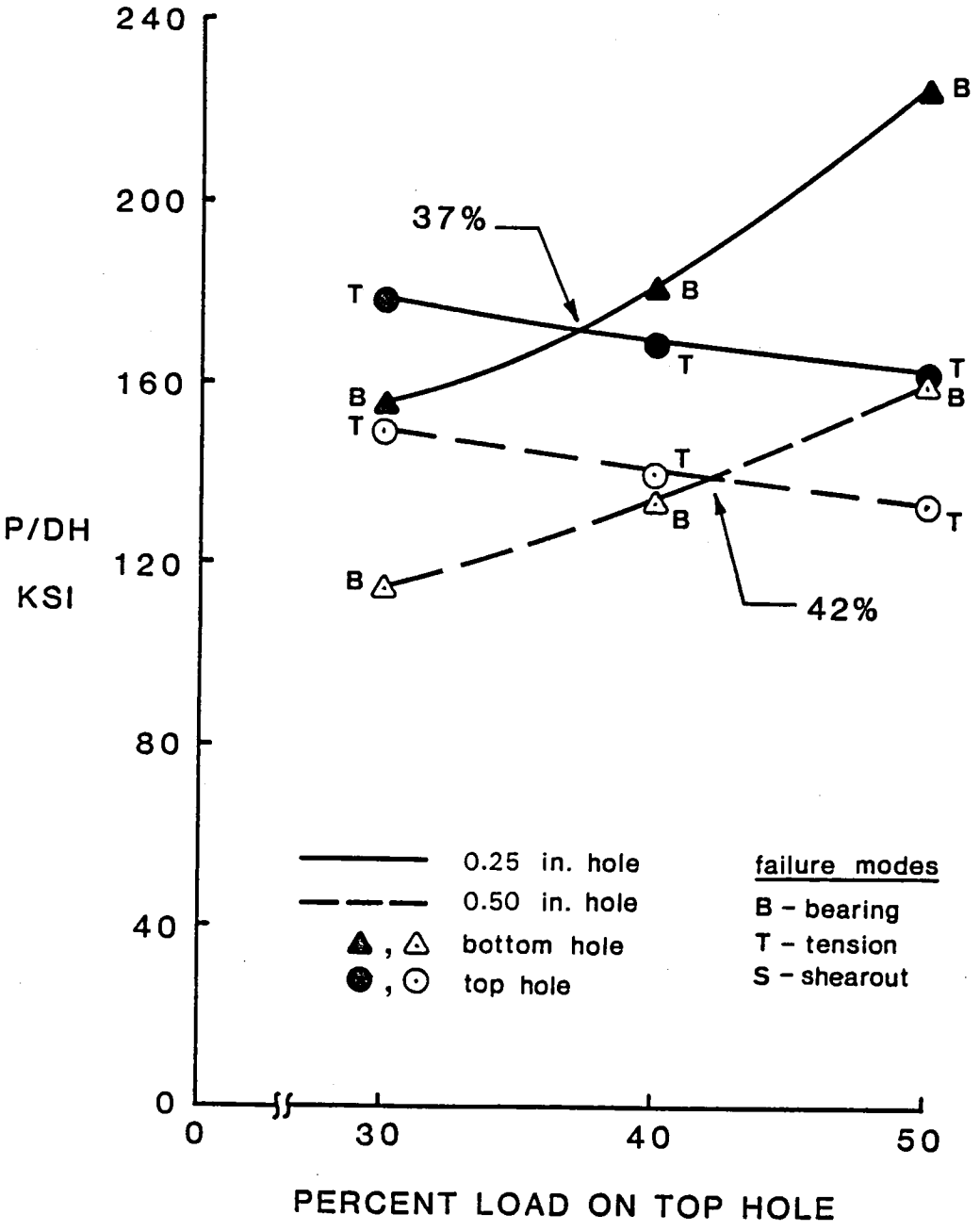

Fig. 6.8 Failure Characteristics for a Quasi-Isotropic Laminate, W/D=5, E/D=3, G/D=3.

with the top hole while the open triangles represent the bottom hole. These dashed loci intersect when the percent load on the top hole is 42%. This load proportion results in the highest failure load. When the 42-58 ratio is used, the maximum load capacity of the joint increases to 140 ksi. Figs. 6.7c and d show the characteristics of the failure locus at the 42-58 load proportion. The 140 ksi load translates into an increase of 5.3% in joint capacity. With the 42-58 load proportion, the value of F at both the top and bottom holes is unity in the 90 degree ply. The top hole shows a failure mode of net-section tension while the lower hole shows a bearing failure in the same ply. This difference in failure modes at the two holes is explained by realizing that the force reacted by the lower hole produces a tensile stress at the net-section of the top hole. This adds to the tensile stress at the top hole produced by the load being reacted at the top hole. This superposition of stresses is what causes a net-section failure at the top hole in what otherwise might be a bearing failure mode. At the lower hole there is no bypass stress to add to the net-section stresses. The bearing stress plays the dominant role in failure at the lower hole.

It is interesting to note that for this particular case the basic characteristics of Yamada-Sun criteria around each hole is independent of the load proportion. Though the peak

values of F depends on the load proportion, the basic shapes of the criteria as a function of location around the hole are unaffected by load proportion. This indicates the two holes are acting independently, with little interaction of the stress fields.

Fig. 6.9a and 6.9b show the variation of F around the holes for a 50-50 load proportion and the quasi-isotropic baseline geometry when a 1/4 in. diameter hole is used. For this situation failure is predicted in the 90 degree ply at the net-section region of the top hole. The maximum load is 163 ksi. This load is much higher than the 133 ksi capacity of the 1/2 in. diameter case for the 50-50 load ratio. This demonstrates the well observed hole size effect. As expected, all the other plies are at less than capacity. Fig. 6.9b shows all plies of the lower hole to be working at less than 60% of capacity. This means that a larger portion of the load needs to be shifted to the lower hole than was the case for the 1/2 in. diameter hole. The 40-60 and 30-70 load ratio failure characteristics are shown in the solid symbols of Fig. 6.8. The intersection of the top and bottom failure curves occurs when the percent load on the hole is 37%. The variation of F around the two holes for the 37-63 ratio is shown in Fig. 6.9c and 6.9d. The maximum joint load at this optimum ratio is 172 ksi, an increase of roughly 6%. Table 6.1 summarizes the important data for the

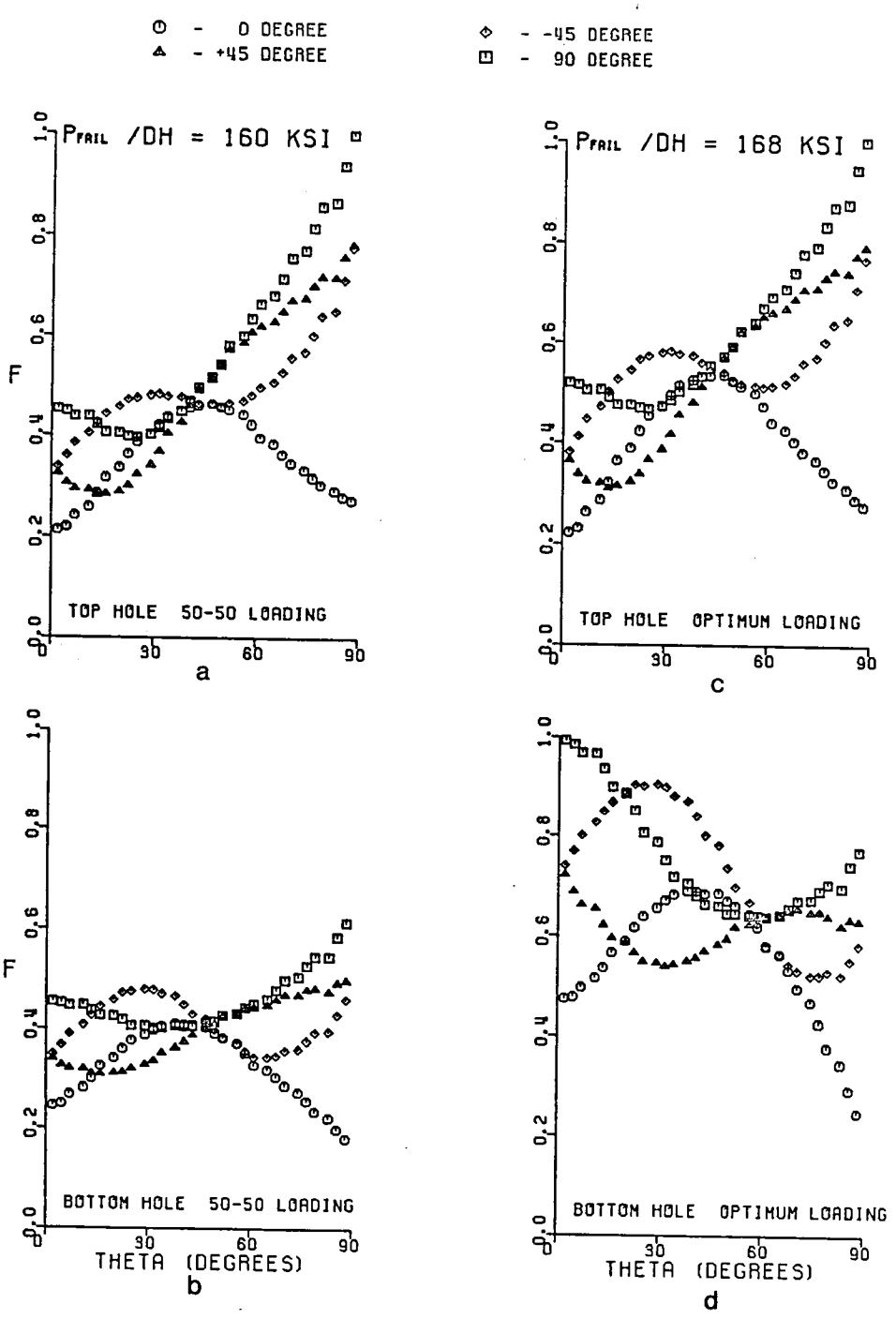

Fig. 6.9 F vs. θ for a Quasi-Isotropic Laminate, W/D=5, E/D=3, G/D=3, D=1/4.

Table 6.1 Results For Quasi-Isotropic Laminates

CASE NO.	GEOMETRY W/D	E/D	G/D	D (in.)	MAXIMUM LOAD 50-50 (ksi)	OPT. (ksi)	OPTIMUM LOAD RATIO (%)	CAPACITY DECREASE (%)
1	5	3	3	1/2	133	140	42	1.00
2	5	3/2	3	1/2	130	135	39	0.96
3	5	3	3/2	1/2	121	130	38	0.93
4	3	3	3	1/2	92	102	18	0.73
5	5	3	3	1/4	160	168	37	1.00
6	5	3/2	3	1/4	158	168	37	1.00
7	5	3	3/2	1/4	145	160	33	0.95
8	3	3	3	1/4	109	121	17	0.72
9	5	3/2	3/2	1/2	114	121	35	0.86
10	3	3	3/2	1/2	90	99	18	0.71
11	3	3/2	3	1/2	91	98	25	0.70
12	3	3/2	3/2	1/2	86	99	24	0.71
13	5	3/2	3/2	1/4	138	156	26	0.93
14	3	3	3/2	1/4	106	119	9	0.71
15	3	3/2	3	1/4	109	116	25	0.69
16	3	3/2	3/2	1/4	102	119	18	0.71

baseline quasi-isotropic laminate, in addition to other quasi-isotropic cases to be discussed. In Table 6.1 the baseline geometry is listed as case 1 for a hole diameter of 1/2 in. and case 5 for a hole diameter of 1/4 in. Table 6.1 indicates the maximum load for the 50-50 load case and for the optimum load ratio. Table 6.1 also includes a column labeled "CAPACITY DECREASE". This will be defined shortly.

The next laminate configuration addressed is a cross-ply layup. While this particular laminate is not often used, it provides a good case study of failure characteristics. Fig. 6.10a and 6.10b show the variation of F for both ply orientations around the top and bottom holes. Note that for this laminate the value of F at both the top and bottom holes appears to be at unity in both plies at the same location around the holes. This means that the 50-50 load ratio is very close to the optimum load ratio for this particular geometry. This is verified in Fig. 6.11. Fig. 6.11 shows the failure characteristics of the laminate as a function of percent load on the top hole. The optimum load ratio of 47-53 is very close to the 50-50 ratio. This translates to a small increase in maximum load capacity. Specifically, the load capacity increases from 80 ksi to 84 ksi or about 3.8 percent. One important difference in this laminate compared to the quasi-isotropic laminate is that the mode of failure is shearout at both holes. For the

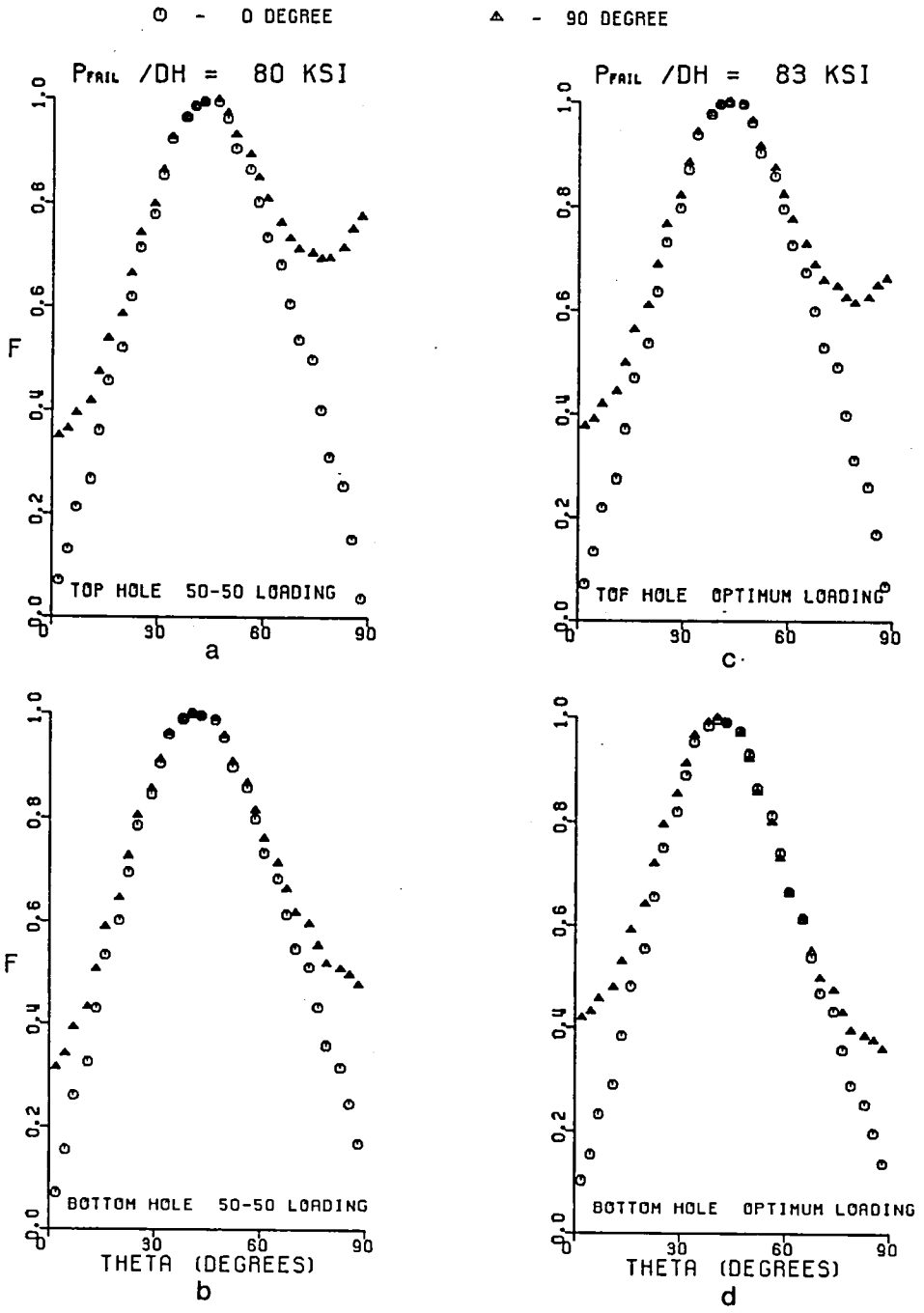

Fig. 6.10 F vs. θ for a Cross-Ply Laminate, W/D=5, E/D=3, G/D=3, D=1/2.

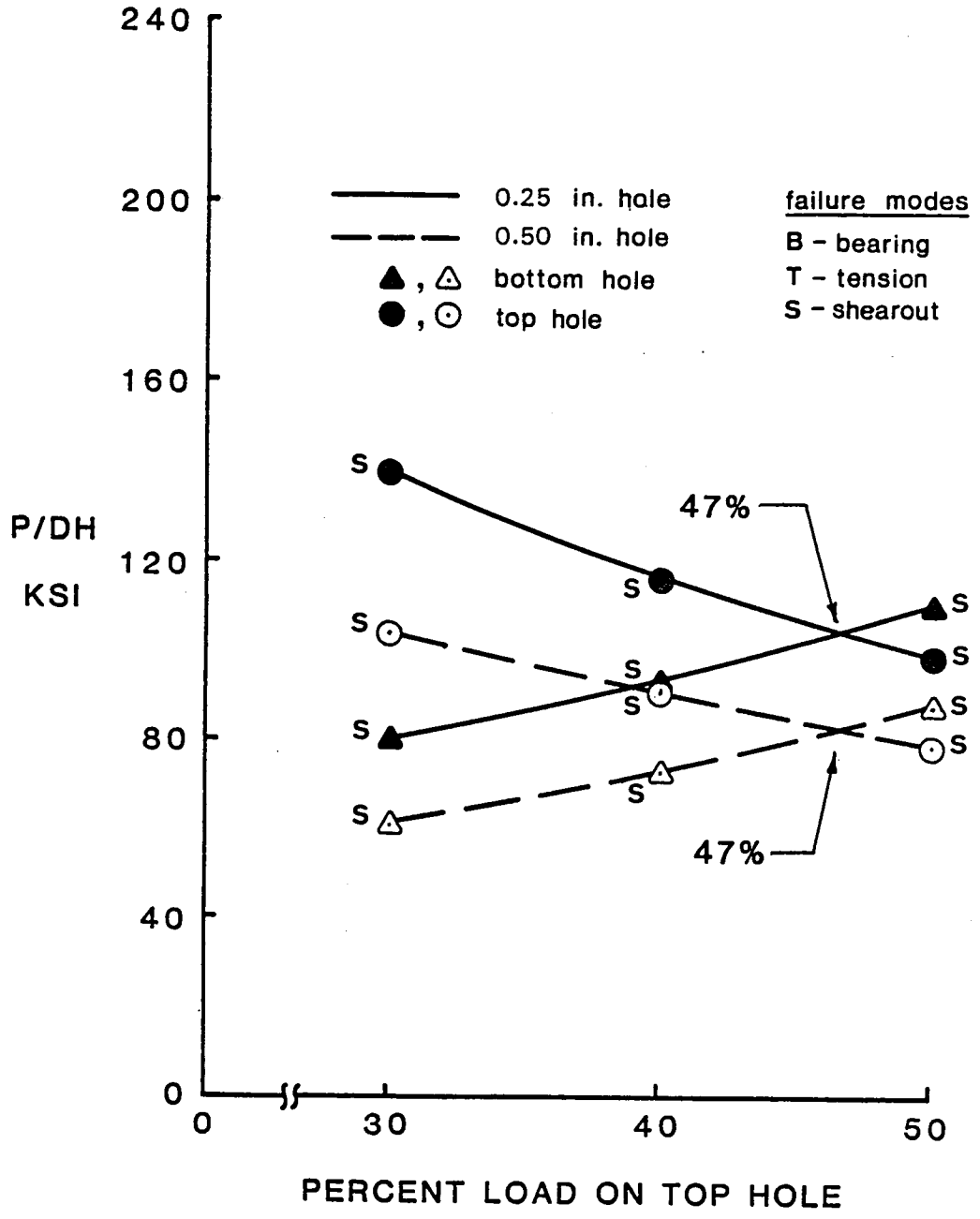

Fig. 6.11 Failure Characteristics for a Cross-Ply Laminate, W/D=5, E/D=3, G/D=3.

quasi-isotropic case the top hole failed in net-section tension and the bottom hole failed in bearing. In addition, for the cross-ply the plies at both orientations fail. This is in contrast to the quasi-isotropic laminate where the 90 degree ply usually governed laminate failure at each hole. This case is shown as case 1 in Table 6.2.

The 1/4 in. diameter hole, case 5 in Table 6.2, for the cross-ply laminate is quite similar in all respects to the 1/2 in. diameter hole case. The variation of F with location around each hole in each ply is shown in Fig. 6.12a-6.12d. The variation of failure load with load proportion is shown as solid lines in Fig. 6.11. The mode of failure, the pattern of the F value variation, the optimum load ratio, and the small increase in maximum load capacity is nearly identical. With a 50-50 load proportion the joint with 1/4 in. diameter hole fails at 99 ksi. At the optimum ratio, the failure load is 106 ksi. There is an increase in the joint capacity when comparing the 1/4 and 1/2 in. cases. This is again due to the hole-size effect on strength. Table 6.2 summarizes the information for this baseline cross-ply case, as well as data to be discussed.

The third laminate in the baseline study is a 45 degree angle-ply layup. Figs. 6.13a and 6.13b show the variation of F in each ply, around each hole. As can be seen, with the 50-50 load ratio both ply orientations fail at the net-

Table 6.2 Results for Cross-Ply Laminates.

CASE NO.	GEOMETRY W/D	E/D	G/D	D (in.)	MAXIMUM LOAD 50-50 (ksi)	OPT. (ksi)	OPTIMUM LOAD RATIO (%)	CAPACITY DECREASE (%)
1	5	3	3	1/2	80	83	47	1.00
2	5	3/2	3	1/2	68	73	53	0.88
3	5	3	3/2	1/2	60	73	41	0.88
4	3	3	3	1/2	73	78	46	0.94
5	5	3	3	1/4	99	106	47	1.00
6	5	3/2	3	1/4	84	92	54	0.87
7	5	3	3/2	1/4	68	88	39	0.83
8	3	3	3	1/4	91	97	45	0.92
9	5	3/2	3/2	1/2	60	63	47	0.76
10	3	3	3/2	1/2	59	70	42	0.83
11	3	3/2	3	1/2	68	70	52	0.83
12	3	3/2	3/2	1/2	59	62	47	0.75
13	5	3/2	3/2	1/4	70	75	45	0.71
14	3	3	3/2	1/4	68	83	39	0.78
15	3	3/2	3	1/4	83	86	52	0.81
16	3	3/2	3/2	1/4	68	73	46	0.69

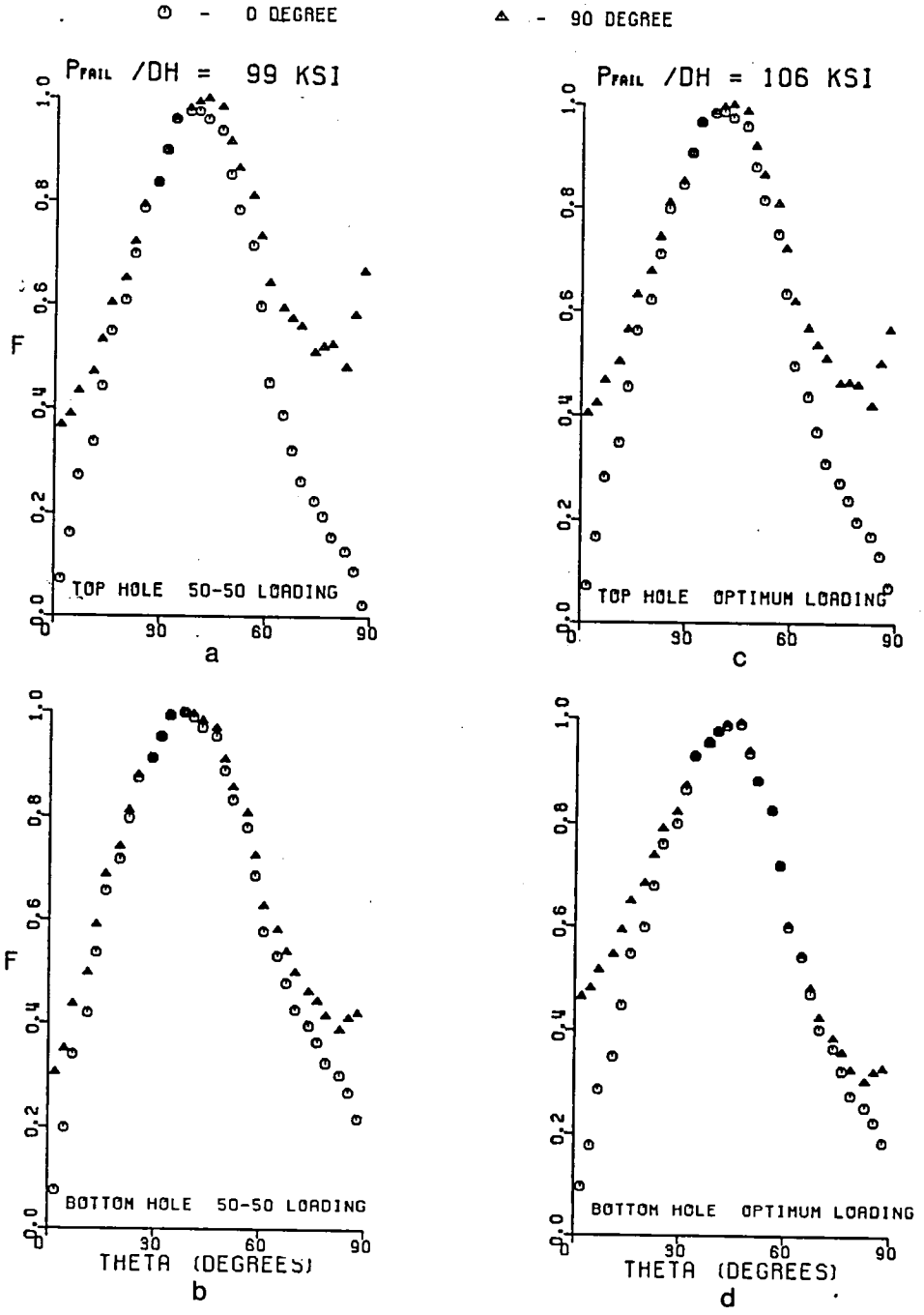

Fig. 6.12 F vs. θ for a Cross-Ply Laminate, W/D=5, E/D=3, G/D=3, D=1/4.

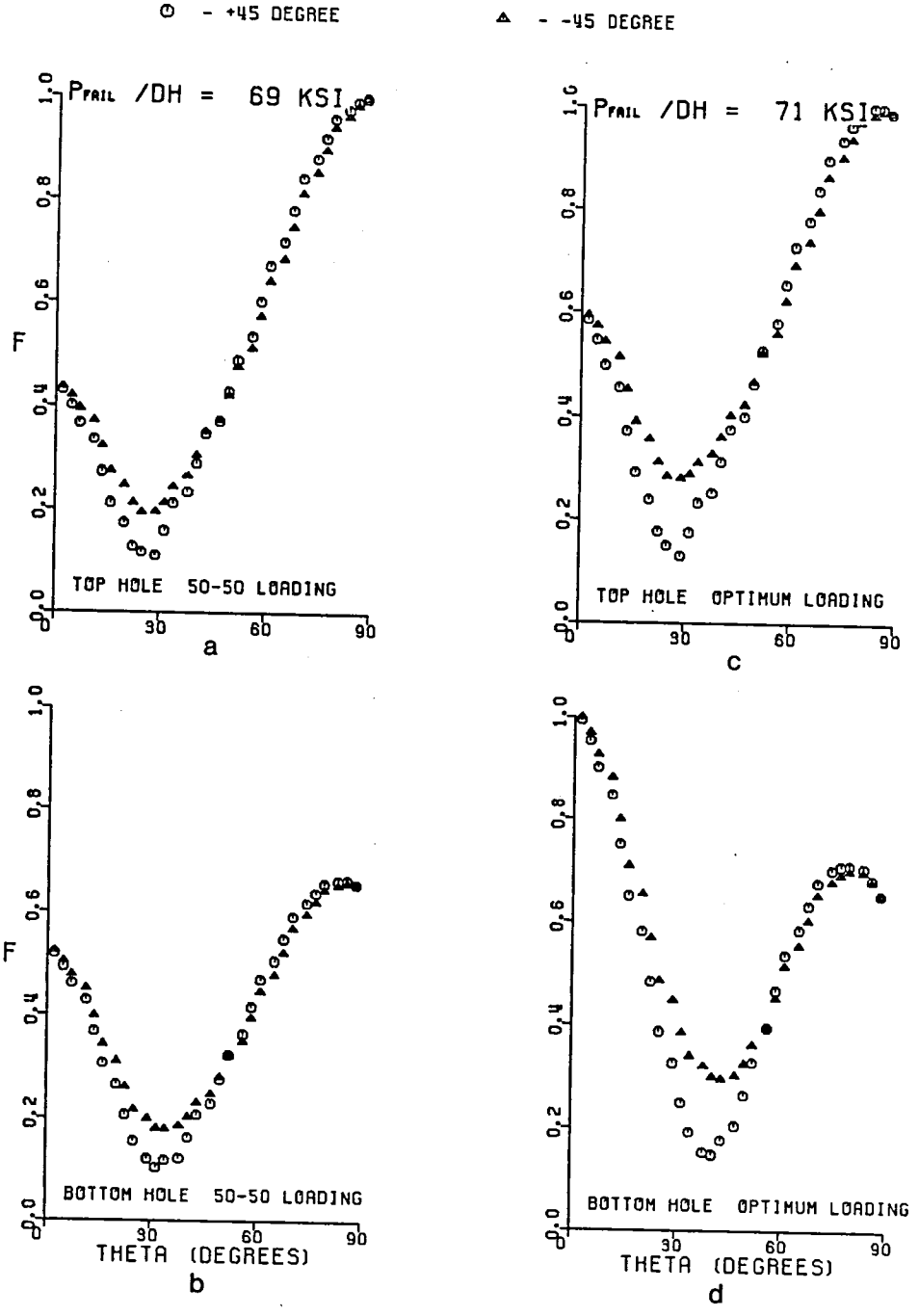

Fig. 6.13 F vs. θ for an Angle-Ply Laminate, W/D=5, E/D=3, G/D=3, D=1/2.

section of the top hole. The bottom hole figure shows the failure mode to be tending to a net-section failure mode. However the lower hole is only at about 70% of its capacity. Fig. 6.14 shows the failure characteristics of the joint as a function of load proportion. The 1/2 in. case, indicated as case 1 in **Table** 6.3, shows an optimum load ratio of 43-57. This ratio results in the variation of F around the hole as shown in Fig. 6.13c and 6.13d. Here it is seen that the top hole failure mode remained the same. There was a small increase in joint capacity, increasing from 69 ksi to 71 ksi, or about 2.9 percent. With the optimum load proportion, the lower hole has changed from a net-section failure to a bearing failure mode. This is seen by observing that the maximum value of F at the bottom hole is at $\theta = 0^{\circ}$. At the 50-50 load ratio, the maximum value of F there occurred at $\theta = 90^{\circ}$.

The variation of F with θ for the 1/4 in. diameter hole, case 5 in **Table** 6.3, is shown in Fig. 6.15a-6.15d. The general shape of these variations are very similar to the 1/2 in. hole case. Referring to Fig. 6.14, the optimum load ratio, however, is quite different for this smaller hole. The maximum joint capacity occurs when the first hole carries only 32% of the total load. The optimum load ratio results in an increase of the joint maximum capacity from 75 ksi at the 50-50 load ratio to 83 ksi at the preferred ratio

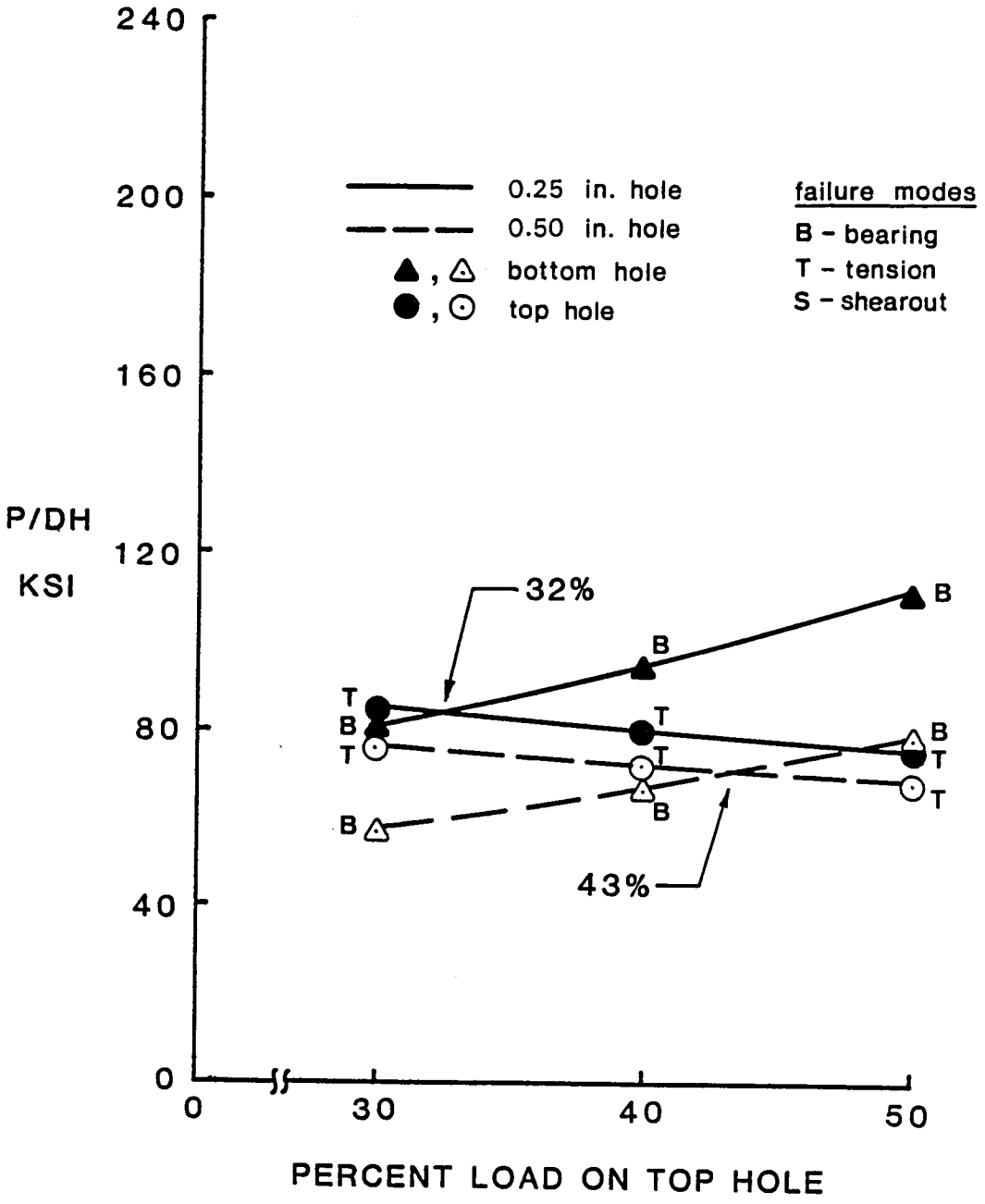

Fig. 6.14 Failure Characteristics for an Angle-Ply Laminate, W/D=5, E/D=3, G/D=3.

Table 6.3 Results for Angle-Ply Laminates.

CASE NO.	GEOMETRY W/D	E/D	G/D	D (in.)	MAXIMUM LOAD 50-50 (ksi)	OPT. (ksi)	OPTIMUM LOAD RATIO (%)	CAPACITY DECREASE (%)
1	5	3	3	1/2	69	71	43	1.00
2	5	3/2	3	1/2	70	70	50	0.99
3	5	3	3/2	1/2	64	66	44	0.93
4	3	3	3	1/2	44	49	18	0.69
5	5	3	3	1/4	75	83	32	1.00
6	5	3/2	3	1/4	77	80	42	0.96
7	5	3	3/2	1/4	74	78	30	0.94
8	3	3	3	1/4	48	54	18	0.65
9	5	3/2	3/2	1/2	60	60	50	0.85
10	3	3	3/2	1/2	42	46	17	0.65
11	3	3/2	3	1/2	44	46	22	0.65
12	3	3/2	3/2	1/2	42	45	23	0.63
13	5	3/2	3/2	1/4	66	68	38	0.82
14	3	3	3/2	1/4	48	52	10	0.63
15	3	3/2	3	1/4	48	52	26	0.63
16	3	3/2	3/2	1/4	46	53	20	0.64

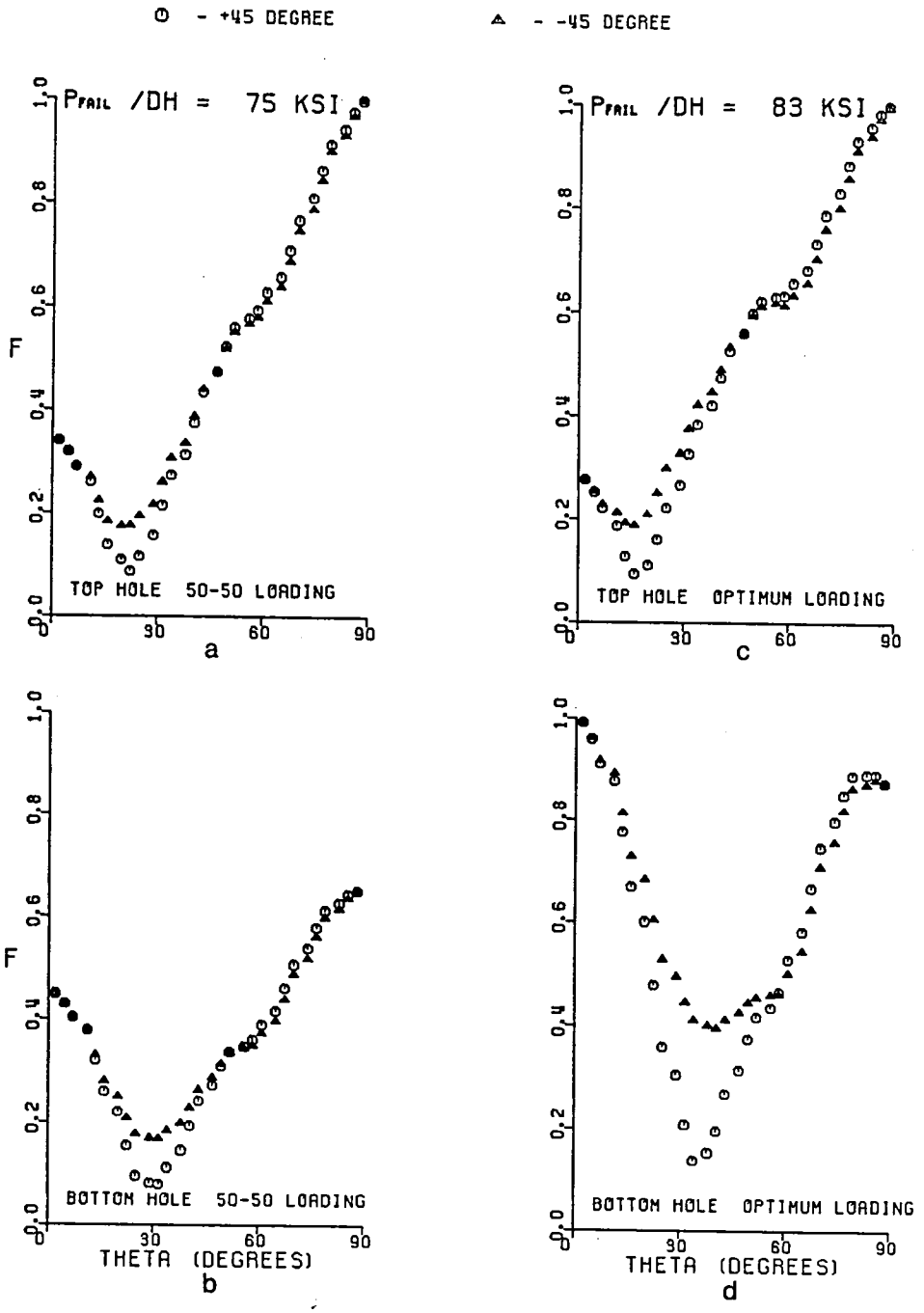

Fig. 6.15 F vs. θ for an Angle-Ply Laminate, W/D=5, E/D=3, G/D=3, D=1/4.

of 32-68, an increase of 10.7%. Table 6.3 summarizes these and other results for the angle-ply case.

Before proceeding further, it is important to determine the significance of the results obtained so far. From the results, it appears that for the baseline geometry, the load capacity of a quasi-isotropic joint can be increased by 5-6%, depending on hole diameter, if a load ratio other than 50-50 is used. For the cross-ply laminate, a load ratio of 47-53 results in about a 4% increase in capacity. For the angle-ply laminate, the increase in capacity is from 3% and 11%, for the 1/2 in. and 1/4 in. diameter holes, respectively. In no case does the number represent a large increase in capacity. Why? This is due primarily to the insensitivity of the top hole failure load to load proportion. This is evidenced by the shallow slope of the top hole failure characteristic vs. load proportion in each of the three figures, Figs. 6.8, 6.11, 6.14. Based on these findings, it can be said that for the baseline cases, the redistribution of load between the two holes leads to minimal increases in joint efficiency. Whether or not this is the case for other joint geometries is discussed next.

Geometric Comparisons

To assess the impact of differing geometries on the maximum joint load and on the optimum load proportion, a comparison of the previously discussed baseline case, W/D = 5, E/D = 3, and G/D = 3, with other geometric configurations will be made. This comparison will vary one of the geometric variables and contrast the results to the baseline case. Then another variable will be changed and the results compared again. This variation of parameters will be done until the influence of each particular geometric parameter on the joint load and optimum load ratio has been examined. With three geometric parameters, this comparison results in many different cases to compare with the original baseline case. In addition, two hole sizes are considered. This comparison will be carried out for the three laminates included in this study. The study of the influence of joint geometry on the the optimum failure load is important because changes in geometry translate into changes in the amount of material in a joint, and hence changes in weight. If load capacity drops only a slight amount for a significant decrease in joint weight, the design with smaller load capacity could be warranted.

Quasi-Isotropic Laminates

Recall that Fig. 6.8 showed the failure load characteristics for 1/2 in. and 1/4 in. diameter holes for

the baseline geometry of W/D = 5, E/D = 3, and G/D = 3 for the quasi-isotropic laminate. Fig. 6.16 shows the failure load characteristics for the case where the end distance E/D has been shortened by a factor of two, i.e., W/D = 5, E/D = 3/2, and G/D = 3. This is case 2 in Table 6.1. Comparing the 1/2 in. diameter hole cases (dashed lines) in **Figs.** 6.8 and 6.16 it is clear that the optimum load ratio shifts from 42-58 to 39-61 as end distance shortens. However the maximum joint load remains about the same, namely 135 ksi. Also, the mode of failure remains the same for both cases, tension at the top hole and bearing at the bottom hole. For the 1/4 in. diameter hole case (solid lines) the optimum load ratio stays the same, 37-63 for both cases. Also the maximum joint load is the same, 168 ksi. One important change, however, is the change in failure mode. In the baseline case with E/D = 3, the mode of failure at the bottom hole is bearing. However, when the edge distance ratio E/D is shortened to 3/2, the failure mode shifts from bearing to net-section tension at the bottom hole.

The second case of differing geometry is shown in Fig. 6.17. This figure shows the failure load characteristics for the case where the two holes are closer together than the baseline geometry, namely, W/D = 5, E/D = 3, G/D =3/2. This is case 3 in Table 6.1. Comparing the 1/2 in. diameter case of the baseline geometry, **Fig.** 6.8, with this altered

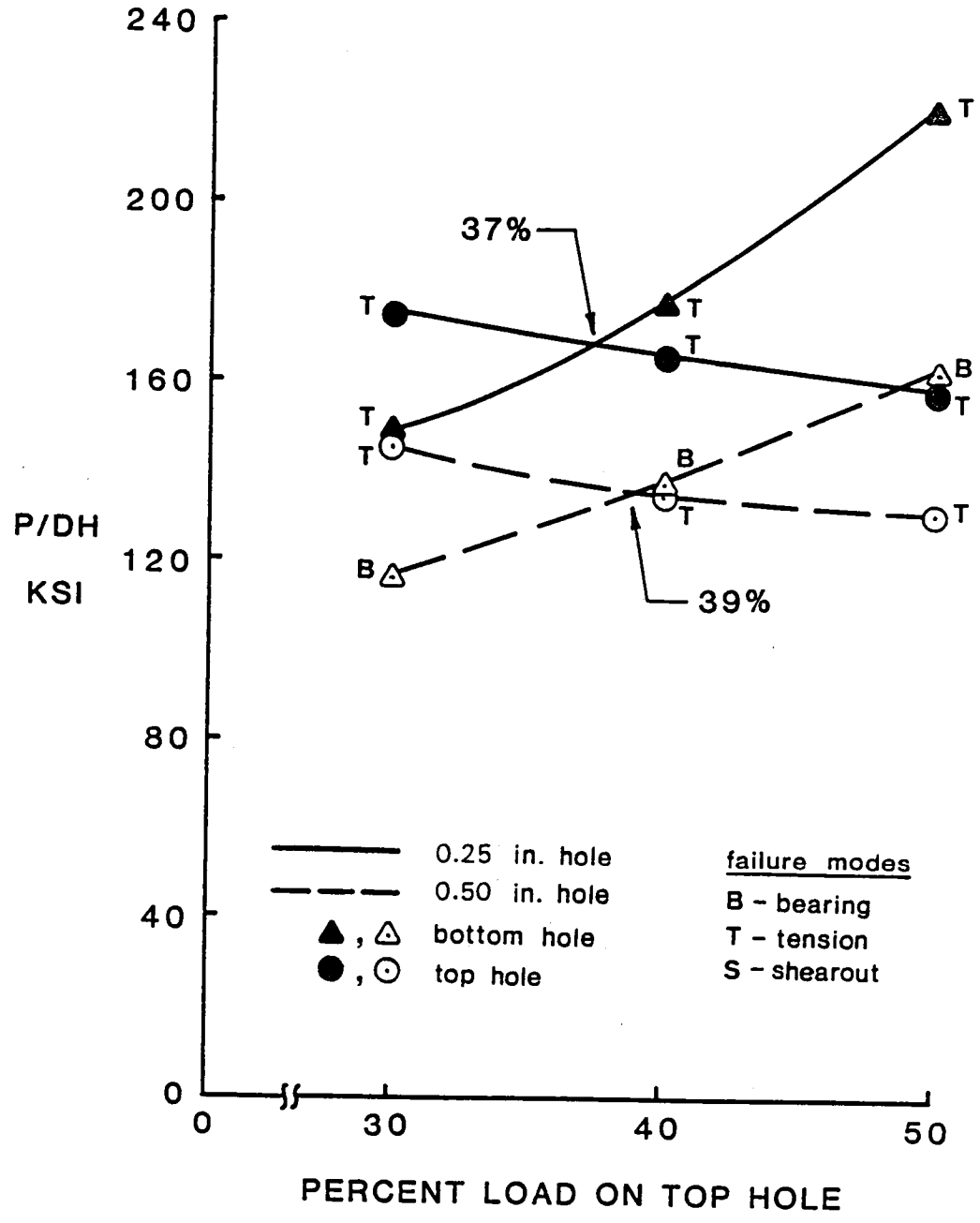

Fig. 6.16 Failure Characteristics for a Quasi-Isotropic Laminate, W/D=5, E/D=3/2, G/D=3.

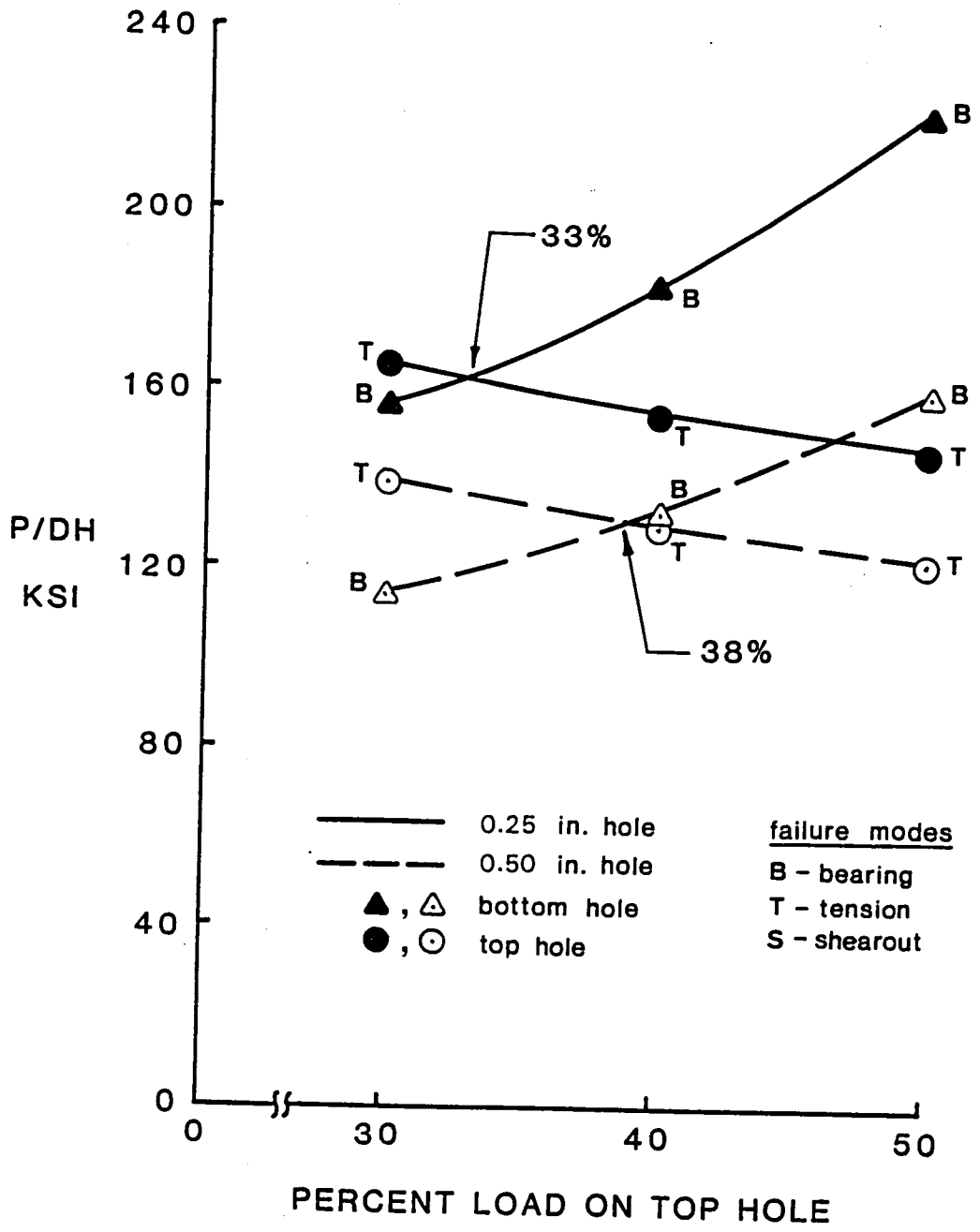

Fig. 6.17 Failure Characteristics for a Quasi-Isotropic Laminate, W/D=5, E/D=3, G/D=3/2.

geometry it is clear that the optimum load ratio is shifted from 42-58 to 38-62 due to moving the holes closer together. In addition, the failure load is reduced from 135 ksi to about 130 ksi. These changes are fairly small in magnitude and would not warrant attention in the design stage. The failure mode for baseline and closer hole geometric configurations is the same at both holes.

Examining the influence of the hole being closer together in the 1/4 in. diameter hole, case 7 of Table 6.1, a shift in the optimum load ratio from 37-63 to 33-67 and a slight decrease in maximum joint load from 167 ksi to 162 ksi is observed. As in the 1/2 in. case, the failure modes remain unaffected by this change in geometry.

The final geometry variation, case 4 of Table 6.1, is the reduction of the joint width from W/D = 5 to W/D = 3, the other variables being E/D = 3, and G/D = 3. This results in a much narrower joint. Fig. 6.18 shows the failure load characteristics for this case of W/D = 3, E/D = 3, and G/D = 3. Compared to the baseline case of W/D = 5, E/D = 3, G/D = 3, Fig. 6.8, some dramatic differences can be observed. In the 1/2 in. diameter case the optimum load ratio has dropped from 42-58 to 18-82. This represents a large reduction of load being reacted at the top hole. Also compared to the baseline case, the maximum joint load is reduced from 140 ksi to 102 ksi. The failure mode is the

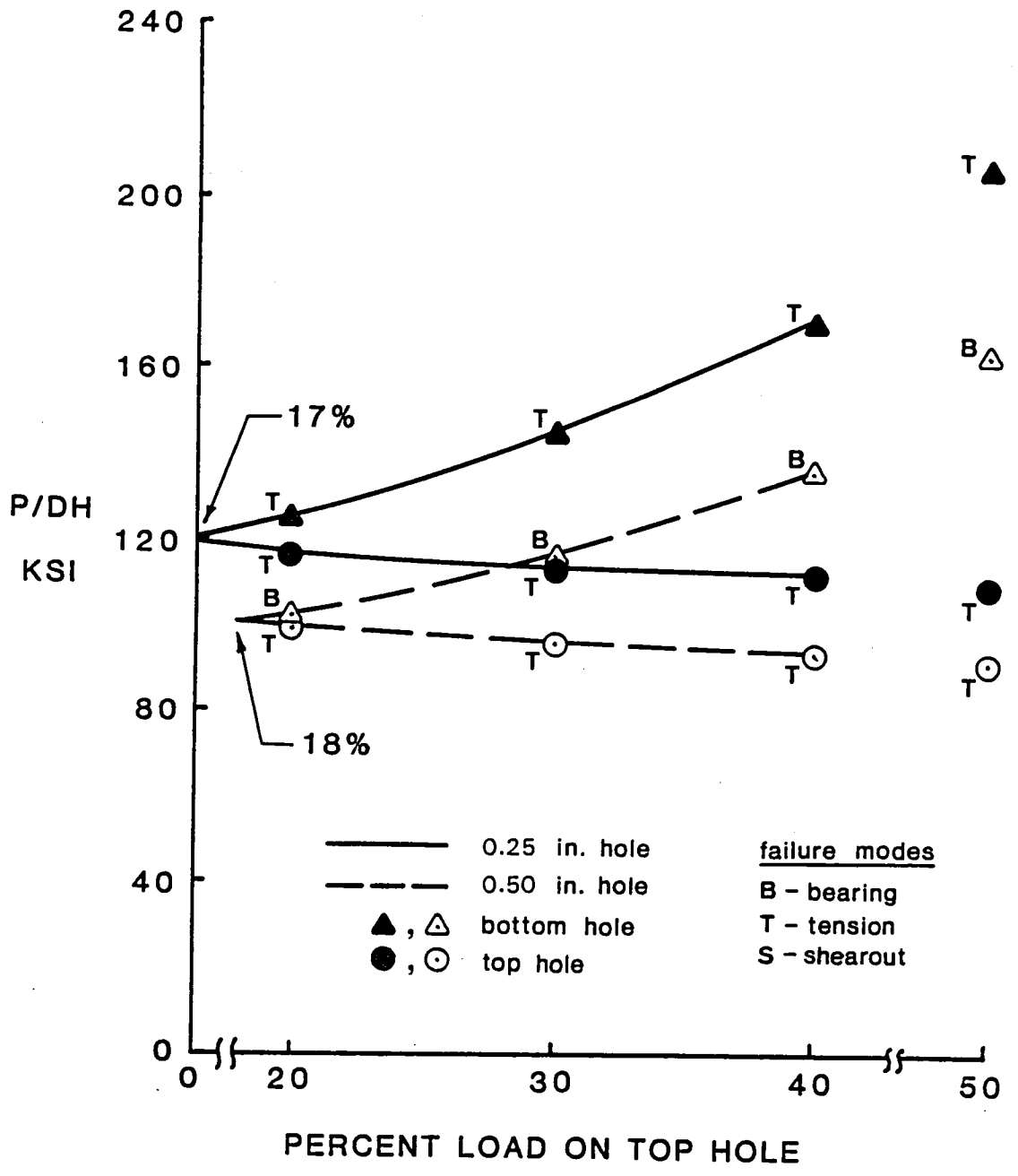

Fig. 6.18 Failure Characteristics for a Quasi-Isotropic Laminate, W/D=3, E/D=3, G/D=3.

same for both the baseline and narrower joint cases, net-section tension at the top hole and bearing at the bottom hole. The 1/4 in. diameter hole also suggests large changes in the optimum load ratio due to changing joint width, changing from 37-63 to 17-83. The maximum joint load is reduced from 168 ksi to about 121 ksi. In addition, there is a shift in the failure mode at the bottom hole. The shift is from bearing in the baseline case to net-tension in the case where the width is reduced to W/D = 3.

The three comparisons just discussed were made to show the influence of a particular geometric parameter on failure load, optimum load ratio, and mode of failure of quasi-isotropic laminates. Table 6.1 can be used to quickly assess the effects of these changes. Table 6.1, and also Tables 6.2 and 6.3, show a column labeled CAPACITY DECREASE. This is the optimum load for a particular set of geometric parameters and a particular hole size, divided by the optimum load for the baseline case, with the same hole size. For example, the 0.73 in case 4 of Table 6.1 is the optimum load of 102 ksi divided by the 140 ksi optimum load for a joint with 1/2 in. diameter holes, case 1. Likewise, the 0.72 of case 8 is the result of computations for the 1/4 in. diameter hole, i.e., 121/168 = 0.72.

Before considering the influence of the parametric changes on the other two laminates it is important to

summarize the influence of these geometric changes on load capacity and optimum load ratio for the quasi-isotropic laminate.

Shortening the end distance does little to influence the optimum load ratio or the optimum load capacity. Because it is slightly shorter, this geometric change results in a sightly lighter joint. The change in failure mode, relative to the baseline case, at the bottom hole from bearing to tension for the 1/4 in. hole diameter case is not considered significant.

Moving the holes closer together lowers joint capacity more than shortening end distances. This is because the stresses around one hole are influenced by the proximity of the other hole. This situation should be avoided unless the weight savings from the shorter joint offsets the decreased capacity.

Using a narrower joint greatly alters the situation relative to the baseline case. For both hole sizes capacity is reduced a significant amount. For the narrower joint, the failure locus of the top hole moves downward and thus intersects the locus of the bottom hole at a much lower load proportion and also at a much lower failure load. In addition, the failure locus of the bottom hole drops some. It is clear that the closeness of the hole to the edge of the joint is responsible for this behavior.

Cross-ply Laminates

Fig. 6.11 showed the failure characteristics for the baseline geometry of W/D = 5, E/D = 3, and G/D = 3 for the cross-ply laminate. For both hole diameter cases the optimum load ratio was 47-53. Also, the mode of failure at both hole locations was shearout. Fig. 6.19 shows the failure characteristics for cross-ply joints with shorter end distances, i.e. W/D = 5, E/D = 3/2, and G/D = 3. This is case 2 in Table 6.2. It can be seen that for both the 1/2 and 1/4 in. diameter holes the optimum load ratio occurs when the first hole is loaded more than the second hole! The failure modes are also shearout for both holes. The failure load for the 1/2 in. hole in the baseline geometry case at the optimum load ratio is about 82 ksi. In the case where the E/D ratio is 3/2, the maximum joint strength at the optimum load ratio is 73 ksi, a decrease in capacity. For this case the optimum load ratio occurs at 53-47.

For the 1/4 in. holes the baseline case yields a joint strength at the optimum load ratio of 106 ksi while the E/D = 3/2 (case 6 of Table 6.2) yields a value of 92 ksi. Shearout is the failure mode. For this shorter joint the optimum load proportion is 54-46.

Fig. 6.20 illustrates the result on the failure characteristics of the cross-ply laminate of changing the hole spacing ratio, G/D, to 3/2. In the 1/2 in. case the

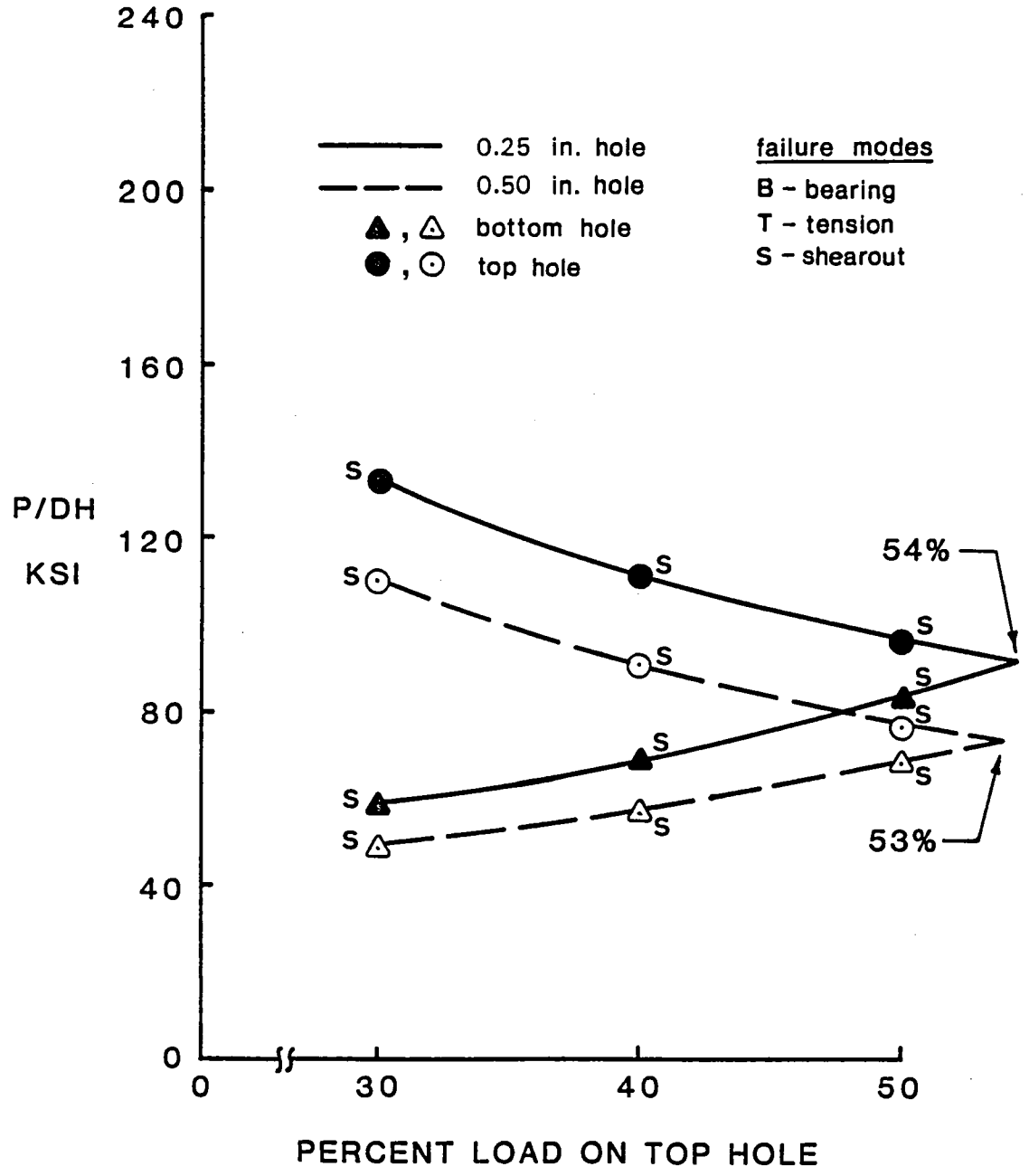

Fig. 6.19 Failure Characteristics for a Cross-Ply Laminate, W/D=5, E/D=3/2, G/D=3.

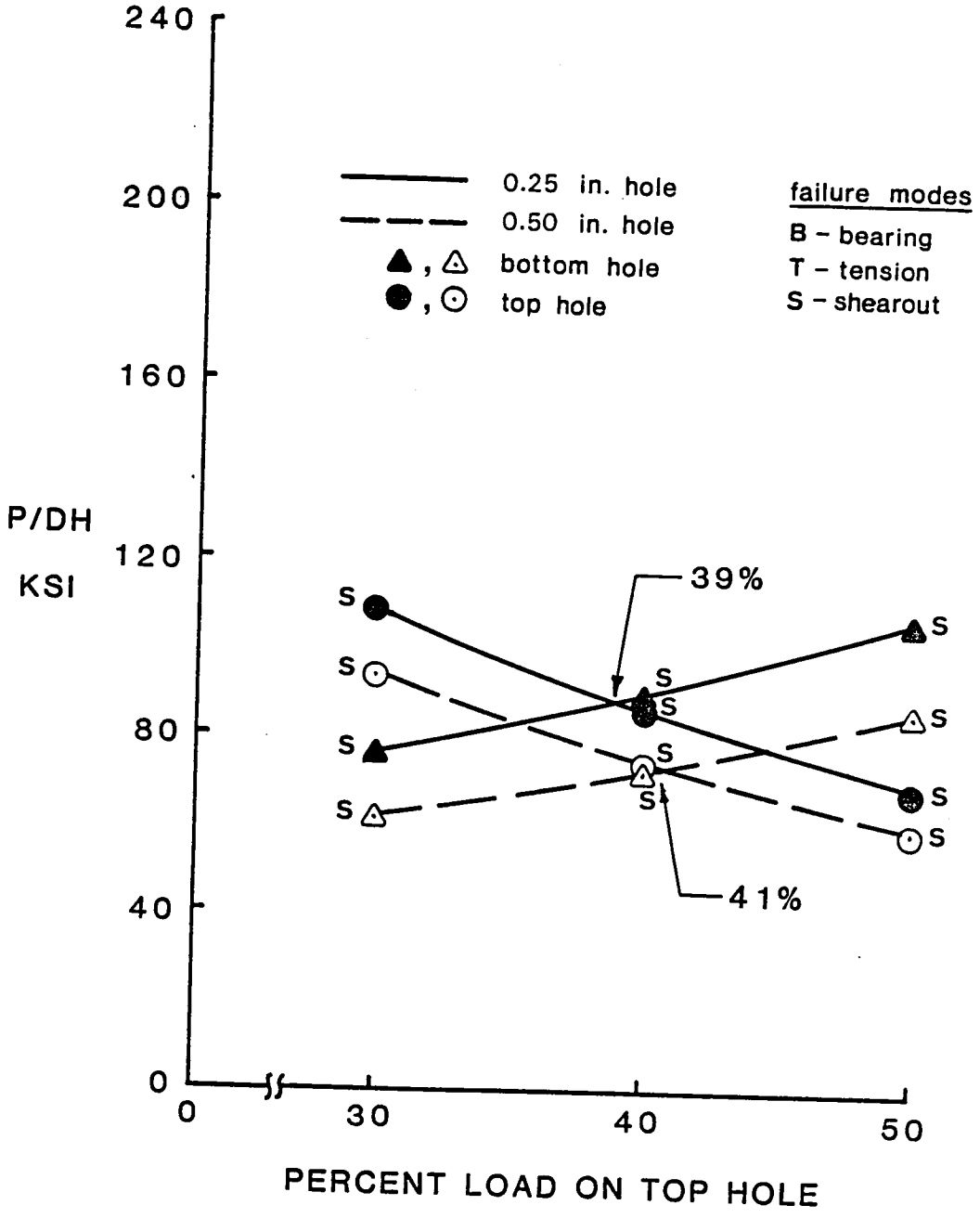

Fig. 6.20 Failure Characteristics for a Cross-Ply Laminate, W/D=5, E/D=3, G/D=3/2.

optimum load ratio is 41-59 compared to 47-53 for the baseline case. The maximum joint load at the optimum load ratio decreases from 83 ksi in the baseline case to 73 ksi for the G/D = 3/2 case. The joint with a 1/4 in. diameter hole shows a reduction from 106 ksi in the baseline case to about 88 ksi for this value of G/D. Again, for all situations the mode of failure is shearout.

Fig. 6.21 illustrates the effect of narrowing the cross-ply joint from a W/D = 5 to a W/D = 3. Recall, this reduction of joint width resulted in significantly less strength for the quasi-isotropic case. In the case of the cross-ply we see similar results but the reduction is somewhat less. As seen in **Fig.** 6.11, the baseline case showed the optimum load ratio for both the 1/2 and 1/4 in. holes to be about 47%. The W/D = 3 case yields similar results, the optimum ratios being 45% and 46%, respectively for the 1/2 in. and 1/4 in. diameter holes. The baseline case has a maximum joint strength for the 1/2 in. hole of about 83 ksi and the narrowed geometry has about a 73 ksi strength. Similarly the 1/4 in. hole with W/D = 5 and W/D = 3 have joint strengths of 106 ksi and 88 ksi, respectively. The failure modes for all load ratios is again, shearout.

Before proceeding to the third laminate, the influences of these geometric changes on the cross-ply joints should be summarized. Table 6.2 summarizes information for this

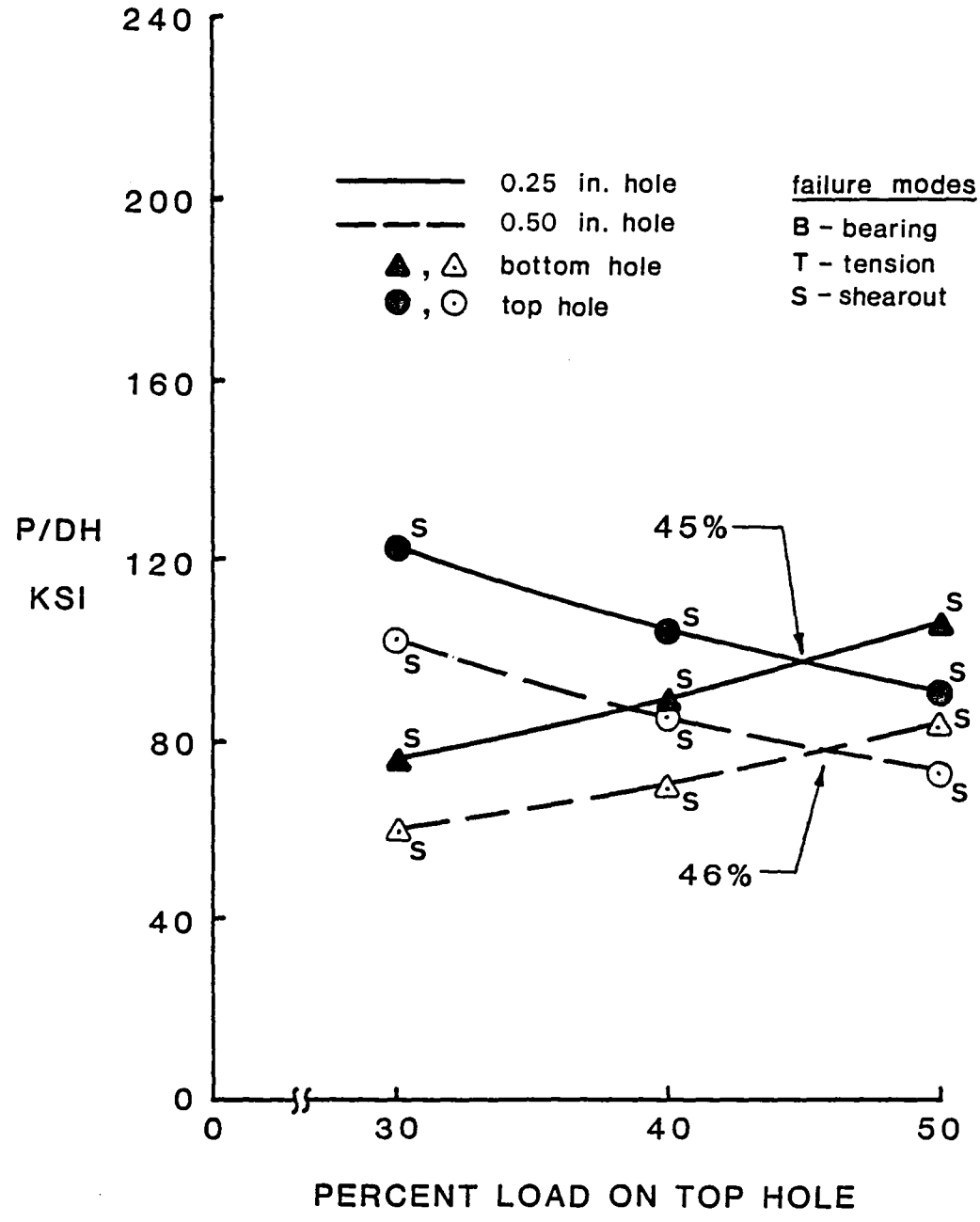

Fig. 6.21 Failure Characteristics for a Cross-Ply Laminate, W/D=3, E/D=3, G/D=3.

cross-ply case, particularly the capacity decrease.

Compared to the baseline case, shortening the end distance in the cross-ply joint decreases the optimum load capacity. From Fig. 6.19 it can be seen that the decreased capacity is due to a weaker second hole. The failure loci for the top holes are about the same for both the E/D = 3 and E/D = 3/2 cases (**Figs.** 6.11 and 6.19). However, the failure loci for the bottom holes drop significantly when E/D changes from 3 to 3/2. This drop results in lower load capacity.

Moving the holes closer together does not influence the failure locus of the bottom hole, for either the 1/2 in. or 1/4 in. diameter holes. However, for both the 1/2 in. and 1/4 in. diameter holes, the failure locus of the top hole is lowered by moving the holes closer together. As a result both the load proportion and the optimum load decrease relative to the baseline case.

Making the joint narrower decreases capacity. However, compared to the effect of narrowing a quasi-isotropic joint, narrowing a cross-ply joint does not have as dramatic an effect. This is because the cross-ply joint fails in the shear-out mode. For this mode, interaction with the sides of the joint is not important as it is with net-section tension, the mode that controls failure of the quasi-isotropic joint.

Angle-ply Laminates

Fig. 6.14 showed the failure loci for the baseline geometry for the angle-ply laminate used in this study. Comparison of this baseline case to the case with E/D = 3/2, W/D = 5, G/D = 3, shown in Fig. 6.22, shows a change in the optimum load ratio to 50-50 for the 1/2 in. diameter hole and to 42-58 for the 1/4 in. diameter hole. The modes of failure are the same as in the baseline case for both 1/2 in. and 1/4 in. diameter holes, net-tension occurring at the top hole and bearing failure at the bottom hole. The optimum load for the 1/2 in. diameter hole is basically unaffected by shortening the end of the joint. The load capacity for the 1/4 in. diameter hole case decreases by 4% by shortening the joint.

The failure loci for the case with G/D = 3/2 are shown in Fig. 6.23. The optimum load ratio for the 1/2 in. hole (case 3 in Table 6.3) is 44-56. This is nearly the same as the baseline value of 43-57. The 1/4 in. hole loci yield a value of 30-70 for the optimum load ratio. Again, this compares closely with the 32-68 ratio of the baseline case. The failure modes for the holes closer together are the same as the baseline case, net-tension at the top hole and bearing at the bottom hole. The maximum joint load for the 1/2 in. hole at the optimum load ratios decreases from 70 ksi for the baseline case to 66 ksi for the G/D = 3/2

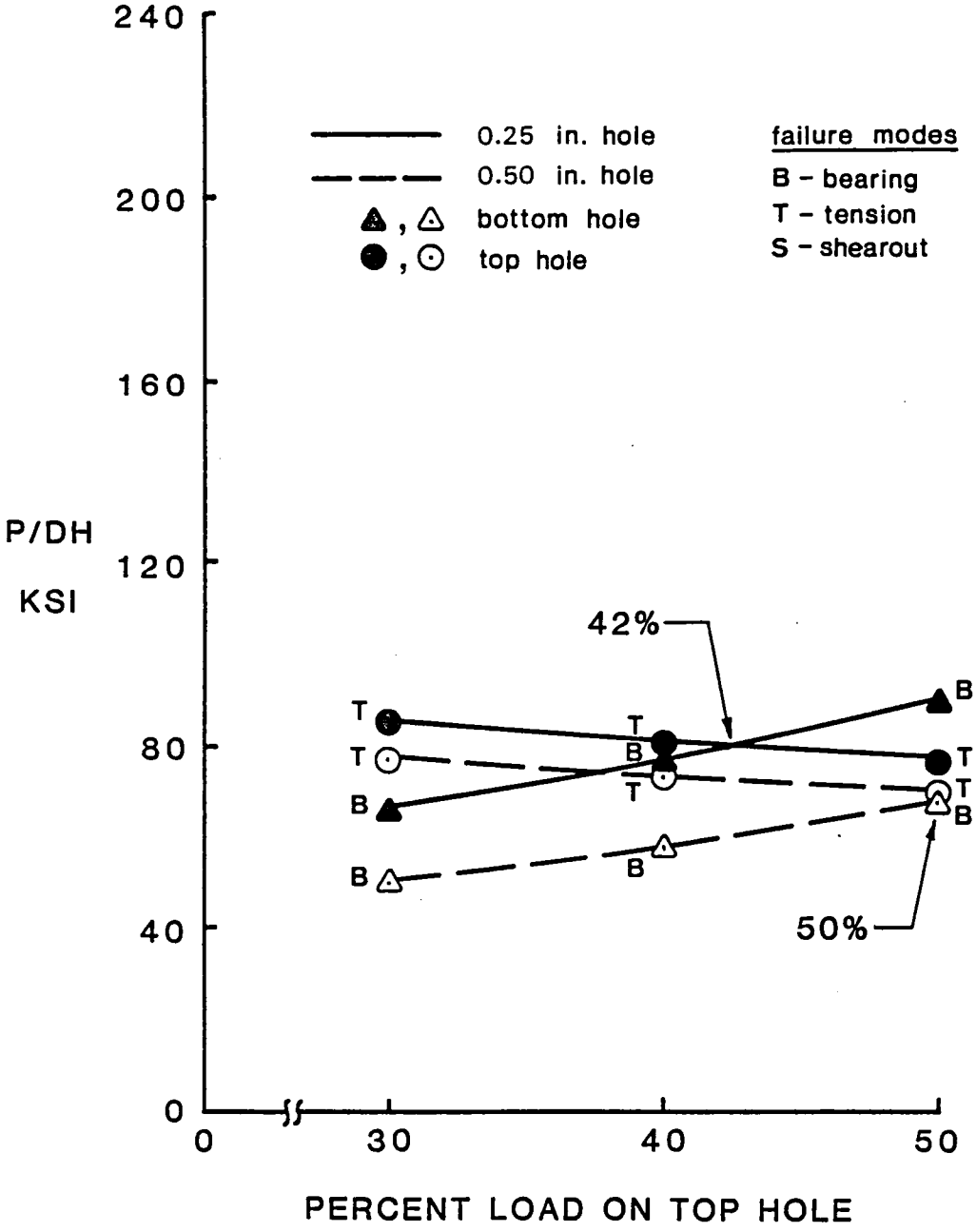

Fig. 6.22 Failure Characteristics for an Angle-Ply Laminate, W/D=5, E/D=3/2, G/D=3.

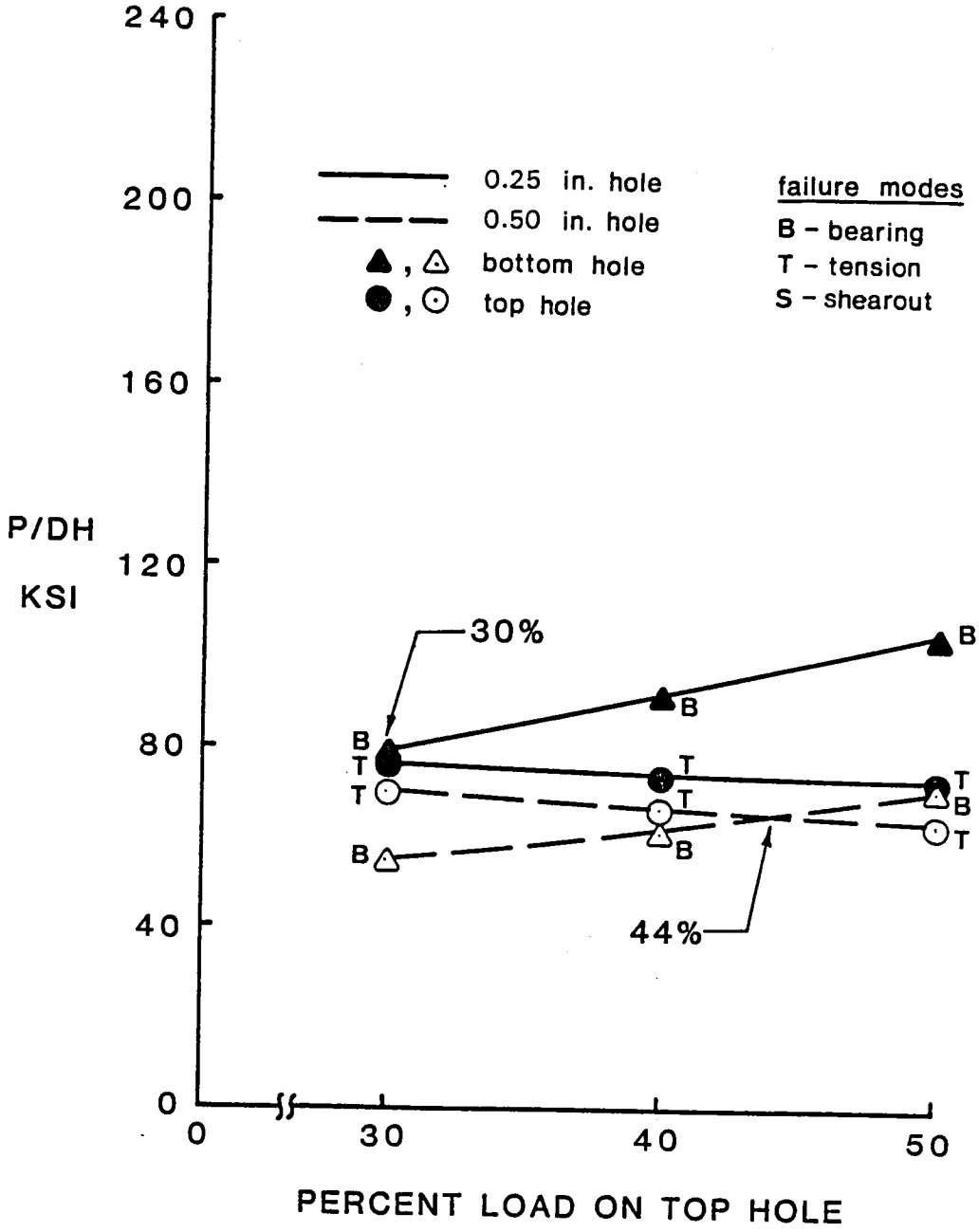

Fig. 6.23 Failure Characteristics for an Angle-Ply Laminate, W/D=5, E/D=3, G/D=3/2.

case. The 1/4 in. hole yields a similar decrease in load from 83 ksi to 78 ksi. These reflect a 6 and 7% decrease in load, respectively.

The effect of narrowing the angle-ply joint is shown in Fig. 6.24. For the 1/2 in. hole (case 4 of Table 6.3) the optimum load ratio is drastically reduced from the 43-57 for the baseline case to a load ratio of 18-82 for the narrower joint. Similarly for the 1/4 hole in. hole the load ratio is reduced from 32-68 to 18-82. In both cases the load capacity is significantly reduced. In addition, the mode of failure changes at the bottom hole to a net-tension mode. This is an expected result since the plate width is much narrower and the amount of material at net section is significantly reduced, thus increasing the tensile stress values. Narrowing the joint decreases the optimum failure load from 71 ksi for the 1/2 in. baseline case to 48 ksi. For the 1/4 in. hole narrowing the joint decreases the capacity from 83 ksi in the baseline case to 53 ksi for the case where W/D = 3.

Influence of Combined Geometric Variations

The previous text covered the effects of a variation of the geometry parameters. However, each of these parameters was varied independently and the ramifications due to a specific geometric parameter were addressed. It is obvious more than one parameter can be varied at one time. To fully

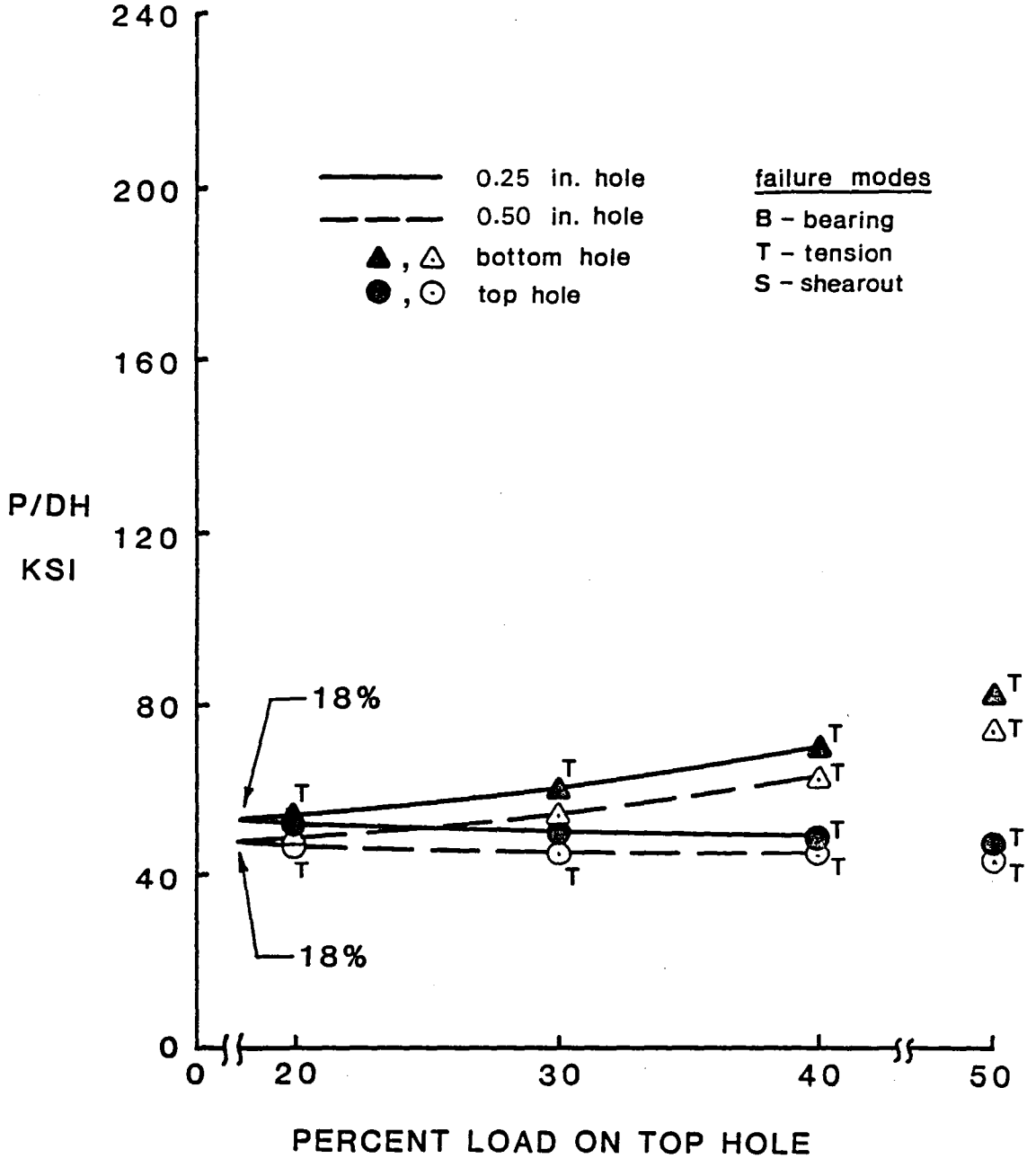

Fig. 6.24 Failure Characteristics for an Angle-Ply Laminate, W/D=3, E/D=3, G/D=3.

cover all of the combinations of the geometric parameter variations would entail many more comparisons, some of which would be repetitive. Therefore, the rest of this chapter will deal with only the geometric combinations which yield peculiar results for a particular laminate. The tables summarize the important information for all combinations studied.

Quasi-Isotropic Laminates

The influence of a shorter edge distance, E/D = 3/2, when used with a narrow, W/D = 3, joint is apparent in Fig. 6.25. The overall joint capacity is not changed relative to the 50-50 case to any great extent. However, the optimum load ratio is reduced to about **25-75.** This points out the fact that with this geometric configuration, the joint reacts most of the load at the top hole. In order to improve joint efficiency, a high proportion of the total joint load needs to be reacted at the lower hole. In addition, the mode of failure has an influence on the magnitude of the optimum lower hole load. Fig. 6.25 shows that for the 1/4 in. diameter hole case, the top hole hole is failing in a net-section tensile mode. This is usual for this laminate. However, the bottom hole has made a transition from a bearing mode to a tensile-bearing failure mode. This clearly shows the influence of reducing the end distance. The reduction induces a tensile failure mode at

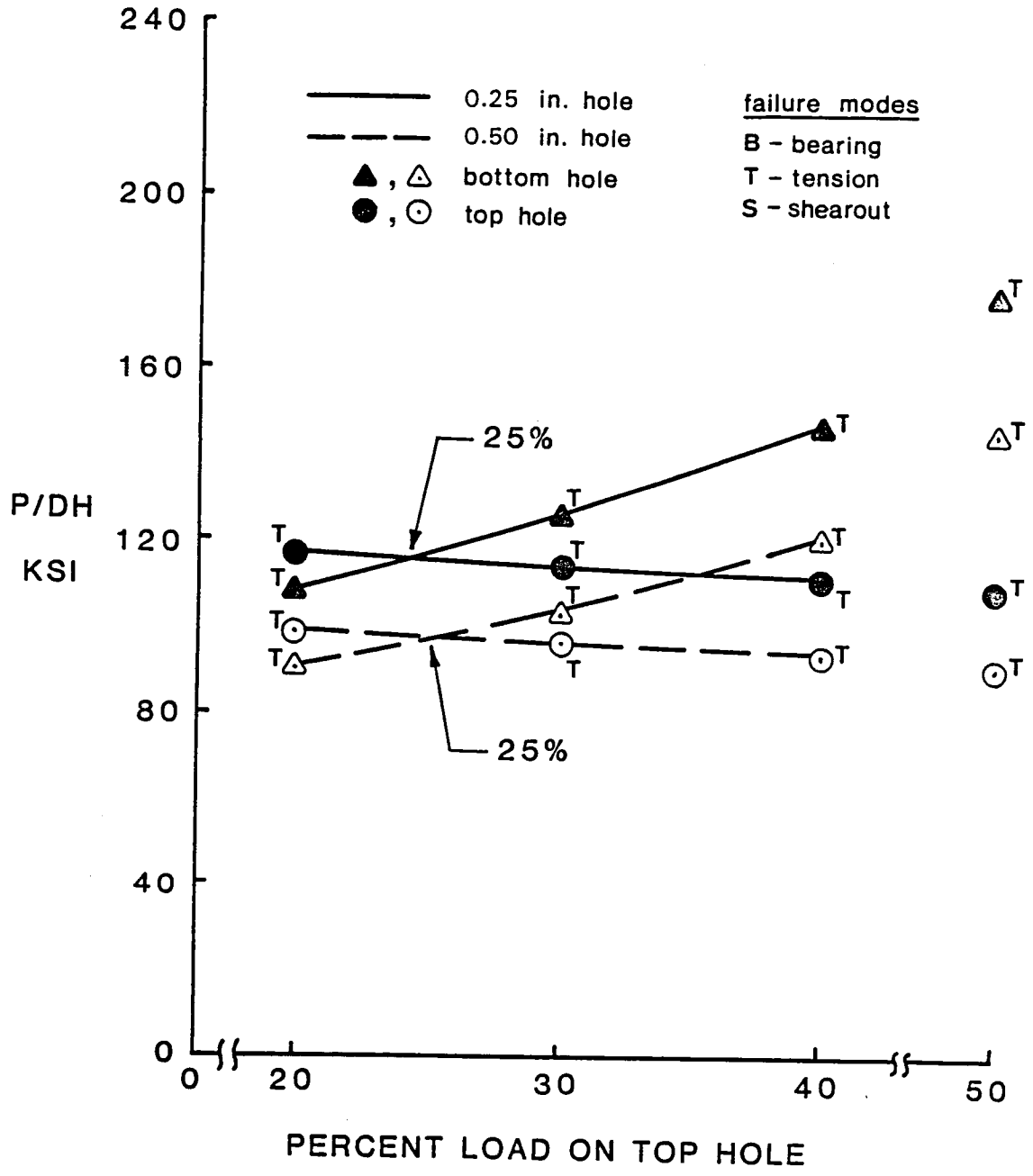

Fig. 6.25 Failure Characteristics for a Quasi-Isotropic Laminate, W/D=3, E/D=3/2, G/D=3.

the bottom hole.

The geometric factor which has the largest impact on overall joint capacity for the quasi-isotropic laminate is the W/D ratio. For both hole diameters, the narrower joint showed a marked decrease in load capacity. In addition, for the 1/4 in. diameter case, a narrower joint induced a change in failure mode at the bottom hole from bearing to net-section tension. This influence did not show up in the 1/2 in. diameter hole case.

Cross-Ply Laminates

In contrast to the quasi-isotropic laminate, the major influence on load capacity was not the W/D ratio but rather shortening the end distance, or reducing the hole spacing, or a combination of both. When these two parameters were changed, there was a large decrease in joint capacity. This illustrates again the interaction of the mode of failure with the geometric parameters. This laminate fails in a shearout mode in all cases. When the holes are moved closer together, the interacting stress fields will have a large influence on the shearout stresses. Likewise, when the end distance is shortened, the amount of material to dissipate the shearout stress is reduced, thus increasing the importance of this mode of failure. When the joint width is narrower, the influence on joint capacity is rather small. This reinforces the observation that the shearout stresses

and the mode of failure associated with them are concentrated in a region near the holes and they do not extend toward the edges of the plate.

For the cross-ply case one geometry, W/D = 3, E/D = 3/2, and G/D = 3 shown as cases 11, 15 in **Table** 6.2, indicated that for maximum joint performance the top hole should react a higher portion of the load than the bottom hole. This is illustrated in Fig. 6.26.

Angle Ply Laminates

When compared to the quasi-isotropic cases this laminate showed similar failure modes. Like the quasi-isotropic case, the major geometric parameter in terms of influence on joint capacity and optimum load ratio was the W/D ratio. The most extreme of these was the case where W/D =3, E/D = 3, and G/D = 3/2, as shown in Fig. 6.27. The 1/4 in. diameter hole, case 14, indicated that a load ratio of 10-90 should be used for maximum joint capacity. The load ratio for the 1/2 in. case was found to be 17-83. These are rather extreme values and indicate the great influence of geometry on the optimum load ratio.

Comments on the Failure Criteria

The failure analysis of these three laminates was based on the Yamada-Sun failure criteria. As was pointed out earlier, this criteria assumes that the σ_2 stress has little influence on the ultimate failure of the laminate. To

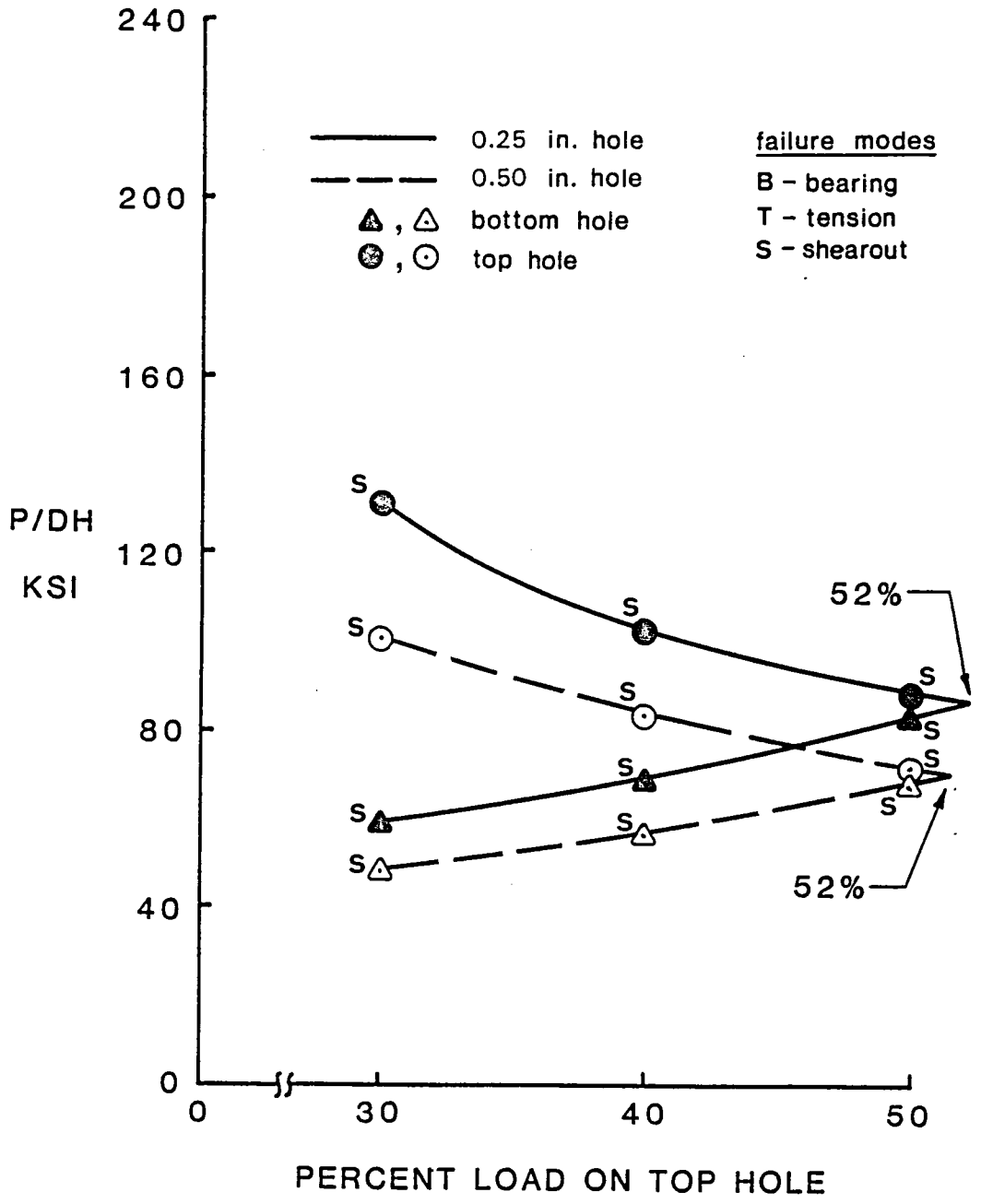

Fig. 6.26 Failure Characteristics for a Cross-Ply Laminate, W/D=3, E/D=3/2, G/D=3.

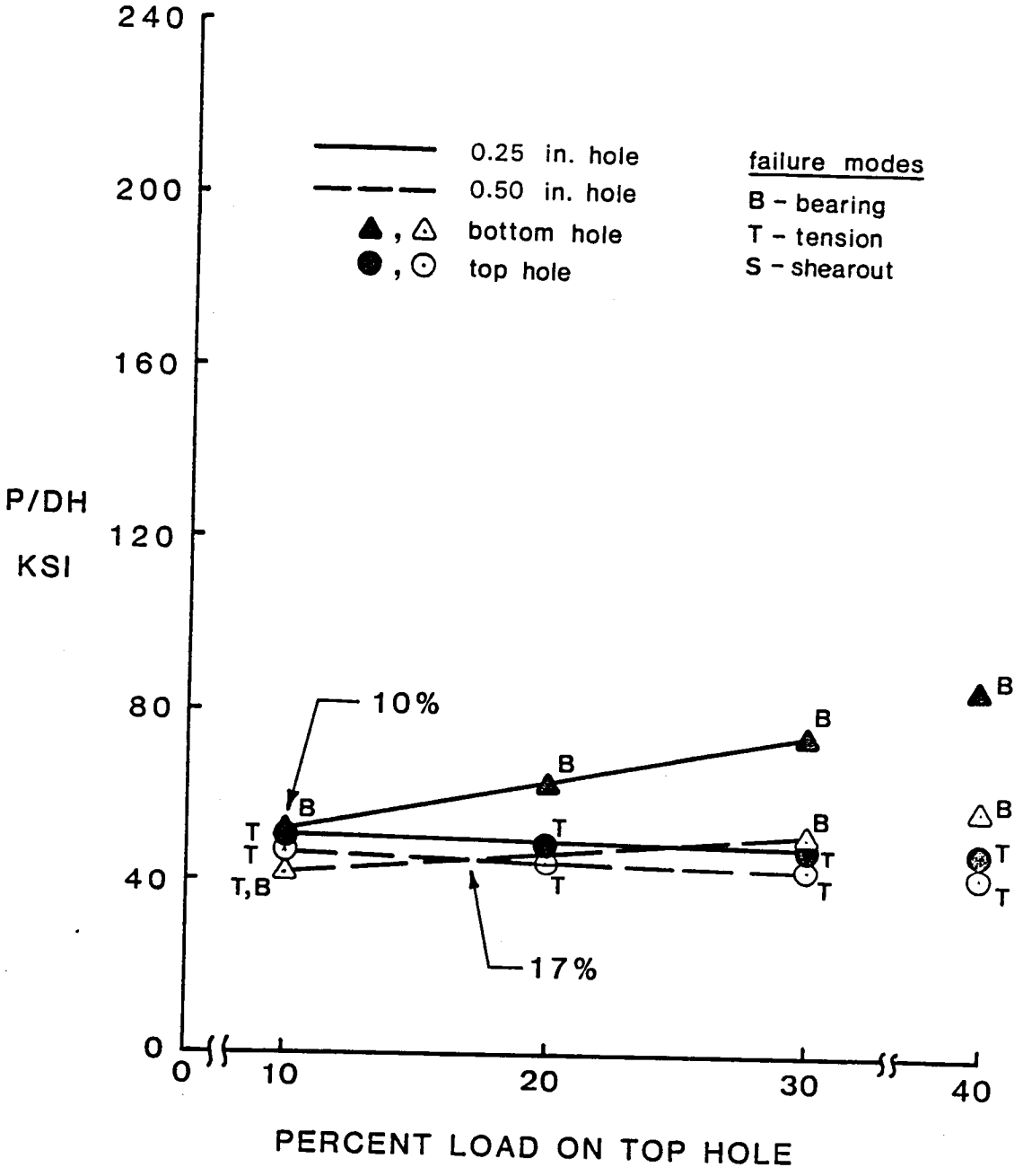

Fig. 6.27 Failure Characteristics for an Angle-Ply Laminate, W/D=3, E/D=3, G/D=3/2.

address this assumption, a short study was conducted to compare the Yamada-Sun with two other criteria. One of these other two criteria is a Yamada-Sun-like criteria with a σ_2 term included. The other is a maximum stress criteria. Appendix A contains the results of this study as well as a brief explanation of the details of this analysis.

The failure characteristics vs. load ratio and also the Yamada-Sun values for each laminate are available in ref. 31. For the sake of brevity, these are not included here.

CHAPTER 7

SUMMARY AND CONCLUSIONS

The major phases of this study can be categorized into four major areas:

1) A literature review was conducted to determine the extent of work previously done to investigate the stress state in one and two-hole bolted joints. The scope of this review was limited to applications which had a direct bearing on the main thrust of this study.

2) Finite-element analyses of a single-hole pin-loaded plate were conducted. This was considered as a validation step for the finite-element model used in this study and also to briefly acquaint the reader with the stress states around a loaded hole in a orthotropic plate. These results were compared to previous work.

3) Finite-element studies were made to examine a two-hole bolted joint. Some of these results were compared with work performed by another investigator. Since many of the results presented from this phase of the study do not seem to be available elsewhere, this work represents a contribution to the literature.

4) A 'graphical' optimizing algorithm was implemented to find the load proportion which resulted in maximum load capacity. Implicit in the algorithm was a failure criteria, specifically the Yamada-Sun criteria, used in conjunction with the idea of a characteristic curve.

5) The load proportion that resulted in the maximum capacity was found for three laminates and for variations in the important geometric parameters.

From the last phase of the study, it can be concluded that,

1) In general, to achieve the maximum joint capacity of a two-hole joint, 50% of the load should not be reacted at each hole. For most cases, the lower hole should react a higher percentage of the total load than the top hole.

2) The percentage of load to react at each hole is highly dependent on both geometry and laminate elastic properties.

3) Although the optimum load ratio can differ from the standard 50-50 to as much as 9-91, the gain in using the optimum load ratio is quite small,

usually only 5-10%. In a few cases a capacity increase of 15-29% is indicated.

4) The mode of failure is influenced by both the laminate elastic properties and the geometry of the joint.

Although this study has addressed and answered some important questions about joint behavior, there are some avenues where further work would be important for advancements in the state of the art of bolted composite joints.

1) Conduct experimental investigations to verify the current stress predictions. These tests would also confirm the findings of the study if the strengths determined experimentally did not vary outside normal experimental scatter, reinforcing the fact that most cases indicate little gain in overall joint capacity.

2) Investigate other laminates and geometries which indicate a larger payoff for the load tailoring concept.

REFERENCES

1. W.G. Bickley, "The Distribution of Stress Around a Circular Hole in a Plate, Philos. Trans. R. Soc. London, Ser. A, Vol. 227, Aug. 1928, pp. 383-415.

2. D.W. Oplinger, "On the Structural Behavior of Mechanically Fastened Joints in Composite Structures", Fibrous Comp. in Structural Design, 1980, pp. 575-602.

3. J.P. Waszcak, T.A. Cruse, "Failure Mode and Strength Predictions of Anisotropic Bolt Bearing Specimens", J. Comp. Mat., Vol. 5, July 1971, pp. 421-425.

4. J.H. Crews, C.S. Hong, I.S. Raju, "Stress-Concentration Factors for Finite Orthotropic Laminates with a Pin-Loaded Hole", NASA TP 1862, May 1981.

5. T.A. Collings, "The Strength of Bolted Joints in Multi-Directional CFRP Laminates", Composites, Vol. 8, Jan. 1977, pp. 43-55.

6. T.A Collings, M.J. Beauchamp, "Bearing Deflection Behaviour of a Loaded Hole in CFRP", Composites, Vol. 15, Jan. 1984, pp. 33-38.

7. G.R. Pyner, F.L. Matthews, "Comparison of Single and Multi-Hole Bolted Joints in Glass Fibre Reinforced Plastic", J. Comp. Mat., Vol. 13, July 1979, pp. 232-239.

8. E.W. Godwin, F.L. Matthews, P.F. Kilty, "Strength of Multi-Bolt Joints in GRP", Composites, Vol. 13, No. 3, July, 1982, pp. 268-272.

9. E.W. Godwin, F.L. Matthews, "A Review of the Strength of Joints in Fibre-Reinforced Plastics", Composites, Vol. 11, July 1980, pp. 155-160.

10. J.R. Eisenmann, J.L. Leonhardt, "Improving Composite Bolted Joint Efficiency by Laminate Tailoring", Joining of Composite Materials, ASTM STP 749, 1981, pp. 117-130.

11. S.R. Soni, "Failure Analysis of Composite Laminates with a Fastener Hole", Joining of Composite Materials, ASTM 749, 1981, pp. 145-164.

12. S. W. Tsai, E. M. Wu, "A General Theory of Strength for Anisotropic Materials", J. Comp. Mat., Vol. 5, 1971, pp. 58-60.

13. L. J. Hart-Smith, "Bolted Joints in Graphite-Epoxy Composites", NASA CR-144899, June 1976.

14. L. J. Hart-Smith, "Mechanically Fastened Joints for Advanced Composites - Phenomenological Considerations and Simple Analysis", Fibrous Composites in Structural Design, 1980, pp. 543-574.

15. S. P. Garbo, J. M. Ogonowski, "Effect of Variances and Manufacturing Tolerances on the Design Strength and life of Mechanically Fastened Composite Joints", AFWAL-TR-81-3041, Vols. 1-3, April 1981.

16. S. P. Garbo, D. L. Buchanan, "Design of High-Load Transfer Joints", A Collection of Technical Papers, AIAA, Paper No. 83-0905-CP, Lake Tahoe, Nevada, May 1983.

17. S. P. Garbo, M. L. Becker, "Carbon/Epoxy Laminates Under Combined Fastener Bearing and Tension Bypass Loading", A Collection of Technical Papers, AIAA, Paper No. 83-0967, Lake Tahoe, Nevada, May 1983.

18. M. W. Hyer, J. C. Perry, M. C. Lightfoot, "Load Transfer in Composite Bolted Joints", A Collection of Technical Papers, AIAA, Paper No. 80-0779-CP, Seattle, WA., May 1980.

19. M. W. Hyer, E. C. Klang, "Contact Streses in Pin-Loaded Orthotropic Plates", VPI-E-84-14, April 1984.

20. Hyer, M. W., Klang, E. L., and Cooper, D. E., "The Effects of Pin Elasticity, Clearance, and Friction on the Stresses in a Pin-Loaded Orthotropic Plate," VPI-E-85-09.

21. Klang, E. C. and Hyer, M. W., "The Stress Distribution in Pin-Loaded Orthotropic Plates," VPI-E-85-13.

22. Hyer, M. W. and Klang, E. C., "Contact Stresses in Pin-Loaded Orthotropic Plates," to appear, Int. J. Solid and Structures.

23. R. E. Rowlands, M. U. Rahman, T. L. Wilkinson, Y. I. Chiang, "Single- and Multiple-Bolted Joints in Orthotropic Materials", Composites, Vol. 13, No. 3, July 1982, pp. 273-278.

24. M. R. Rahman, "Stress and Strength Analysis of Double-Bolted Mechanical Joints in Orthotropic Materials", Ph.D. Dissertation, The University of Wisconsin-Madison, 1981.

25. F. K. Chang, R. A. Scott, G. S. Springer, "Strength of Mechanically Fastened Composite Joints", J. Comp. Mat., Vol. 16, Nov. 1982, pp. 470-494.

26. J. M. Whitney, R. J. Nuismer, "Stress Fracture Criteria for Laminated Composites Containing Stress Concentrations", J. Comp. Mat., Vol. 8, July 1974, pp. 253-265.

27. S. E. Yamada, C. T. Sun, "Analysis of Laminate Strength and Its Distribution", J. Comp. Mat., Vol. 12, pp. 275-284.

28. J. M. Bathe, E. A. Wilson, "Numerical Methods in Finite Element Analysis", Prentice-Hall, 1976.

29. R. M. Jones, "Mechanics of Composite Materials", McGraw-Hill, 1975.

30. F. K. Chang, "Strength of Bolted Joints in Laminated Composites", Ph.D. Dissertation, The University of Michigan, 1983.

31. Chastain, P. A., "Effects of Load Proportion on the Capacity of Multiple-Hole Composite Joints," M. S. Thesis in Engineering Mechanics, Virginia Polytechnic Institute and State University, 1985.

Appendix A

FAILURE CRITERIA ANALYSIS

Every failure criteria used for determination of the failure of a composite material incorporates assumptions regarding material behavior. The Yamada-Sun criteria [27] is no exception. As mentioned in Chapter 3, this criteria assumes that the σ_2 stress is not important in determination of the final failure load. Chang et al [25] have used this criteria successfully in strength determination of single- and double-hole joints. This appendix will verify the validity of the Yamada-Sun assumption.

Three failure criteria were used to study failure in two geometric configurations for three laminates. A unit loading with a load proportion of 50-50 was used. These criteria included the Yamada-Sun criteria, which is denoted as F in the following figures, the Maximum Stress criteria, represented as H in the figures, and a Yamada-Sun-like criteria with a σ_2 term included, denoted as G in the figures. This new term is the σ_2 stress divided by a strength value denoted as Y. This is the strength of a unidirectional laminate when loaded perpendicular to the fiber direction. In the absence of any specific data for this value, the value of the cross-ply shear strength, $S_{0/90}$, is used. This strength value is fairly close in magnitude to the matrix direction in-situ strength, Y.

Specifically, the three criteria are

$$F = \left(\frac{\sigma_1}{X}\right)^2 + \left(\frac{\tau_{12}}{S_{0/90}}\right)^2 \qquad (A.1)$$

$$G = \left(\frac{\sigma_1}{X}\right)^2 + \left(\frac{\sigma_2}{Y}\right)^2 + \left(\frac{\tau_{12}}{S_{0/90}}\right)^2 \qquad (A.2)$$

$$H = \left(\frac{\sigma_1}{X}\right)^2 \qquad (A.3)$$

The first geometric configuration is the baseline case, W/D=5, E/D=3, W/D=3, and D=1/2. Fig. A.1 shows the three criteria plotted as a function of the location around the top hole of a quasi-isotropic laminate. This figure shows F, G, and H values in each lamina. As can be seen, in the 0°, $+45^\circ$, and -45° plies there is a moderate discrepency between these criteria. There is some correlation, however, at the bearing and net-section regions around the hole. However, when examining the 90° ply, all three criteria coincide at both the net-section and bearing portion of the hole. It is important to keep in mind that the 90° ply corresponds to fibers in the direction of applied load. Recall that this particular case failed in net-section tension mode in both the experiment and finite-element model predictions. This is verified here by noting that the maximum value of F, G, and H occurs at the net-section

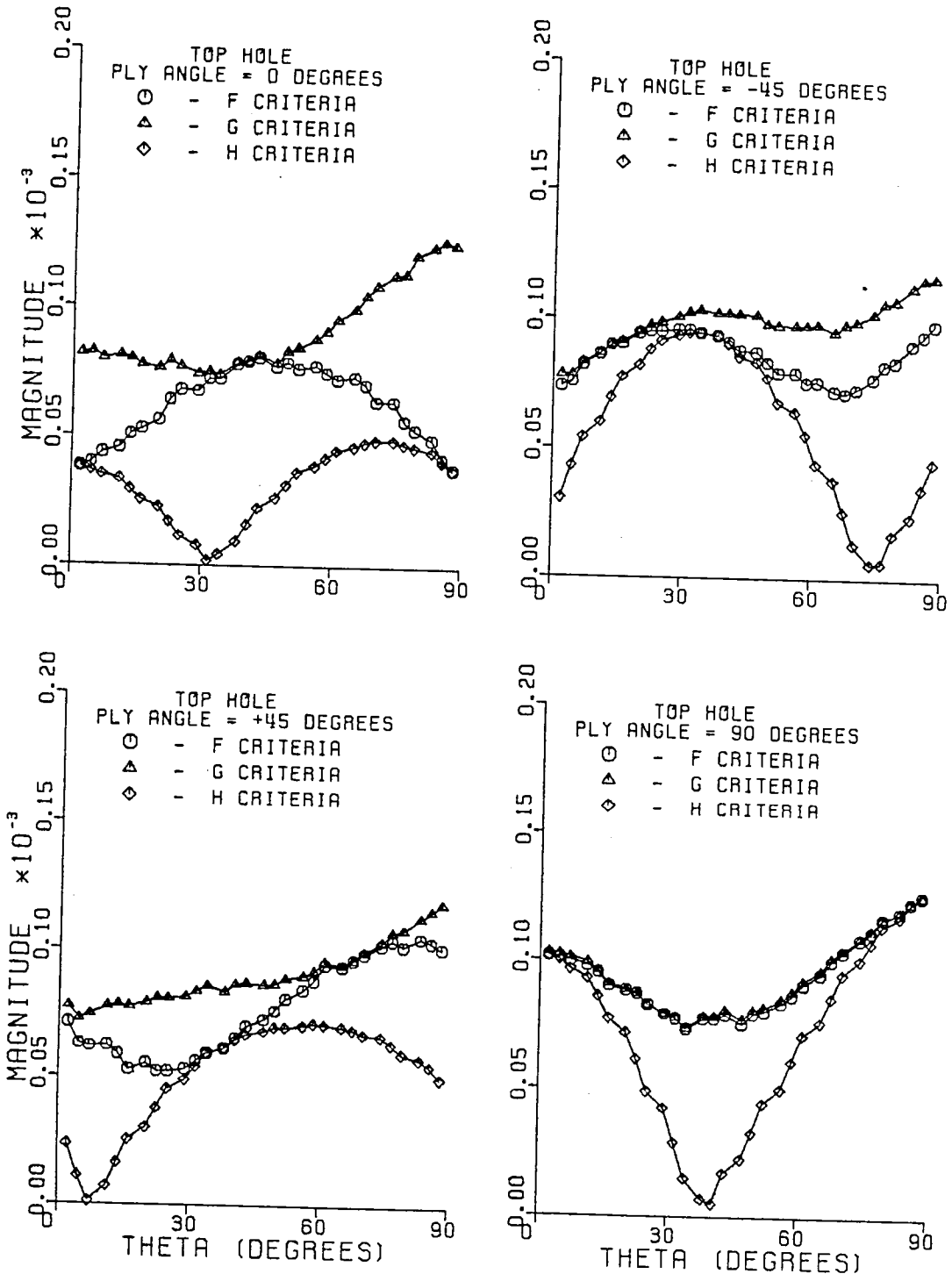

Fig. A.1 F, G, H vs. θ for a Quasi-Isotropic Laminate, Top Hole, W/D=5, E/D=3, G/D=3, D=1/2.

region of the hole in the 90° ply. This maximum value also occurs in the 0° ply at the net-section region. However, it is not practical to use the 0° ply as a reference for total laminate failure since a net-section failure would require fiber failure.

In Fig. A.2, the F, G, and H values are shown at the bottom hole for the same geometry and laminate. Note that again, the 90° ply shows a maximum value for all three. This time the maximum occurs at the bearing region of the hole. This was shown earlier in Chapter 6. All three of the criteria coincide at $\theta = 0^{\circ}$ in this ply. That is because this ply is the key ply to laminate failure.

Fig. A.3 shows the three criteria values at the top hole for a cross-ply laminate with the baseline geometry. One immediately notices that the Maximum Stress criteria (H) is nearly zero at the top hole. The F and G criteria, however, each have their maximums occurring near the 45° region around the hole in the 0° ply. A similar occurence can be seen the 90° ply also. This indicates that for this laminate, the τ_{12} term is important and σ_2 is not. Recall again, that the results shown in Chapter 6 indcated that this case failed in a shearout mode. Fig. A.4 shows very similar behavior for the bottom hole. A similar conclusion can be drawn that both the F and G criteria are appropriate to use for failure prediction. However, the σ_2 term

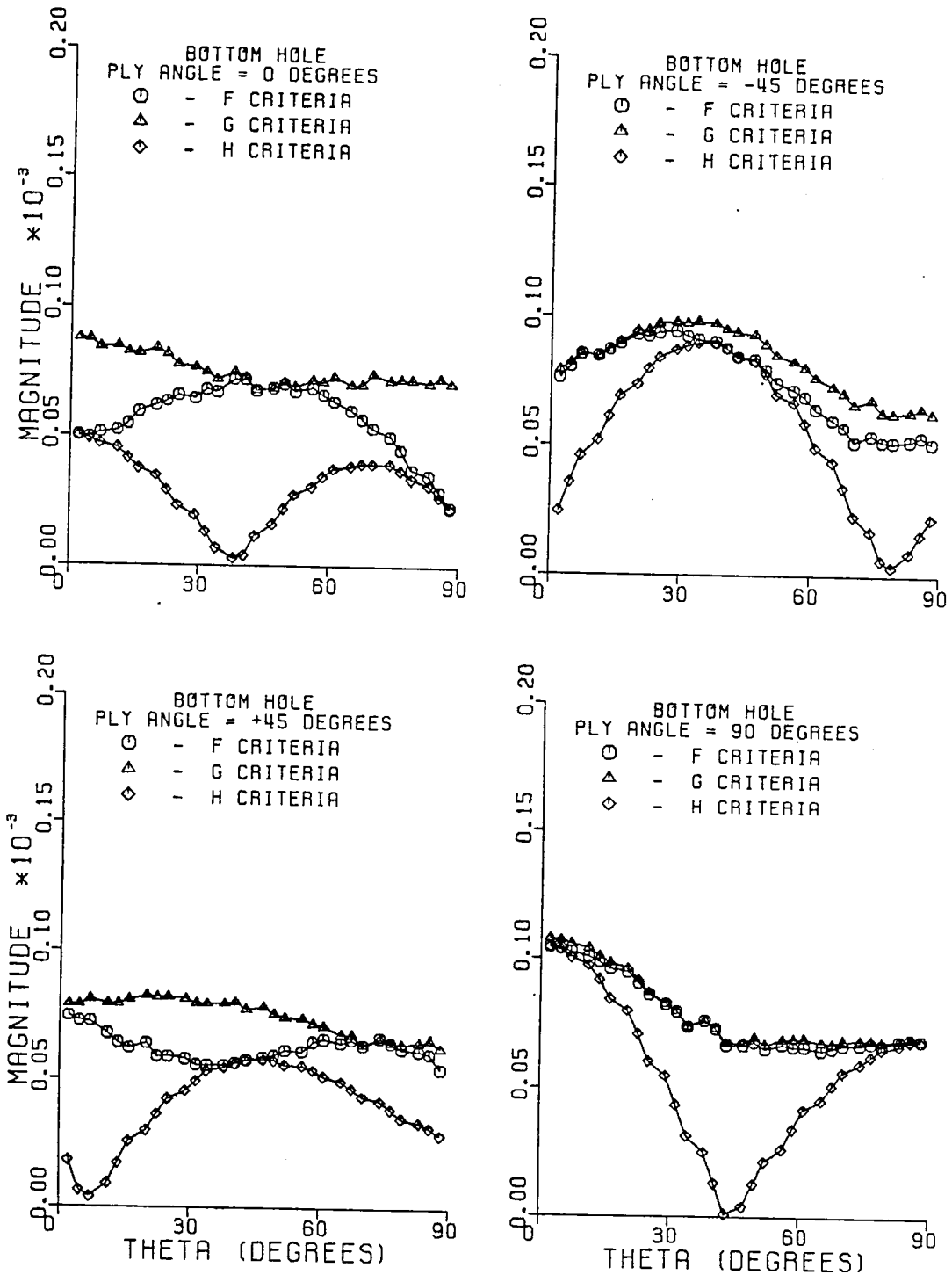

Fig. A.2 F, G, H vs. θ for a Quasi-Isotropic Laminate, Bottom Hole, W/D=5, E/D=3, G/D=3, D=1/2.

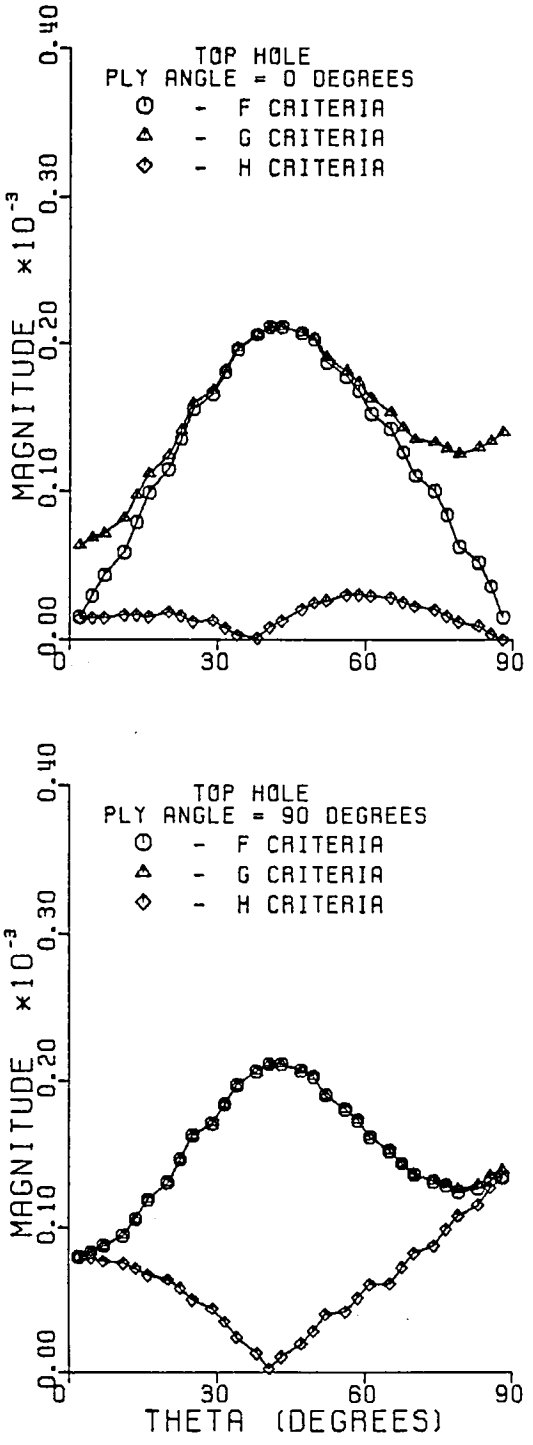

Fig. A.3 F, G, H vs. θ for a Cross-Ply Laminate, Top Hole, W/D=5, E/D=3, G/D=3, D=1/2.

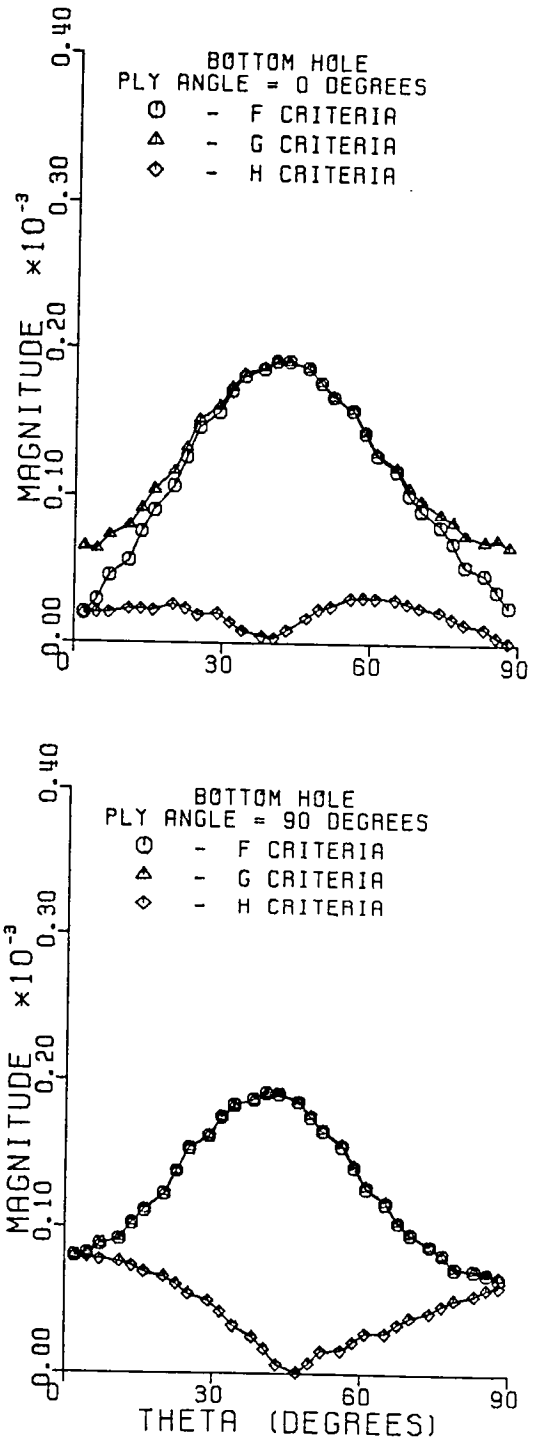

Fig. A.4 F, G, H vs. θ for a Cross-Ply Laminate, Bottom Hole, W/D=5, E/D=3, G/D=3, D=1/2.

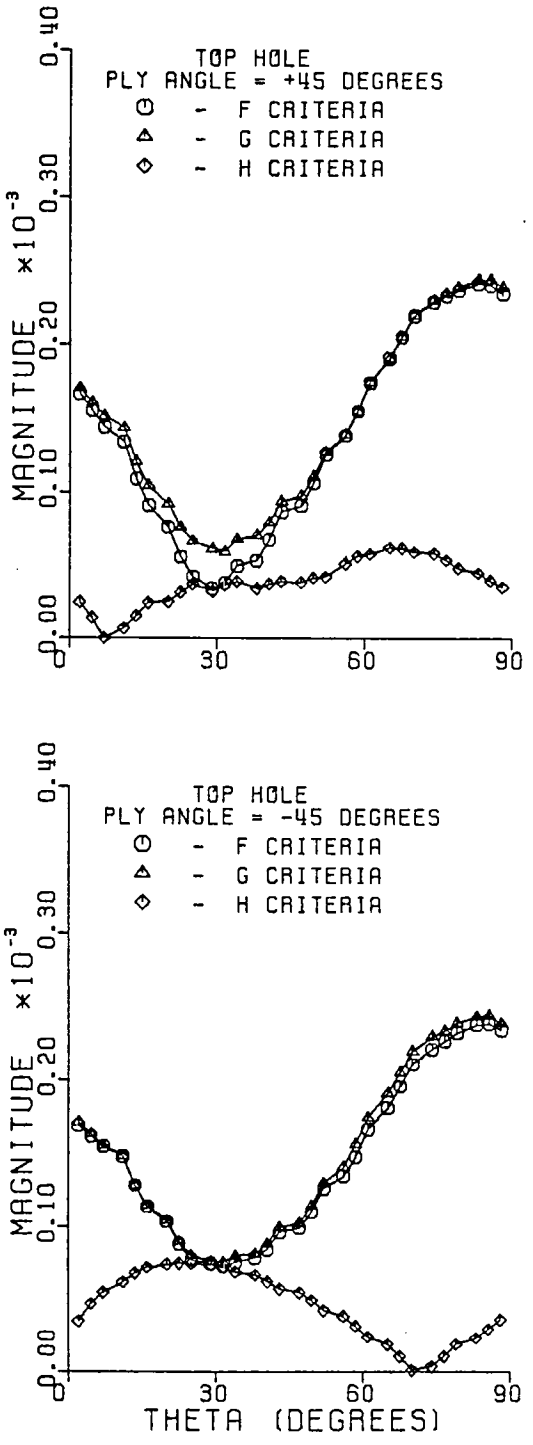

Fig. A.5 F, G, H vs. θ for an Angle-Ply Laminate, Top Hole, W/D=5, E/D=3, G/D=3, D=1/2.

contributes nothing.

Fig. A.5 illustrates results for the angle-ply laminate and the baseline geometry case. As was seen before, the F and G criteria agree on the maximum load and the mode of failure. The failure mode is indicated as net-section tension by the location of either the maximum F or G values. Similar results are seen for both plies. Fig. A.6 shows these same results for the bottom hole. Here again, the F and G criteria indicate maximum values at the bearing region of the hole. The Maximum Stress criteria does not accurately predict failure for this case. The other two criteria however, correspond almost exactly. This indicates that the effect of the σ_2 term is quite small in relation to the τ_{12} term.

The other geometry addressed in this analysis of failure criteria was the case where W/D=3, E/D=3/2, G/D=3/2, and D=1/2. This geometry was thought to provide an extreme case in relation to the baseline geometry. If the Yamada-Sun criteria proved to be appropriate for this geometry, then it would be fairly safe to assume that geometric cases in between these two would also be correctly predicted. Fig. A.7 shows the F, G, and H criteria each ply in a quasi-isotropic laminate at the top hole. As was the case in fig. A.1, all three criteria coincide at the net-section region in the key ply in the laminate, namely, the 90° layer. This

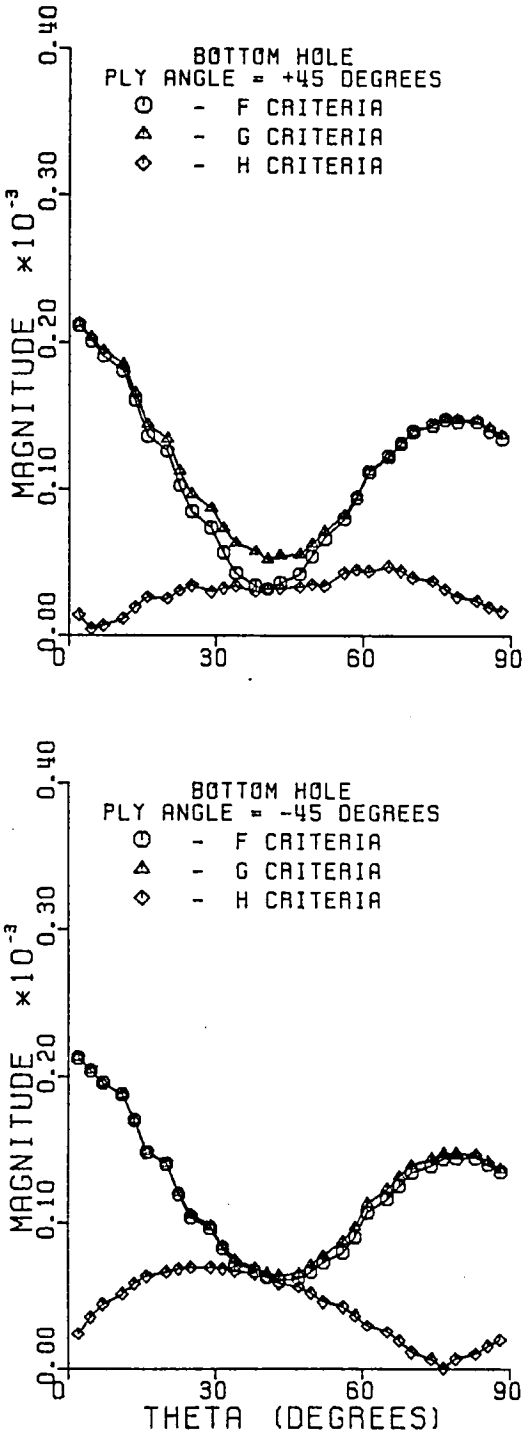

Fig. A.6 F, G, H vs. θ for an Angle-Ply Laminate, Bottom Hole, W/D=5, E/D=3, G/D=3, D=1/2.

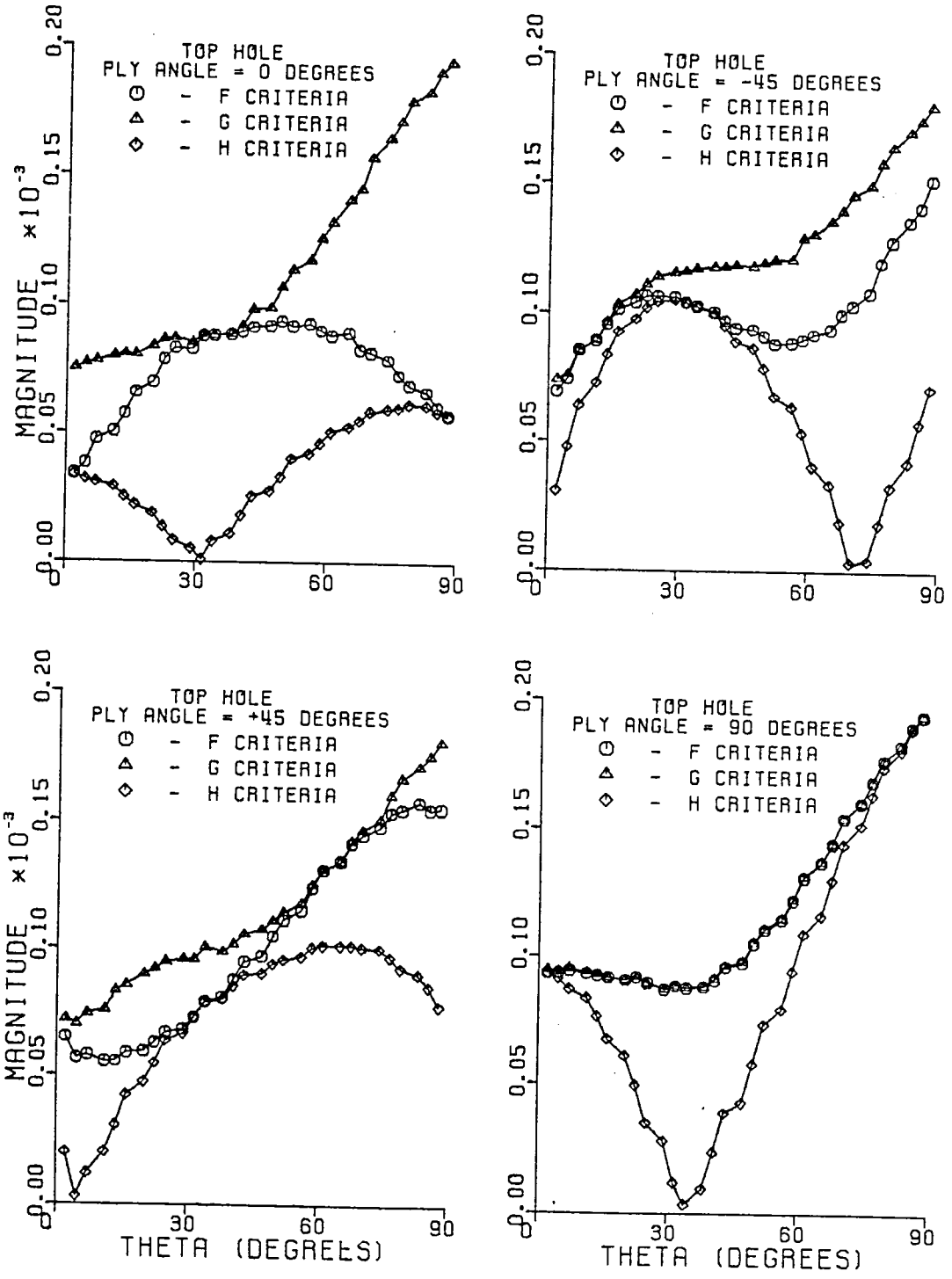

Fig. A.7 F, G, H vs. θ for a Quasi-Isotropic Laminate, Top Hole, W/D=3, E/D=3/2, G/D=3/2, D=1/2.

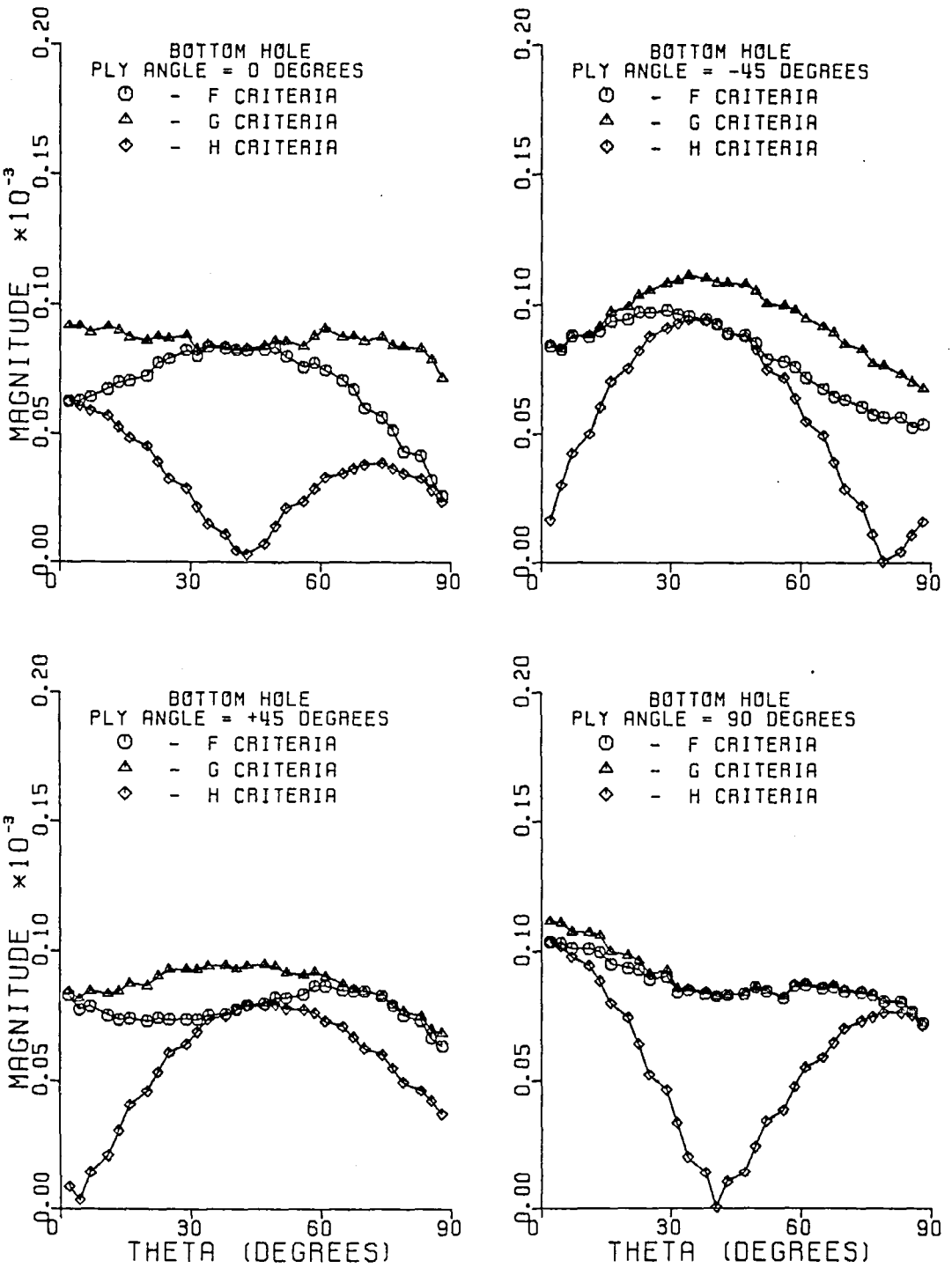

Fig. A.8 F, G, H vs. θ for a Quasi-Isotropic Laminate, Bottom Hole, W/D=3, E/D=3/2, G/D=3/2, D=1/2.

indicates that the dominant term in the determination of failure for this case is the σ_1 term.

Fig. A.8 shows these values for the same laminate at the bottom hole. In this case, the G criteria shows a slightly higher value at the maximum than the F criteria. This occurs in the -45° and 90° plies. Although the mode of failure is predicted to be the same by all three criteria, the inclusion of the σ_2 term would lower the failure strength by about 9%.

Figs. A.9 and A.10 show the results for a cross-ply laminate at the top and bottom holes respectively. The results are similar to the situation observed in the baseline geometry case. Both the F and G criteria agree on their maximum values and would predict the same failure load. This indicates that the σ_2 term is not important in this case.

Figs. A.11 and A.12 show results for an angle-ply laminate at the top and bottom holes. Again, the results are nearly the same as for the baseline geometry. The H criteria is definitely not appropriate for failure prediction in this case. The F and G criteria predict the nearly the same failure load and also match with the failure mode prediction. This prediction is similar to results in Chapter 6.

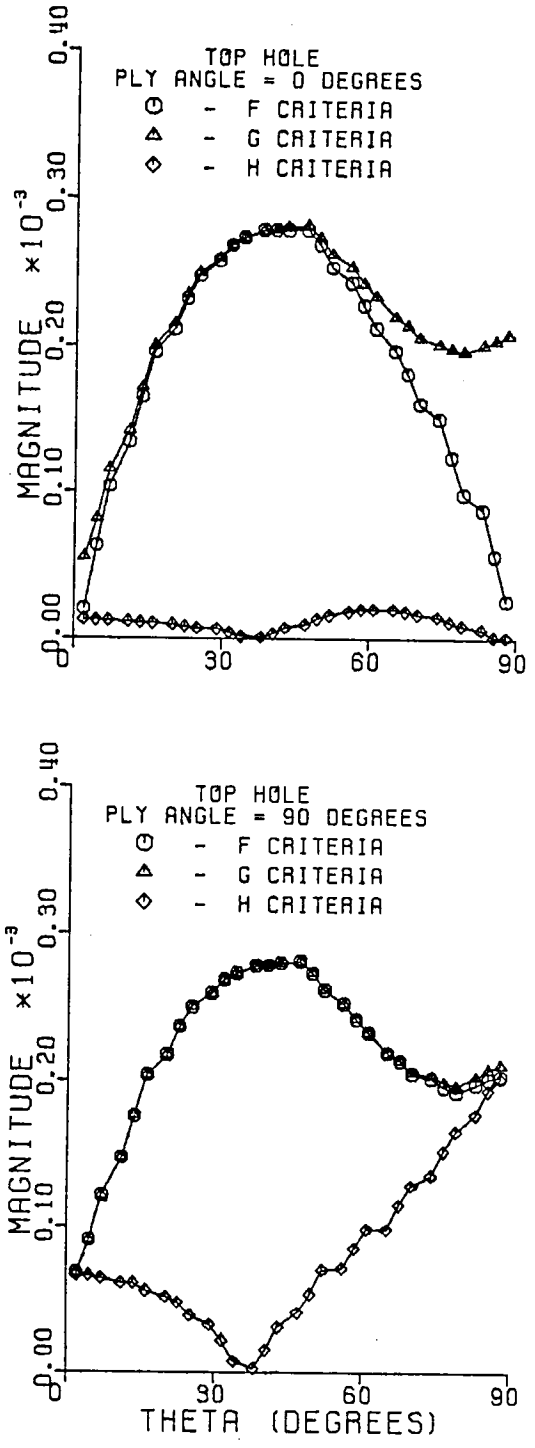

Fig. A.9 F, G, H vs. θ for a Cross-Ply Laminate, Top Hole, W/D=3, E/D=3/2, G/D=3/2, D=1/2.

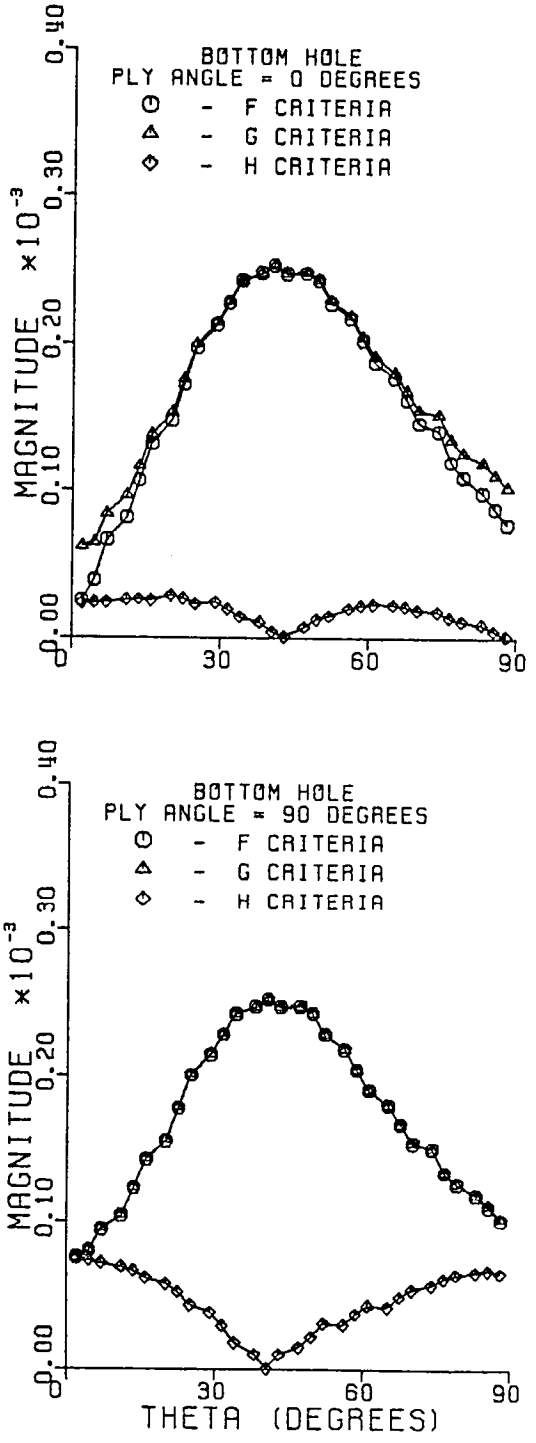

Fig. A.10 F, G, H vs. θ for a Cross-Ply Laminate, Bottom Hole, W/D=3, E/D=3/2, G/D=3/2, D=1/2.

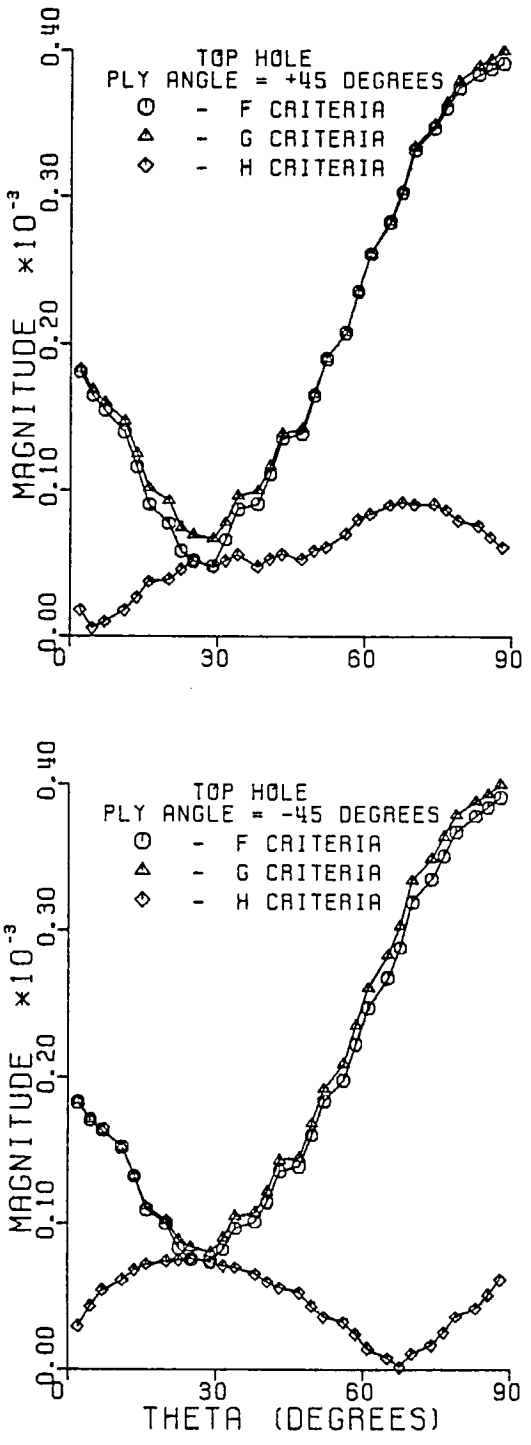

Fig. A.11 F, G, H vs. θ for an Angle-Ply Laminate, Top Hole, W/D=3, E/D=3/2, G/D=3/2, D=1/2.

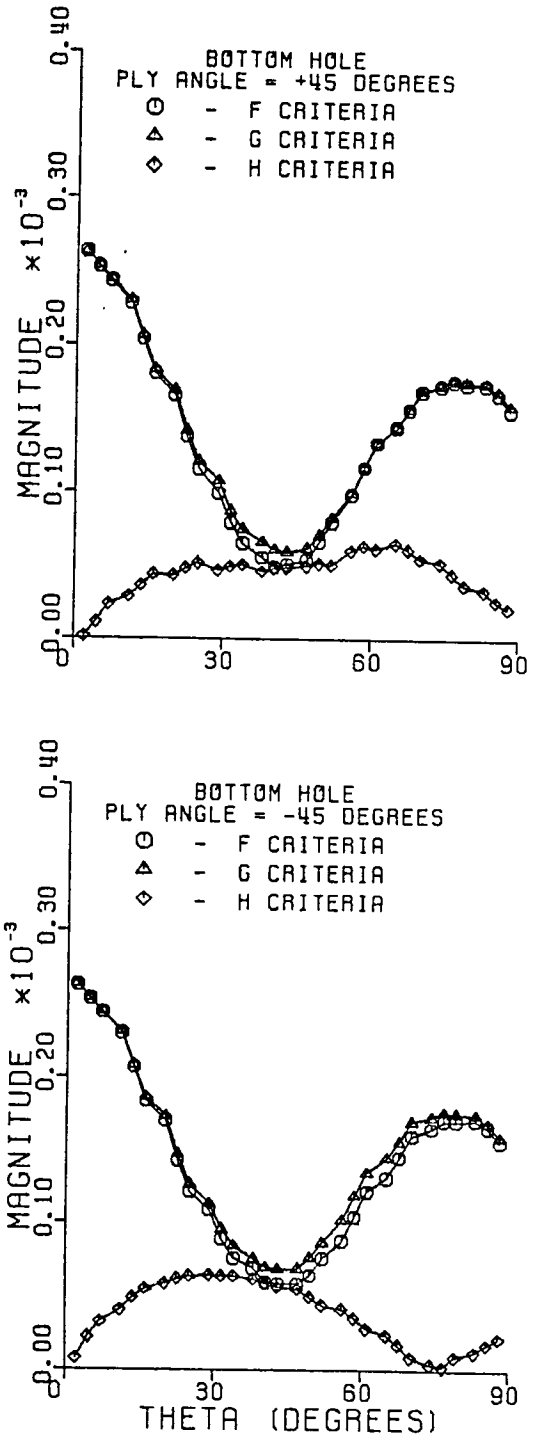

Fig. A.12 F, G, H vs. θ for an Angle-Ply Laminate, Bottom Hole, W/D=3, E/D=3/2, G/D=3/2, D=1/2.

1. Report No.	2. Government Accession No.	3. Recipient's Catalog No.
NASA CR-178019		

4. Title and Subtitle	5. Report Date
Effects of Load Proportioning on the Capacity of Multiple-Hole Composite Joints	November 1985
	6. Performing Organization Code

7. Author(s)	8. Performing Organization Report No.
M.W. Hyer, University of Maryland, College Park, MD 20742 P.A. Chastain, Aerojet Strategic Propulsion Co., Sacramento, CA 95813	

9. Performing Organization Name and Address	10. Work Unit No.
Department of Engineering Science and Mechanics Virginia Polytechnic Institute and State University Blacksburg, VA 24061-4899	
	11. Contract or Grant No. NAG1-343
12. Sponsoring Agency Name and Address	13. Type of Report and Period Covered Final, 3/84-3/85 Contractor Report
National Aeronautics and Space Administration Washington, D.C. 20546	14. Sponsoring Agency Code 505-63-01-06

15. Supplementary Notes The research effort which led to the results presented here was financially supported by the Structures Laboratory, USARTL (AVSCOM). The technical monitor was Donald J. Baker of the NASA Langley Research Center.

16. Abstract This study addresses the issue of adjusting the proportion of load transmitted by each hole in a multiple-hole joint so that the joint capacity is a maximum. Specifically two-hole-in-series joints are examined. The results indicate that when each hole reacts 50% of the total load, the joint capacity is not a maximum. One hole generally is understressed at joint failure. The algorithm developed to determine the load proportion at each hole which results in maximum capacity is discussed. The algorithm includes two-dimensional finite-element stress analysis and failure criteria. The algorithm is used to study the effects of joint width, hole spacing, and hole to joint-end distance on load proportioning and capacity. To study hole size effects, two hole diameters are considered. Three laminates are considered: a quasi-isotropic laminate; a cross-ply laminate; and a 45 degree angle-ply laminate. By proportioning the load, capacity can be increased generally from 5 to 10%. In some cases a greater increase is possible.

17. Key Words (Suggested by Author(s))	18. Distribution Statement
composite joints, composite materials, pin-loaded holes, composite material failure criteria, stress concentration factors in composites	unclassified-unlimited subject category 39

19. Security Classif. (of this report)	20. Security Classif. (of this page)	21. No. of Pages	22. Price
unclassified	unclassified	178	A09

For sale by the National Technical Information Service, Springfield, Virginia 22161